UNIVERSITA' DEGLI STUDI DI PARMA

Dottorato di ricerca in Biologia e Patologia Molecolare

Ciclo XXVIII

Determinants of biological activity of nanomaterials in innate immunity cells: the role of aspect ratio, environmental contaminants and protein corona

Coordinatore:
Chiar.mo Prof. Valeria Dall'Asta

Tutor:
Chiar.mo Prof. Ovidio Bussolati

Dottorando: Manfredi Allegri

Alla mia cara e indistruttibile nonna
Vanda che ha potuto vedere anche
questo mio traguardo

INDEX

SUMMARY

As defined by the European Union, " 'Nanomaterial' (NM) means a natural, incidental or manufactured material containing particles, in an unbound state or as an aggregate or agglomerate, where, for 50 % or more of the particles in the number size distribution, one or more external dimensions is in the size range 1 nm-100 nm " (2011/696/UE). Given their peculiar physico-chemical features, nanostructured materials are largely used in many industrial fields (e.g. cosmetics, electronics, agriculture, biomedical) and their applications have astonishingly increased in the last fifteen years.

Nanostructured materials are endowed with very large specific surface area that, besides making them very useful in many industrial processes, renders them very reactive towards the biological systems and, hence, potentially endowed with significant hazard for human health. For these reasons, in recent years, many studies have been focused on the identification of toxic properties of nanostructured materials, investigating, in particular, the mechanisms behind their toxic effects as well as their determinants of toxicity.

This thesis investigates two types of nanostructured TiO_2 materials, TiO_2 nanoparticles (NP), which are yearly produced in tonnage quantities, and TiO_2 nanofibres (NF), a relatively novel nanomaterial. Moreover, several preparations of MultiWalled Carbon Nanotubes (MWCNT), another nanomaterial widely present in many products, are also investigated.-

Although many *in vitro* and *in vivo* studies have characterized the toxic properties of these materials, the identification of their determinants of toxicity is still incomplete. The aim of this thesis is to identify the structural determinants of toxicity, using several *in vitro* models. Specific fields of investigation have been a) the role of shape and the aspect ratio in the determination of biological effects of TiO_2 nanofibres of different length; b) the synergistic effect of LPS and TiO_2 NP on the expression of inflammatory markers and the role played therein by TLR-4; c) the role of functionalization and agglomeration in the biological effects of MWCNT.

As far as biological effects elicited by TiO_2 NF are concerned, the first part of the thesis demonstrates that long TiO_2 nanofibres caused frustrated phagocytosis, cytotoxicity, hemolysis, oxidative stress and epithelial barrier perturbation. All these effects were mitigated by fibre shortening through ball-milling. However, short TiO_2 NF exhibited enhanced ability to activate acute pro-inflammatory effects in macrophages, an effect dependent on phagocytosis. Therefore, aspect ratio reduction mitigated toxic effects, while enhanced macrophage activation, likely

rendering the NF more prone to phagocytosis. These results suggest that, under *in vivo* conditions, short NF will be associated with acute inflammatory reaction, but will undergo a relatively rapid clearance, while long NF, although associated with a relatively smaller acute activation of innate immunity cells, are not expected to be removed efficiently and, therefore, may be associated to chronic inflammatory responses.

As far as the relationship between the effects of TiO_2 NP and LPS, investigated in the second part of the thesis, are concerned, TiO_2 NP markedly enhanced macrophage activation by LPS through a TLR-4-dependent intracellular pathway. The adsorption of LPS onto the surface of TiO_2 NP led to the formation of a specific bio-corona, suggesting that, when bound to TiO_2 NP, LPS exerts a much more powerful pro-inflammatory effect. These data suggest that the inflammatory changes observed upon exposure to TiO_2 NP may be due, at least in part, to their capability to bind LPS and, possibly, other TLR agonists, thus enhancing their biological activities.

Finally, the last part of the thesis demonstrates that surface functionalization of MWCNT with amino or carboxylic groups mitigates the toxic effects of MWCNT in terms of macrophage activation and capability to perturb epithelial barriers. Interestingly, surface chemistry (in particular surface charge) influenced the protein adsorption onto the MWCNT surface, allowing to the formation of different protein coronae and the tendency to form agglomerates of different size. In particular functionalization a) changed the amount and the type of proteins adsorbed to MWCNT and b) enhanced the tendency of MWCNT to form large agglomerates. These data suggest that the different biological behavior of functionalized and pristine MWCNT may be due, at least in part, to the different tendency to form large agglomerates, which is significantly influenced by their different capability to interact with proteins contained in biological fluids.

All together, these data demonstrate that the interaction between physico-chemical properties of nanostructured materials and the environment (cells + biological fluids) in which these materials are present is of pivotal importance for the understanding of the biological effects of NM. In particular, bio-persistence and the capability to elicit an effective inflammatory response are attributable to the interaction between NM and macrophages. However, the interaction NM-cells is heavily influenced by the formation at the nano-bio interface of specific bio-coronae that confer a novel biological identity to the nanostructured materials, setting the basis for their specific biological activities.

SOMMARIO

Come definito dall'Unione Europea, con il termine nanomateriale si intende " un materiale di origine naturale, accidentale o industriale contenente particelle, in uno stato non aggregato, aggregato o agglomerato, in cui almeno il 50% delle particelle ha almeno una dimensione compresa tra 1 e 100 nm " (2011/696/UE). I materiali nanostrutturati, date le loro peculiari caratteristiche fisico-chimiche, sono largamente impiegati in numerosi settori industriali (es. cosmetica, elettronica, agricoltura, campo biomedicale) e il loro utilizzo è cresciuto esponenzialmente negli ultimi quindici anni. I materiali nanostrutturati sono caratterizzati da una notevole area superficiale che, nonostante li renda molto utili in numerosi processi industriali, li rende estremamente reattivi nei confronti dei sistemi biologici e, quindi, potenzialmente pericolosi per la salute umana. Per questi motivi, negli ultimi anni, numerosi studi si sono focalizzati sull'identificazione delle proprietà tossiche dei materiali nanostrutturati, studiando in particolar modo i meccanismi alla base dei loro effetti tossici così come i loro determinanti strutturali di tossicità.

In questa tesi si studieranno due materiali nanostrutturati di TiO_2, le nanoparticelle (TiO_2 NP), la cui produzione consiste di decine di tonnellate ogni anno, e le nanofibre (TiO_2 NF), un materiale relativamente nuovo. Inoltre saranno oggetto di studio anche diverse preparazioni di nanotubi di carbonio a parete multipla (MWCNT), un altro nanomateriale a larga diffusione. Nonostante le proprietà tossiche di questi materiali siano state caratterizzate in numerosi studi *in vivo* e *in vitro*, l'identificazione dei determinanti di tossicità dei NM risulta ancora incompleta. Lo scopo di questa tesi consiste nell'identificazione di determinanti strutturali di tossicità, utilizzando diversi modelli *in vitro.* Più nello specifico si è indagato a) il ruolo della morfologia e dell'aspect ratio nella determinazione degli effetti biologici prodotti da TiO_2 NF di diversa lunghezza; b) l'effetto sinergico di LPS e TiO_2 NP sull'espressione di marker infiammatori e il ruolo del TLR-4 in questo fenomeno; c) il ruolo della funzionalizzazione e dell'agglomerazione nella determinazione degli effetti biologici dei Nanotubi di Carbonio a Parete Multipla (MWCNT).

Per quanto riguarda gli effetti biologici prodotti dalle TiO_2 NF, nella prima parte della tesi si dimostra che TiO_2 NF lunghe causano fagocitosi frustrata, citotossicità, emolisi, stress ossidativo e alterano l'integrità della barriera epiteliale. Tutti questi effetti erano mitigati dall'accorciamento delle fibre attraverso il processo di ball-milling. Al contrario, le TiO_2 NF corte erano in grado di stimolare maggiormente l'espressione di marker infiammatori acuti nei macrofagi, un effetto dipendente dalla fagocitosi. La riduzione dell'aspect ratio, quindi, mitigava gli effetti tossici,

mentre stimolava maggiormente l'attivazione dei macrofagi, fenomeno riconducibile ad un'aumentata fagcocitosi di queste fibre. Questi risultati suggeriscono che, *in vivo,* le NF corte potrebbero essere associate a una reazione infiammatoria acuta ma, parallelamente, essere soggette ad una clearance relativamente più rapida. Al contrario, le NF lunghe, stimolando in misura minore fenomeni di attivazione macrofagica, potrebbero essere rimosse in maniera meno efficiente e, quindi, essere associate a fenomeni infiammatori cronici.

Per quanto riguarda la relazione tra gli effetti delle TiO_2 NP e del LPS, approfondite nella seconda parte della tesi, è stato dimostrato che le nanoparticelle potenziavano fortemente l'attivazione dei macrofagi indotta dal LPS mediante un pathway intracellulare mediato dal recettore TLR-4. L'adsorbimento del LPS sulla superficie delle TiO_2 NP portava alla formazione di una specifica bio-corona, indicando che, quando legato alle TiO_2 NP, il LPS induce effetti pro-infiammatori significativamente maggiori. Questi dati suggeriscono che i fenomeni infiammatori osservati in seguito all'esposizione alle TiO_2 NP potrebbero essere dovuti, almeno parzialmente, alla loro capacità di legare il LPS e, probabilmente, altri agonisti dei TLR, aumentandone l'attività biologica.

E' stato infine valutato il ruolo della funzionalizzazione e dell'agglomerazione negli effetti biologici di MWCNT, ed è stato dimostrato che la funzionalizzazione superficiale dei MWCNT con gruppi aminici o carbossilici mitigava gli effetti tossici dei MWCNT in termini di attivazione di macrofagi e di alterazione delle barriere epiteliali. La chimica di superficie (in particolare la carica superficiale) influenzava l'adsorbimento di proteine sulla superficie dei MWCNT, portando alla formazione di diverse bio-corone e influenzando la tendenza a formare agglomerati di differenti dimensioni. Questi risultati suggeriscono che il diverso comportamento biologico dei MWCNT pristini e funzionalizzati potrebbe essere associato, almeno in parte, alla differente tendenza a formare grandi agglomerati, che, a sua volta, sembrerebbe influenzata in maniera significativa dalla differente capacità di interagire con le proteine presenti nei fluidi biologici.

In conclusione, i dati presentati in questa tesi dimostrano che la comprensione degli effetti biologici dei nanomateriali richiede non solo la caratterizzazione delle loro proprietà fisico-chimiche ma, soprattutto, delle interazioni tra essi e l'ambiente biologico (cellule + fluidi biologici). In particolare, la biopersistenza e la capacità di determinare un'efficace risposta infiammatoria sono attribuibili all'interazione con i macrofagi. Inoltre, l'interazione tra cellule e materiali è notevolmente influenzata dalla formazione di specifiche bio-corone all'interfaccia bio-nano. La

formazione della bio-corona conferisce una nuova identità biologica ai materiali nanostrutturati, costituendo così la base per specifiche attività biologiche.

List of abbreviations

BET, Brunauer, Emmett and Teller; BM- TiO_2NF, Ball-Milled TiO_2NF; BSA, Bovine Serum Albumin; CFE, Colony Forming Efficiency; CLI-095, Ethyl (6R)-6-[N-(2-chloro-4-fluorophenyl)sulfamoyl]-cyclohex-1-ene-1-carboxylate; CNT, Carbon Nanotubes; Cro, Crocidolite; CVD, Carbon Vapor Deposition; DMEM, Dulbecco's Modifed Eagle Medium; DRAQ5, 1,5-Bis[2-(di-methylamino) ethyl]amino-4, 8-di- hydroxyanthracene-9,10-dione; EDX, Energy Dispersive X-Ray Analysis; FBS, Fetal Bovine Serum; FT-IR, Fourier transform infrared spectroscopy; LPS, Lipopolysaccharide; NF, Nanofibres; NM, nanomaterials; NP, nanoparticles; MWCNT, Multi-Walled Carbon Nanotubes; NO, Nitric Oxide; PAMP, Pathogen-associated molecular pattern; P-TiO_2NF, Pristine TiO_2NF; SB203580, 4-(4-Fluorophenyl)-2-(4-methylsulfinylphenyl)-5-(4-pyridyl)-imidazole; SSA, Specific Surface Area; SWCNT, Single-Walled Carbon Nanotubes; TBS, Tris-buffered saline; TEER, Trans-Epithelial Electrical Resistance; TLR-4, Toll-like receptor 4; U0126, 1,4-Diamino-2,3-dicyano-1,4-bis[2-aminophenylthio]butadiene; XRD, X-Ray Diffraction.

INTRODUCTION

Nanoparticles and Nanomaterials

As defined by the European Union in 2011, " 'Nanomaterial' means a natural, incidental or manufactured material containing particles, in an unbound state or as an aggregate or as an agglomerate and where, for 50 % or more of the particles in the number size distribution, one or more external dimensions is in the size range 1 nm-100 nm " (2011/696/UE).

Nanoparticles (NP) are endowed with peculiar physico-chemical properties that promote their use in many industrial applications and that derive not only from their chemical composition, but also from their size and shape; since, within certain limits, both size and shape can be controlled, it is possible to synthesize NP with defined properties. Moreover, given that NP are defined in the nanometric range, they are endowed with a very large specific surface area.

As far as NP origin is concerned, we can distinguish antropic and natural NP (Guzman, Taylor et al. 2006). Natural NP have been present in the ecosystem for millions of years coming for example from volcanisms, combustion processes of various type, microbes etc. Anthropic NP can be classified in intentional and non-intentional (or ultrafine) (Banfield, Veblon et al. 1990). Intentional NP (metals, semiconductors, organic polymer etc.) are largely used in a lot of industrial fields (e.g. cosmetics, electronics, agriculture, biomedical) and their applications have astonishingly increased in the last fifteen years.

The human organism has been exposed for millennia to natural and non-intentional nanostructures, but with the increasing number of nano-related products, the concerns of governments and the general public about related health hazards, with particular emphasis on occupational exposure and consumers' safety, have rapidly grown. As underlined before, NP are endowed with a very large specific surface area that, besides making them very useful in many industrial processes, renders them potentially very reactive towards the biological systems and, hence, endowed with significant risks for human health (Oberdorster, Oberdorster et al. 2005). Promotion of inflammatory responses is one of the proposed pathogenic mechanisms for a variety of different nanomaterials; in fact, tissues of animals exposed to nanosized materials (nanomaterials, NM) often present changes linked to inflammation, such as oxidative stress, DNA damage, infiltrates, and fibrosis (Landsiedel, Sauer et al. 2014; Luo, Chang et al. 2015). Inflammation may even constitute a mechanistic paradigm for a predictive assessment of

nanomaterial toxicity (Nel, Xia et al. 2006), at least for the so called Granular Biodurable nanoParticles (GBP) (Gebel, Foth et al. 2014).

To investigate the effects of NP on human health, a new branch of toxicology, called nanotoxicology, progressively developed in the last 10-15 years. The aim of nanotoxicology is to:

- Characterize biological risks linked to the exposure to NP and NM
- Characterize, in the case NP or other NM are found to be endowed with significant toxicity, the mechanisms behind their toxic effects
- Identify determinants of toxicity

The last goal is extremely important, due to the fact that the identification of a particular determinant of toxicity can allow its elimination or preventive mitigation, thus decreasing its toxicity while preserving NM properties.

Titanium Dioxide Nanostructures

Within the range of metal oxide nanoparticles, titanium dioxide (TiO_2) NP occupy a prominent position with a widespread use as sun blocking filters in cosmetics and self-cleaning, antibacterial and anti-polluting coatings onto different substrates, due to their photocatalytic activity. The increasing use of TiO_2 NP has promoted their large-scale production and, at the same time, has led to a growing concern about the risks to human health, in particular for the workers more regularly exposed, and to the environment. Indeed, although bulk TiO_2 has been classified as a biologically inert material for humans and animals (Lindenschmidt, Driscoll et al. 1990), evidence has been repeatedly reported on TiO_2 NP toxicity in several animal models *in vivo*, with inflammation (Shi, Magaye et al. 2013), enhanced proliferation of pulmonary cells at relatively high doses (Grassian, O'Shaughnessy P et al. 2007; Ma-Hock, Burkhardt et al. 2009), and carcinogenicity (Dankovic, Kuempel et al. 2007).

Despite the high number of contributions regarding the identification of the biological effects of TiO_2 NP both *in vivo* and *in vitro*, no attempt has been made so far to give an overall picture of the relationship between TiO_2 NP and the inflammatory response. More importantly, no study has specifically addressed the identification of structural determinants of TiO_2 NP linked to pro-inflammatory activity.

Structural toxicity determinants of TiO_2 nanostructures

Several structural determinants have been linked to the pro-inflammatory effects of nanomaterials (Braakhuis, Park et al. 2014). In the case of TiO_2 NP, comparison of NP differing for one or more structural features has been performed in several studies. However, it should be remarked that for a rigorous assessment of each determinant, nanomaterials different for a single physico-chemical characteristic should be compared under the same experimental conditions.

Agglomeration has been shown to play an important role in the effects of TiO_2 NP after inhalation (Noel, Cloutier et al. 2013). In fact, while exposure to the larger agglomerates (>100 nm) had significant acute pro-inflammatory effects, the smaller (<100 nm) did not, although indicators of cytotoxicity and oxidative stress where higher with the latter preparation.

As far as NP size is concerned, some authors suggest that NP smaller than 5 nm are more inflammogenic than NP with larger diameter (Kobayashi, Naya et al. 2009), while other authors suggest that the NP smaller than 5 nm or larger than 50 nm induce milder effects. Size is a key feature in the determination of nanomaterial bioavailability and of its distribution in different tissues and organs as well as of cell uptake. Bachler et al. (Bachler, von Goetz et al. 2015) have modeled the biodistribution of TiO_2 NP concluding that at high internal exposure, TiO_2 NP *in vivo* agglomerate and are subsequently internalized by macrophages in the various compartments. If smaller than 100 nm, TiO_2 NP can enter cells not only through phagocytosis, so that NP can enter both phagocytic and non-phagocytic cells without significant differences (Getts, Shea et al. 2015). Conversely, micrometric sizes favor phagocytosis, at least until the size of the agglomerate exceeds that of the phagocyte (Getts, Shea et al. 2015).

Shape has been identified as another important determinant of toxicity. Phagocytosis and, therefore, the clearance of NP is influenced by shape with rounded NP or agglomerates more easily internalized than the high aspect ratio nanostructures (Champion and Mitragotri 2006). In recent years, a lot of fibre-like TiO_2 nanostructures, such as nanotubes, nanobelts, nanofibres, have been synthesized for many industrial applications. Many authors described a significantly greater biological activity of these fibrous nanostructures compared with spherical counterparts both *in vitro* (Xia, Hamilton et al. 2013; Hamilton, Wu et al. 2014) and *in vivo* (Hurbankova, Cerna et al. 2013; Silva, Teesy et al. 2013). Comparing the effects of TiO_2 nanobelts of two different lengths (short 3 µm, long 9 µm) with TiO_2 nanospheres after an acute administration, Porter et al. (Porter, Wu et al. 2013) demonstrated that nanobelts were more capable of inducing inflammation than nanospheres. In particular, authors showed that after 112 days of exposure, although inflammatory changes were apparently reversible, lung burden of long nanobelts was much higher than that of nanospheres suggesting an impaired of the clearance of the long fibrous material. These findings seems to be in accordance with the fibre paradigm, which indicates that a fibre length larger than 5 µm leads to frustrated phagocytosis, a phenomenon in which macrophages, the main cells responsible for the clearance of NM from tissues, cannot efficiently internalize them, leading to the increased biopersistence of the material (Schinwald and Donaldson 2012). Moreover it has been suggested that length needs to exceed the micrometric range to exert a significant influence on the biological activity of NM since no significant differences in pro-inflammatory effects were caused by TiO_2 nanodots or short nanorods (length:200 nm) (Warheit, Webb et al. 2006).

Surface reactivity has been proposed to be the single best parameter to predict the pro-inflammatory activity of nanoparticles since it is influenced by other relevant structural determinants (Braakhuis, Park et al. 2014), which include, in the case of TiO_2 nanomaterials, shape, size, and surface area. However, given the high capability of NP of adsorbing different molecules, surface reactivity can be modified depending on the medium in which NP are dispersed and, therefore, on the specific molecules they can adsorb onto their surface.

Mechanisms of pro-inflammatory effects of TiO_2 nanostructures

In the last years many authors have investigated the mechanism linked to the *in vivo* pro-inflammatory activity of TIO_2 NP and from those studies it is possible to enucleate several main hypotheses.

The first hypothesis suggests that TiO_2 NP may cause direct cell damage leading to a significant release of Damage Associated Molecular Patterns (DAMPS), which could activate different "sentinel receptors" on the immune and non-immune cells such as Toll Like Receptors (TLRs) or Nod Like Receptors (NLRs).

In general, however, TiO_2 NP are characterized by a very low cytotoxic activity, most of that is observed at very high doses used in *in vitro* experiments which are not comparable to those used detectable after *in vivo* exposure. With this important limitation in mind, it is interesting to note that different authors report that the exposure to TiO_2 NP can trigger different types of cell death. In particular, several reports indicate that TiO_2 NP can induce necrosis and necrosis associated to apoptosis, two types of cell death characterized by the release of DAMPS (Hussain, Thomassen et al. 2010; Sang, Li et al. 2013; Sheng, Wang et al. 2013). Others demonstrate that cells exposed to titania NP activate pro-apoptotic pathways which lead to cell death (Meena, Kajal et al. 2015; Orazizadeh, Daneshi et al. 2015; Wang, Cui et al. 2015). Moreover it has been demonstrated that TiO_2 NP, like other metal-based NP, are able to induce autophagy, another type of cell death (Chang, Xie et al. 2015; Yu, Sung et al. 2015). This mechanism is considered an adaptive mechanism involved in cell survival in situations characterized by the activation of ER stress, a condition that follows a significant accumulation of misfolded proteins inside cells. When ER stress overcomes some threshold, there is a switch from autophagy as a survival mechanism to a process that leads to cell death. In this phase several mediators are released which act as DAMPs.

Recently, it has been demonstrated both *in vivo* and *in vitro* that TiO_2 NP are able to trigger ER stress (Chang, Xie et al. 2015; Sheng, Ze et al. 2015; Yu, Sung et al. 2015), suggesting an involvement of this biological process in the determination of pro-inflammatory effect of TiO_2 NP.

One of the most supported hypothesis about the pro-inflammatory mechanism of TiO_2 NP does not identify the inflammation as a consequence of direct cell damage with the release of DAMPs but identifies TiO_2 NP as particles able to activate several pro-inflammatory transduction pathways focusing in particular on the activation of MAPKs and NF-κB transcription factor (Husain, Saber et al. 2013; Li, Ze et al. 2013) but also on an array of proteomic (Triboulet, Aude-Garcia et al. 2015) and epigenetic changes (Lu, Miousse et al. 2015). However, most of contributions indicate that TiO_2 NP are able to generate, in cells exposed to the material, high levels of ROS, with phagocytosis often involved in the oxidative stress. Indeed, TiO_2 NP can trigger oxidative stress once internalized in phagocytic cells leading to NADPH assembly. Oxidative stress may be triggered not only after phagocytosis in phagocytic cells, but it can be generated also form the external cell surface. This fact could be due to the fact that TiO_2 NM are redox active materials (Rasmussen, Mast et al. 2014) and could give the explanation for the triggering of oxidative stress also in non-phagocytic cells exposed to TiO_2 NP (Aueviriyavit, Phummiratch et al. 2012; Gerloff, Fenoglio et al. 2012). Biological effects of TiO_2 NP seems to be extremely related to their capability of inducing oxidative stress and, therefore, alterations of the intracellular signaling pathways. In particular, the oxidative stress induced by TiO_2 NP has been linked to genotoxic damage in A431 human epidermal cells and to macrophage activation in murine Raw264.7 macrophages in which the high increase of ROS has been correlated to an over activation of ERK1/2 and a marked stimulation of pro-inflammatory cytokine secretion (Kang, Moon et al. 2008). ROS generation has been also linked to enhancement of p38 phosphorylation and NF-kB activation, which lead to an increase pro-inflammatory cytokine expression.

Recently, many authors have suggested that TiO_2 NP can elicit pro-inflammatory effects acting as PAMPS or DAMPS, activating the innate immunity receptors. TiO_2 NP have been indeed involved in the activation of inflammasome in dendritic cells with a significant increase in IL-1beta secretion (Winter, Beer et al. 2011) and it has been demonstrated that this activation required NP internalization (Morishige, Yoshioka et al. 2010; Cho, Duffin et al. 2013).

With their large SSA NP and NM can interact with many compounds in biological fluids or in the environment, adsorbing them onto their surface. The binding between macromolecules, in

particular proteins, and nanostructures has been documented since several years and it has been demonstrated that these interactions can heavily affect the biological behavior of NM (Lynch, Cedervall et al. 2007; Lundqvist, Stigler et al. 2008; Lesniak, Fenaroli et al. 2012; Salvati, Pitek et al. 2013). More in general, the possibility that the observed biological effects of nanoparticles derive, or are modulated, by adsorbed compounds including environmental contaminants, and in particular endotoxins (LPS, lipopolysaccharide) has been documented since at least 2006 for gold nanoparticles (Vallhov, Qin et al. 2006) and for other different NM including TiO_2 NP (Esch, Han et al. 2010).

Carbon NanoTubes

After their discovery by Iijima in 1991 (Iijima 1991), carbon nanotubes (CNTs) have been increasingly used in advanced industrial applications. CNTs are graphitic hollow filaments of variable lengths, up to several hundred micrometers, depending on the production method. Single-walled carbon nanotubes (SWCNTs) are composed of a single cylindrical sheet of graphene, while multi-walled carbon nanotubes (MWCNTs) consist of several concentric, coaxial rolled up graphene sheets (Murray, Kisin et al. 2012) (Figure 1). Specifically, the CNT diameter is typically from 0.4 to 3 nm for SWCNTs and from 1.4 to 100 nm for MWCNTs (Tagmatarchis and Prato 2004). Chemical Vapor Deposition (CVD) method is the most frequently used for CNT synthesis and is the dominant technique for mass production of CNTs due to its easy scaling-up (Charitidis, Georgiou et al. 2014). CNTs can exist as particles if they have defects and therefore 'grow' as tangles, like balls of string. Whilst the CNT in such bundles are tubular, they are particulate as far as cells are concerned, since the bundles of tubules are in a compact form. However, if the CNT have a number or few defects, the tubules can grow straight and the CNT can adopt a fibrous, high-aspect shape (Poland, Duffin et al. 2008).

Owing to their excellent physicochemical, electrical and mechanical properties, they are applied in numerous technological fields such as polymer composites, microelectronics, energy storage and sensors (De Volder, Tawfick et al. 2013).

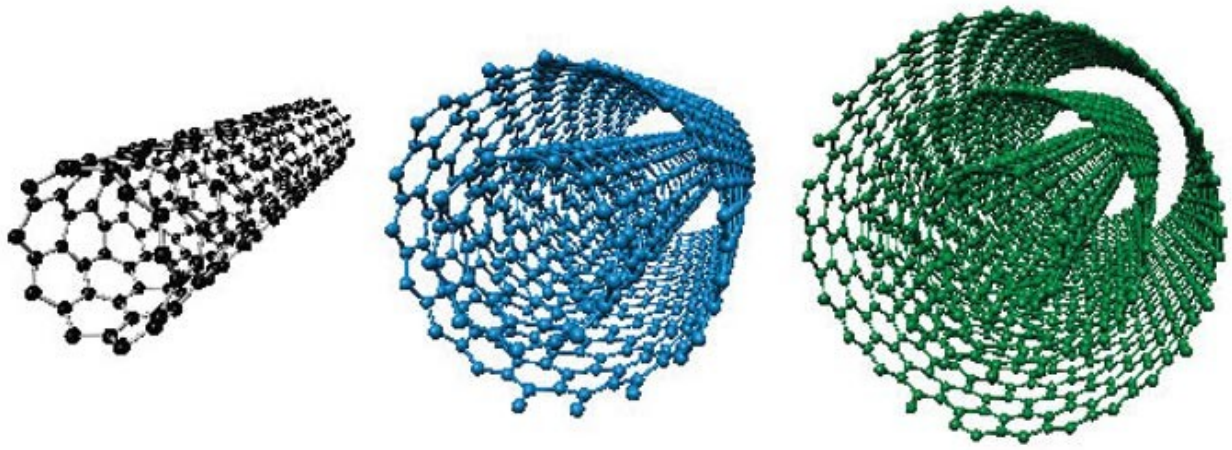

Figure 1. Schematic representation of Single Walled (left), Double Walled (center), Multi Walled (right) Carbon Nanotubes

Toxicological profile of Carbon Nanotubes

The increased large-scale production of CNTs, which are endowed with evident morphological similarities with asbestos fibres, has raised many concerns about their safety for human health. Many *in vitro* and *in vivo* findings suggest that CNTs exert significant toxic effects towards the biological systems. The conventional view point is that SWCNTs exhibit significant cytotoxicity to human and animal cells through various mechanisms (Manna, Sarkar et al. 2005; Chen, Tam et al. 2006; Kagan, Tyurina et al. 2006), whereas MWCNTs are considered endowed with lower toxicity (Jia, Wang et al. 2005). However, increasing evidence suggest that MWCNTs can be inflammogenic and fibrogenic in rodents.

Concerning the biological effects elicited by CNTs, a direct correlation in human population between lung disease and CNT exposure has not been demonstrated yet, but several *in vivo* studies focusing on the pulmonary toxicity of CNT have revealed that this NM share a very similar pattern of toxic effects with asbestos fibres including acute neutrophilic inflammation (Muller, Huaux et al. 2005; Shvedova, Kisin et al. 2005), cytokine production (Shvedova, Kisin et al. 2005), granulomatous inflammation (Lam, James et al. 2004; Shvedova, Kisin et al. 2008), interstitial thickening (Porter, Hubbs et al. 2013) and fibrosis (Mercer, Hubbs et al. 2011).

It has been proposed that the generation of reactive oxygen species (ROS) and reactive nitrogen species (RNS), originated by the direct release from the material or after its interaction with immune cells, may be the mechanism underlying the toxic effect of CNTs as in the case of asbestos fibres (Kamp 2009). For asbestos, the redox cycling triggered by the iron integrated in its crystalline structure generates the release of damaging free radicals such as Hydroxyl (Gilmour, Brown et al. 1997). Analogously, most of the pulmonary pro-inflammatory effects observed after CNTs administration may be attributable to the release of free radicals which may originate from the contaminant transition metals within their structure (derived by production processes) or from their structural defects, which can generate free bonds in the graphenic backbone (Muller, Huaux et al. 2008).

Murphy et al. (Murphy, Schinwald et al. 2012) and Brown et al. (Brown, Kinloch et al. 2007) observed that ROS formation and oxidative stress phenomena can be generated also after the interaction of CNTs with inflammatory cells. In particular they showed that long CNTs were endowed with the ability to stimulate frustrated phagocytosis in macrophages *in vitro,* a

pathogenic mechanism also described for asbestos fibres. This phenomenon occurs when macrophages are unable to completely internalize very long fibres (> 15 μm (Schinwald, Chernova et al. 2012)) leading to an incomplete clearance of the materials that, extrapolating the situation to an *in vivo* context, generate an accumulation in the respiratory regions. Frustrated phagocytosis is accompanied by the generation of oxidative stress (Hansen and Mossman 1987), release of cytokines (Brown, Kinloch et al. 2007) as well as lysosomal destabilization (Hamilton, Wu et al. 2009), increasing recruitment of inflammatory cells to the lungs and activating the surrounding epithelial cells, eventually leading to a sustained inflammatory response.

The role of bio-coronae in the determination of the biological identity of nanomaterials

Physico-chemical characteristics of NM are crucial for the determination of the interactions with biological structures. High-SSA NP adsorb onto their surface different biomolecules present in biological fluids, especially proteins but also lipids, forming the so-called “bio-corona”. The most studied bio-corona is represented by the “protein corona” which is formed by proteins or small peptides. This layer is dynamic with exchanges between surface-bound and bulk proteins occurring on different time scales (Miclaus, Bochenkov et al. 2014) (Figure 2).

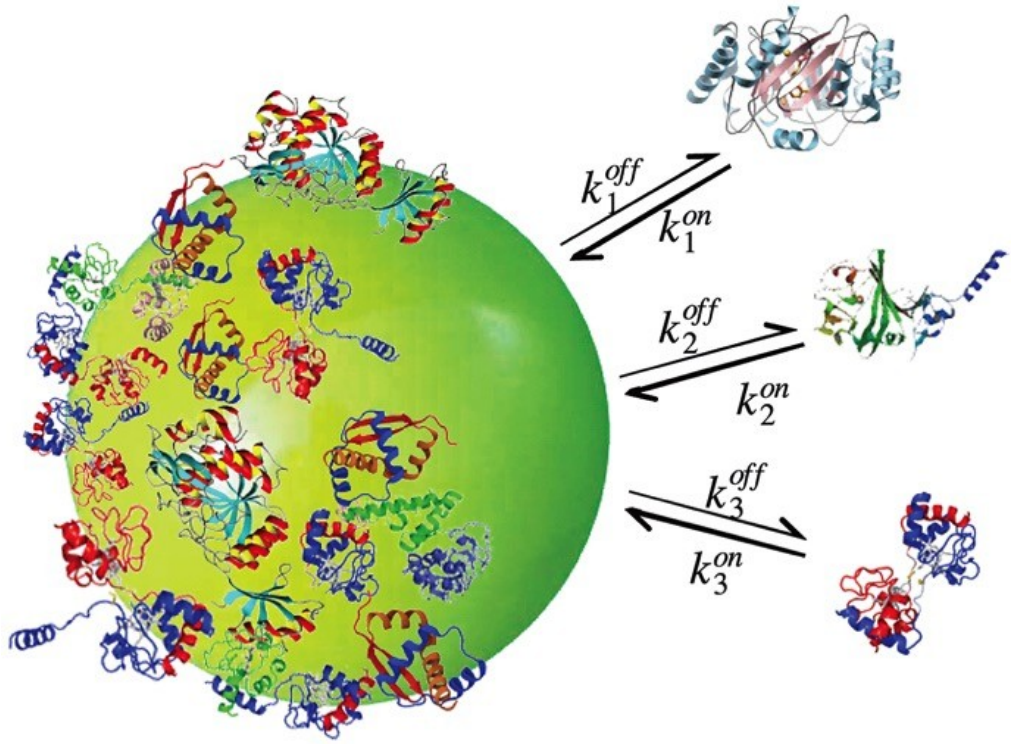

Figure 2. Schematic representation of proteins adsorption and desorption onto the surface of NP. Adapted from (Darabi Sahneh, Scoglio et al. 2013).

According to this model, proteins with higher affinity for the surface exchange slowly (over periods of hours) forming the most stable corona called “hard corona”; instead, low affinity proteins are quickly replaced, forming the “soft corona” which represents the outer layer. Although the relation between the original surface functionality of NP and the nature of the corona still remains elusive (Monopoli, Walczyk et al. 2011; Lesniak, Fenaroli et al. 2012), it has been demonstrated that surface chemistry, size and charge of NP are key factors able to determine the characteristics of the corona as well as biological fluid properties and composition (Tenzer, Docter et al. 2011; Monopoli, Aberg et al. 2012; Treuel, Brandholt et al. 2014). Subsequent interactions between NP

and biological entities are mediated by the presence and nature of this corona that becomes a key entity at the nano-bio interface. Nowadays, it is widely accepted that the composition of the protein corona strongly determines the biological identity of any NM and, thus, the resultant biological activity and distribution (Casals and Puntes 2012). All current data indicate that proteins contained in the corona and not the NP themselves interact with cells (Walczyk, Bombelli et al. 2010; Monopoli, Aberg et al. 2012) (Figure 3). Therefore, the nature of the corona is more significant in determining biological responses (i.e., immunogenicity) than the bare material properties of the particle itself (Lee, Choi et al. 2015).

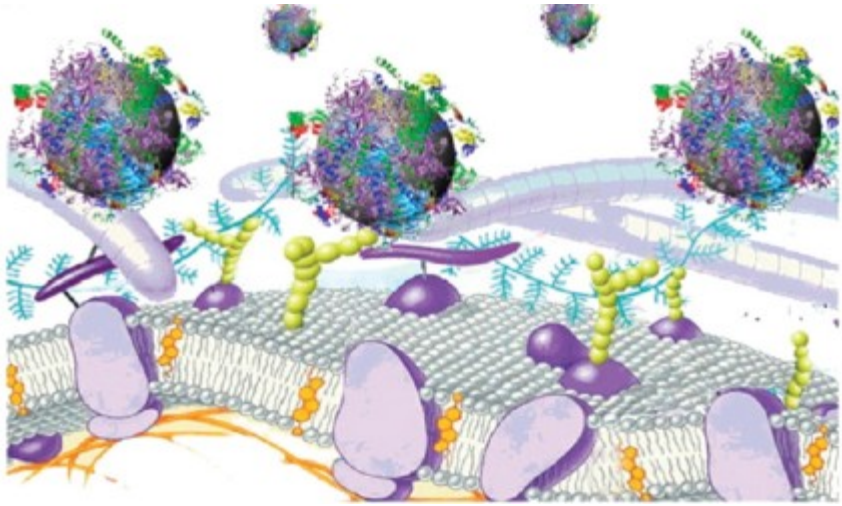

Figure 3. Schematic representation of the interaction between cell surfaces and NP covered by protein corona.
Source:*http://pubs.acs.org/action/showImage?doi=10.1021%2Fja910675v&iName=master.img000.jpg&type=master*

As far as the role of nanomaterial bio-corona is concerned, many authors have reported the possibility that the observed biological effects of nanoparticles could derive, or may be modulated, not only by adsorbed proteins but also by other compounds including environmental contaminants, and in particular endotoxins (LPS, lipopolysaccharide)(Vallhov, Qin et al. 2006; Esch, Han et al. 2010). Given the high-binding activity of NM, the high resilience of these contaminants in the environment, the difficulty to estimate their amount in the NM preparations (Smulders, Kaiser et al. 2012) and the absence of adequate decontaminating procedures (Vallhov, Qin et al.

2006), the LPS contamination represent a severe issue for any experimental evaluation of NP activities.

Aims of the thesis

The aim of this thesis is to identify structural determinants of toxicity of nanomaterials used in industrial production processes. Three experimental lines will be developed, assessing:

a) the role of shape and the aspect ratio in the determination of biological effects of TiO_2 nanofibres, investigating in different cell models their cytotoxic and pro-inflammatory effects as well as their capability to impair the barrier properties of epithelial monolayers
b) the synergistic effect of LPS and TiO_2 NP on the expression of inflammatory markers and the role played therein by TLR-4 in Raw264.7 macrophages
c) the role of functionalization and agglomeration in the determination of biological effects of MWCNT

MATERIALS AND METHODS

Physico-chemical characterization and dispersion of NM

Synthesis and characterization of NM used in this thesis are described within specific chapters.

Cell culture

Biological assays were performed on different cell models, largely adopted in nanotoxicological studies:

a) Mouse peritoneal monocyte-macrophages Raw 264.7 were obtained from the Cell Bank of the IZSLER (Istituto Zooprofilattico Sperimentale della Lombardia e dell'Emilia-Romagna, Brescia, Italy). Raw 264.7 cells were cultured in Dulbecco's modified Eagle's medium (DMEM) supplemented with 10% Fetal Bovine serum (FBS), 4 mM glutamine, and antibiotics (streptomycin 100 µg/mL/ penicillin, 100 U/mL).
b) Murine alveolar macrophages (MH-S), a gift of Prof. Dario Ghigo, University of Torino (Italy), were also originally provided by IZSLER and cultured in RPMI1640 medium supplemented with 10% FBS, antibiotics, L-glutamine (2 mM) and β-mercaptoethanol (0.05 mM).
c) Human alveolar carcinoma epithelial A549 cells were obtained from the Cell Bank of the IZSLER. A549 cells were cultured in F-12 Ham's medium supplemented with 10% FBS, 1 mM glutamine, and antibiotics.
d) Calu-3 cells, derived from a human lung adenocarcinoma and histologically related to serous cells of proximal bronchial airways, were obtained from the IZSLER Cell Bank. Calu-3 cells were cultured in EMEM supplemented with 10% FBS, 2mM glutamine, 1 mM sodium pyruvate, and antibiotics.

All cultures were maintained in a humidified atmosphere of 5% CO_2 in air in 10-cm dishes.

For experimental treatments, if not stated otherwise, culture medium was replaced 24h after cell seeding by fresh medium in the presence of the indicated materials and the exposure prolonged as detailed for each experiment.

Cell viability and cytotoxicity

Cell viability was assessed with the resazurin method (O'Brien, Wilson et al. 2000). Resazurin is a non-fluorescent molecule that is converted by intracellular enzymes in the fluorescent compound resorufin (λem = 572 nm). After the incubation with the materials, cell viability was tested replacing medium with a solution of resazurin (44 µM, Sigma-Aldrich) in serum-free DMEM. After

20 min, fluorescence was measured at 572 nm with a multimode plate reader Perkin Elmer Enspire (Waltham, MA, USA). Since nanomaterials could interfere with cytotoxicity assays, a preliminary test was performed incubating the dye with NM only (at the maximal dose used for the experiment of 128 µg/ml) and then measuring fluorescence. No fluorescence signal was detected above background (data not shown).

Cytotoxicity was assessed with LDH assay after cell treatments with the materials. After the incubation with NM, supernatants were collected and centrifuged at 15000*g* for 15 min to remove particulates. Supernatants were then tested for LDH activity (Cytotoxicity detection kit, Roche Diagnostics Limited, Burgess Hill, UK) according to manufacturer's instructions. Absorbance readings were performed at 550 nm with a plate reader (Fluostar Optima, BMG Labtech, Aylesbury, UK). Maximum LDH release was set to 100 % with cells treated with 0.1% Triton X100 while 0% was set for the untreated control cells. Results were expressed as percentage LDH release as a surrogate for cytotoxicity. Wells without cells were also prepared in order to correct for background LDH activity. Finally, spiking/recovery of the analyte in the presence of materials were also performed in order to assess potential material interference with the assay. None of the materials significantly interfered with the assay (data not shown).

Haemolytic activity

The test samples were suspended in sodium chloride 0.9% at a stock concentration of 6 mg/mL and prepared as previously described. An aliquot of sheep blood in Alsever's solution liquid (Fisher Scientific, Loughborough, UK) was centrifuged at 250*g* for 10 min and then washed 3 times in sodium chloride 0.9%. After centrifugation, the supernatant was discarded, and 200 µL of packed erythrocytes were diluted into 7.2 mL of sodium chloride. One hundred and fifty µL per well of saline with or without the materials were added in a clear 96-well plate. Then 75 µL per well of the erythrocytes suspension were added giving a final concentrations of each material of 4, 2, 1 and 0.5 mg/mL. The plates were incubated for 15 minutes at room temperature protected from light on a plate shaker and then centrifuged at 250 *g* for 15 min to pellet erythrocytes and materials. One hundred µL of supernatant were then transferred into a new clear 96-well plate, and the absorbance was read at 540 nm with a plate reader (Fluostar Optima, BMG Labtech, Aylesbury, UK). Results were expressed as percentage haemolysis, with 0% being set for the saline control and 100% set for Triton X100 0.1% in sodium chloride 0.9%, used as a positive control.

Electronic Paramagnetic Resonance (EPR)

The ability of the materials to generate Reactive Oxygen Species (ROS) was assessed in an a-cellular system using Electron Paramagnetic Resonance (EPR). Materials were suspended at 1 mg/ml in PBS and incubated with the spin trap 1-hydroxyl-2,2,6,6- tetramethyl-4-oxo-piperidine (Tempone-H; 1 mM) immediately before the initial measurement. Tempone-H is a highly sensitive spin trap that shows selectivity for the superoxide anion, as well as for peroxyl radicals and peroxynitrite, forming a stable product that can be measured by EPR (Dikalov, Skatchkov et al. 1997). Samples were maintained at 37°C throughout the incubation and measurements were taken after 1 and 60 minutes after the addition of the Tempone-H by drawing 50 µL of sample into a capillary tube (Scientific Laboratory Ltd., Coatbridge, UK) and sealing it with a plug of soft sealant (Cristaseal, VWR International, Lutterworth, UK). An X-band EPR spectrometer (Magnettech MS-200, Berlin, Germany) was used with the following parameters: microwave frequency, 9.3–9.55 Hz; microwave power, 20 mW; modulation frequency, 100 kHz; modulation amplitude, 1,500 mG; center field, 3,365 G; sweep width, 50 G; sweep time, 30 sec; number of passes, 1. Measurement of intrinsic ROS production was conducted across 3 independent experiments and the mean signal intensity (area under the curve) established across the replicate experiments. Pyrogallol (100 µM) was used as a positive control to generate superoxide radicals (Taylor, Rossi et al. 2004).

Acellular DCFH assay

The acellular production of ROS was also assessed with the DCFH assay. Test materials were prepared in serum-supplemented RPMI culture medium at a concentration of 12.8 mg/mL with vortex mixing and with the addition of 10 min at room temperature (RT) in a bath sonicator (Ultrawave Sonicator QS25, 400W). A 2 mM solution of 2',7'-dichlorofluorescein di-acetate (DCFH-DA, Sigma-Aldrich, Poole, UK) was incubated with sodium hydroxide 0.01 N for 30 min in order to hydrolize the diacetate moiety. The digested probe was then diluted in PBS providing a working solution of the dye at 50 µM. 140 µL per well of PBS was added in a black 96-well plate, followed by 20 µL of the material suspension and, finally, 40 µL of probe solution. The final concentrations of the material were 128, 64 and 32 µg/mL, mimicking the concentrations used to treat the cells. Fluorescence emission was recorded for 20 min at 530 nm (λex 485 nm) using a plate reader (Fluostar Optima, BMG Labtech, Aylesbury, UK). Results were expressed as the change in arbitrary fluorescence unit (RFU) over 20 min compared to control. Experiments were performed with and

without fluorescein acetate (Sigma-Aldrich, Poole, UK) to check for material interference. None of the materials tested interfered significantly with the assay (data not shown).

Cellular DCFH assay

The membrane permeable DCFH-DA probe was also used without alkaline hydrolysis to measure the ability of materials to induce oxidative stress in cells. After internalization, intra-cellular esterases cleave the di-acetate moiety, thus causing probe retention and making it sensitive to ROS. Cells were seeded in 96-well plates as previously described and treated for 24 hours with cell culture medium with or without the materials at the doses of 10, 20 or 40 µg/cm^2. After being washed twice in sodium chloride (0.9%), cells were incubated for 1h at room temperature in a solution of DCFH-DA (10 µM in sodium chloride) to allow internalization of the probe into the cell cytoplasm. Cells were then washed with sodium chloride 0.9% and lysed in 90% DMSO in PBS. Plates were centrifuged at 300 g for 15 minutes to remove cellular debris and particulates. The fluorescence was measured in the supernatants (λ_{ex} 485 nm; λ_{em} 530 nm) using a plate reader (Fluostar Optima, BMG Labtech, Aylesbury, UK). Results are expressed as change in RFU compared to untreated control. Using the same procedure, cells were prepared without the probe to check the material interference. None of the materials tested interfered significantly with the assay (data not shown).

Glutathione assay

After treatments with the materials, cells were washed in ice-cold PBS and then lysed in 200 µL ice-cold 5% trichloroacetic acid in 20 mM HCl, 2.15 mM EDTA and 10 mM ascorbic acid (all reagents from Sigma-Aldrich, Poole, UK). Samples were then transferred to Eppendorf tubes and centrifuged at 15000*g* for 15 minutes at 4°C. 10 µL of each sample (in duplicate) were added to 19 µL of extraction buffer in a 96-well plate. 48 µL of 1 M potassium phosphate (pH 7) were added (Sigma-Aldrich, Poole, UK). After 5 min of incubation, 200 µL of 0.1M potassium phosphate (pH 6.9) were added. Finally, 29 µL per well of *o*-phtalaldehyde (OPT, 5 mg/mL) in methanol was added as the OPT reacts with GSH to form a highly fluorescent product. After 30 minutes incubation, fluorescence (λ_{ex} 350 nm; λ_{em} 420 nm) was measured using a plate fluorimeter (Fluostar Optima, BMG Labtech, Aylesbury, UK). Reduced glutathione concentration was calculated according to standards and results were expressed as GSH level compared to untreated cell control.

Colony Forming Efficiency (CFE) assay

The CFE test is a clonogenic assay that measures the ability of a single cell to form a colony (Franken, Rodermond et al. 2006) and can be used to determine cytotoxic effects induced by nanomaterials. Indeed, since it is a label-free test (non-colorimetric, non-fluorescent), CFE assay lowers the possibility of the occurrence of interference due to nanomaterials (Ponti, Kinsner-Ovaskainen et al. 2014). For the test, 10^2 A549 cells, one of the cell types in which CFE assay was adapted to study the effects of nanomaterials (Ponti, Kinsner-Ovaskainen et al. 2014), were seeded in 10 cm- Petri dishes. After 24h, culture medium was replaced with complete medium supplemented with MWCNTs (2.5 - 5 μg/cm^2), and the exposure prolonged for 72h. After medium renewal, incubation was prolonged for further 72h. Cells were then fixed with a solution of 4% paraformaldehyde for 20 min, washed three times with PBS without Ca and Mg, and stained with a 0.1% crystal violet solution in bi-distilled water. After staining, colonies > 50 cells were counted and data expressed as % of control, untreated cells.

RT- Polymerase Chain Reaction

Total RNA was isolated with GenElute Mammalian Total RNA Miniprep Kit (Sigma–Aldrich). After reverse transcription, aliquots of cDNA from each sample were amplified in a total volume of 25 μl with Go Taq PCR Master Mix (Promega, Italia, Milan, Italy), along with the forward and reverse primers (5 pmol each) reported in Table 1. Real time PCR was performed in a 36-well RotorGeneTM3000, version 5.0.60 (Corbett Research, Mortlake, Australia). For all the messengers to be quantified, each cycle consisted of a denaturation step at 95 °C for 20 s, followed by separate annealing (30s) and extension (30s) steps at a temperature characteristic for each pair of primers (Table 1). Fluorescence was monitored at the end of each extension step. Melting curve analysis was added at the end of each amplification cycle. The analysis of the data was made according to the relative standard curve method (Bustin 2000). RT-PCR data were expressed as the ratio between each investigated mRNA and *Gapdh* mRNA.

Table 1. Primers and temperatures of annealing adopted for RT-PCR experiments

Gene	Forward	Reverse	T (°C)
Inducible Nitric Oxide Synthetase (*Nos2*)	5' - GTT CTC AGC CCA ACA ATA CAA GA – 3'	5' - GTG GAC GGG TCG ATG TCA C – 3'	57
Prostaglandin-endoperoxide synthase 2 (*Ptgs2*)	5'-GCTCAGCCAGGC-AGCAAATC-3'	5'-ATCCAGTCCGG-GTACAGTCA-3'	56
Interleukin 6 *(Il6)*	5'- TAG TCC TTC CTA CCC CAA TTT CC- 3'	5'- TTG GTC CTT AGC CAC TCC TTC- 3'	56
Interleukin 1β *(Il1b)*	5'-GCA ACT GTT CCT GAA CTC AAC T-3'	5'-ATC TTT TGG GGT CCG TCA ACT-3'	58
Glyceraldehyde-3- phosphate dehydrogenase (*Gapdh*)	5' - TGT TCC TAC CCC CAA TGT GT -3'	5' - GGT CCT CAG TGT AGC CCA AG – 3'	57

Nitrite concentration

Nitrite concentration, as a proxy for NO output, was determined in Raw264.7 and/or MH-S macrophages, which are known to be competent for NO production, through a fluorimetric approach, based on the production of the fluorescent molecule 1H-naphthotriazole from 2,3-diaminonaphthalene (DAN) in an acid environment (Misko, Schilling et al. 1993). After indicated time of incubation with the materials, 100 µL of medium were transferred to black 96-well plates with a clear bottom (Corning, Cambridge, MA). DAN (20 µL of a solution of 0.025 mg/mL in 0.31 M HCl) was then added and, after 10 min at RT, the reaction was stopped with 20 µL of 0.7 M NaOH. Standards were performed in the same medium from a solution of 1 mM sodium nitrite. Fluorescence (λ_{ex} 360 nm; λ_{em} 430 nm) was determined with a multimode plate reader Perkin Elmer Enspire (Waltham, Massachussets, USA).

Western Blot Analysis

Cells were lysed in a buffer containing 20 mM Tris–HCl, pH 7.5, 150 mM NaCl, 1 mM EDTA, 1 mM EGTA, 1% Triton, 2.5 mM sodium pyrophosphate, 1 mM β-glycerophosphate, 1 mM Na_3VO_4, 1 mM NaF, 2 mM imidazole and a cocktail of protease inhibitors (Complete, Mini, EDTA-free, Roche, Monza, Italy). Lysates were transferred in Eppendorf tubes, sonicated for 15s and centrifuged at 12,000*g* for 20 min at 4°C. After quantification with the Bio-Rad protein assay, aliquots of 30 µg of

proteins were mixed with Laemmli buffer 4× (250 mM Tris–HCl, pH 6.8, 8% SDS, 40% glycerol, and 0.4M DTT), warmed at 95°C for 10 min and loaded on a 8% gel for SDSPAGE. After electrophoresis, proteins were transferred to PVDF membranes (Immobilon-P, Millipore, Millipore Corporation, MA, USA). Non-specific binding sites were blocked with an incubation of 1h at room temperature in blocking solution (Western Blocking Reagent, Roche) diluted in TBS (Tris-Buffered saline, pH 7.5). The blots were then exposed at 4°C overnight to the following antibodies diluted in 5% BSA in TBS: anti-Nos2 (rabbit polyclonal, 1:400, Santa Cruz Biotechnology, Santa Cruz, CA, USA); anti-phospho-p38 (rabbit polyclonal, 1:500, R&D Systems, Minneapolis, MN, USA); anti-p38, (rabbit polyclonal, 1:400, R&D Systems); anti-actin (mouse monoclonal, 1:4,000, Sigma-Aldrich); anti-tubulin (mouse monoclonal, 1:1,000, Sigma-Aldrich). After washing, the blots were exposed for 1 h at room temperature to HRP-conjugated anti-rabbit or anti-mouse antibodies (Cell Signaling Technology, Danvers, MA, USA), diluted 1:20,000 in blocking solution. Immunoreactivity was visualized with Immobilon Western Chemiluminescent HRP Substrate (Millipore, Merck).

Cytokine assay

TNF-α and IL-6 secretion in the culture media of cells exposed to NM was determined with ELISA RayBio® kit (Ray Biotech, Norcross, GA, USA). After incubation under the conditions indicated for each experiment, 100 µl of medium were transferred in 96-well plates functionalized with anti-TNF-α antibody and incubated overnight at 4°C. Then, 100 µl of biotinylated antibody were added in each well and, after 1 h of incubation at RT, 100 µl of streptavidin solution were added. After 45 min the samples were incubated with 100 µl of the TMB One Step Reagent contained in the kit solution and, after 30 min, reaction was stopped, and absorbance was immediately read at 450 nm with a multimode plate reader Perkin Elmer Enspire. Standards were performed in the Assay Buffer from a solution of 50 ng/ml of recombinant specific protein.

Trans Epithelial Electrical Resistance

Trans-Epithelial Electrical Resistance (TEER) was measured using an epithelial voltmeter (EVOM, World Precision Instruments Inc., Sarasota, FL, USA). For the experiments, Calu-3 cells, an airway epithelial cell line which forms a tight monolayer when cultured in a double chamber culture system, were seeded into cell culture inserts with membrane filters (pore size 0.4 µm) for Falcon 24-well-multitrays (Cat. N° 3095, Becton, Dickinson & Company, Franklin Lakes, NJ, USA), at a density of 2.3×10^4 cells/cm^2, and grown for 12d until a tight monolayer was formed (TEER > 1000

$\Omega \cdot cm^2$). MWCNT were added in the apical chamber from a 1 mg/ml stock solution without changing the medium and TEER was measured at the indicated times of treatment. TEER changes were expressed as the percentage of the initial value adjusted for control cell monolayers according to the following equation (Salem, Bosquillon et al. 2009):

$$\% \, \Delta TEER = \frac{Final\ TEER\ (treated)}{Final\ TEER\ (control)}\ x\ \frac{Initial\ TEER\ (control)}{Initial\ TEER\ (treated)}\ x\ 100$$

Scanning Electron Microscopy (SEM)

Cells were seeded on coverslips in 24-well plates (ThermanoxTM, Scientific Laboratory Supplies Limited, Hessle, UK). After 24h, cells were treated with cell culture medium with or without the various materials at the dose of 10 µg/cm^2. After 24h cells were rinsed in sodium chloride and fixed overnight at 4°C in glutaraldehyde (3% in 0.1 M sodium cacodylate buffer). The preparations were gradually dehydrated with subsequent incubation with ethanol 75%, 85%, 95% and 100%. Coverslips were then treated for 10 min with hexamethyldisilazane and, after drying, mounted on SEM stub. Samples were sputter coated with gold and analyzed using a Scanning Electron Microscope (SEM, Oxford Instruments).

Confocal microscopy

Cells were seeded on four-chamber slides at a density of 15x10^4 cells/cm^2 and treated after 24 h, as described for each experiment. The incubation was prolonged for 24 h. 20 min before the end of exposure, cells were transferred in serum-free medium supplemented with CellTracker® Red CMPTX (8 µM, Molecular Probes, Invitrogen) to label cytoplasm; in the last 5 min 1,5-bis[2-dimethylamino) ethyl]amino-4, 8-dihydroxyanthracene-9,10-dione (DRAQ5®, 20 µM, Alexis Biochemicals, San Diego, CA, USA) was also added to the incubation medium to counterstain nuclei. At the end of the exposure, cell monolayers were rinsed twice in PBS and fixed with 3.7% paraformaldehyde (PFA) at room temperature for 15 min. Specimens were then mounted on glass slides with fluorescence mounting medium (Dako Italia SpA, Milan, Italy) and imaged by confocal microscopy. Confocal analysis was carried out with a LSM 510 Meta scan head integrated with an inverted microscope (Carl Zeiss, Jena, Germany). Samples were observed through a 63x (1.4 NA) oil objective. Image acquisition was carried out in multitrack mode, i.e. through consecutive and independent optical pathways. Excitation at 488 nm and reflectance were used to visualize NM;

excitation at 543 nm and emission recorded through a 580-630 nm band pass barrier filter were used to visualize cytoplasm; excitation at 633 nm and emission through a 670 nm long pass filter were recorded to visualize the nucleus.

Statistical analysis

All experiments were performed a minimum of three times, each at least in duplicate, whenever not stated otherwise. Results were expressed as mean +/- Standard Error of the Mean (SEM) or Standard Deviation (SD), as indicated. Statistical analysis was performed by ANOVA followed by the post hoc test indicated for each experiment or two-tailed *t* test for unpaired data. The Graph Pad Prism^{TM} software version 6.00 (Graph Pad Software Inc., San Diego, CA) was used. The differences were considered significant if $p < 0.05$.

Chemicals

Sigma-Aldrich was the source of the all the chemicals whenever not stated otherwise.

The role of shape and aspect ratio in the determination of biological effects elicited by TiO_2 nanofibres in vitro

Abstract

Titanium dioxide (TiO_2) nanofibres (NF) are a novel fibrous nanomaterial with increasing applications in a wide variety of fields. While the biological effects of TiO_2 nanoparticles have been extensively studied, the toxicological characterization of TiO_2 nanofibres is far from being complete. In this part of the thesis, I evaluated the toxicity of commercially available anatase TiO_2 nanofibres, before and after extensive ball milling with zirconia microbeads which lowered aspect ratio from 1:29 to 1:5. Using TiO_2 nanoparticles and crocidolite as non-fibrous and fibrous benchmarks, I evaluated cell viability, hemolysis, oxidative stress, macrophage activation and trans-epithelial electric resistance (an indicator of the epithelial barrier competence), as well as cell morphology and particle uptake with SEM and confocal microscopy. A possible influence of endotoxin contamination of NF was also investigated. Long, pristine TiO_2 nanofibres were more cytotoxic than shorter counterparts towards alveolar epithelial cells and macrophages. Long nanofibres also exhibited a markedly higher hemolytic activity than short ones and lowered glutathione in macrophages. Moreover, long TiO_2 nanofibres decreased the trans-epithelial electrical resistance of airway cell monolayers, an effect also mitigated after ball-milling. Confocal microscopy indicated that macrophages efficiently internalized short but not long TiO_2 nanofibres, while SEM images demonstrated that the interaction with long TiO_2 nanofibres caused severe cell stretching and deformation. However, aspect ratio reduction enhanced the expression of inflammatory markers (NO production, *Nos2* and *Ptgs2* induction, cytokine secretion) in macrophages, which, however, was also triggered at lower levels by long TiO_2 nanofibres. The enhanced pro-inflammatory effects of short TiO_2 nanofibres were only in part accounted for by LPS contamination but were suppressed by the inhibition of phagocytosis caused by the cytoskeletal drug cytochalasin B. This data indicates that (1) long TiO_2 nanofibres exert significant toxic effects, including loss of viability, hemolysis, impairment of the epithelial barrier integrity, frustrated phagocytosis and macrophage activation; (2) aspect ratio reduction mitigates the effects on cell viability, haemolysis and epithelial barrier competence, but enhances macrophage activation. It is suggested that, in a scenario *in vivo*, phagocytosis-enhanced macrophage activation may contribute to the efficient clearance of short TiO_2 nanofibres, while frustrated phagocytosis, together with increased cytotoxicity, may enhance the toxicity of long TiO_2 nanofibres.

Background

High Aspect Ratio Nanostructures and the Fibre Pathogenicity Paradigm

High aspect ratio nanostructures (HARN), such as nanotubes, nanofibres, nanowires, are increasingly used in many industrial applications from electronics to photovoltaics. However, whilst nanofibres continue to show their utility in many applications, the morphological similarity of these materials to pathogenic fibres such as asbestos has raised serious concerns about the potential health implications of exposure.

This association, based on morphology, is not simply an arbitrary link between very different materials but relies upon the structure-activity relationship that has been identified to promote fibre-type pathogenicity as opposed to particle toxicity mediated by other mechanisms such as surface reactivity (Fubini 1997) or release of cytotoxic ions (Cho, Duffin et al. 2012). This structure activity relationship, known as the "fibre pathogenicity paradigm" (FPP), identifies three critical features that are required for a fibrous particle to present a fibre-type health hazard: aspect ratio and length (dimension), persistence of a particle in the biological environment and its resistance to breakage and dissolution (durability) and, most crucially for consideration of risk, the exposure to the particle in question (dose) (Donaldson and Tran 2004). These components of dimension, durability and dose, or the 3 Ds, provide the cornerstone of the FPP and have recently been reviewed alongside other determinants of particle induced toxicity (Donaldson, Murphy et al. 2011; Donaldson and Poland 2013; Donaldson, Schinwald et al. 2013).

The role of length and aspect ratio in the FPP

Whilst durability and dose are key variables and determinants of fibre-induced pathogenicity, the focus of this study is the role of aspect ratio and length on the pathogenicity of titanium dioxide nanofibres. The role of length in fibre pathogenicity has long been established from the early work of Stanton, subsequently developed into the Stanton hypothesis (Stanton, Laynard et al. 1977; Stanton, Layard et al. 1981), to more recent evaluations of nanofibres (Schinwald, Chernova et al. 2012). Such a role is in part reflected in the definition of a respirable fibre by the World Health Organisation (1997), which defines a minimum length and aspect ratio (5 µm and 3:1, respectively). Over the years there have been numerous experimental studies looking at the contribution of length to fibre toxicity either by comparing samples containing different proportions of long mineral fibres (Davis, Addison et al. 1991) or modifying the length (e.g. via ball

milling) to assess the impact on toxicity (Davis and Jones 1988; Davis, Addison et al. 1991). Two such examples are those of Wright and Kuschner (Wright and Kuschner 1975) and Davis *et al.* (Davis, Addison et al. 1986). Kuschner and Wright used vitreous fibres that were ground to be much shorter than the parent long fibre material; the short fibres showed virtually no pathology in rats when instilled but there was severe fibrosis with the long fibre material. Davis *et al.* ground long amosite asbestos to shortness and again found virtually no pathology after years of inhalation exposure to the short ones, but lung cancer, fibrosis and a single mesothelioma were detected in animals inhaling the long parent material (Davis, Addison et al. 1986). Similar results have been found in numerous other studies looking at the respiratory effects as well as the pleural/peritoneal effects of nanofibres (relevant for the development of mesothelioma, a cancer almost exclusively associated with asbestos exposure) (Goodglick and Kane 1990). The relevance of such results, gained from the analysis of more conventional mineral fibres to the new generation of nanomaterials has been under increased scrutiny with the intense interest that surrounded the development of carbon nanotubes as an industrially and commercially relevant material. Numerous studies have now shown that carbon nanotubes can elicit a toxic effect in the lungs of laboratory rodents (Ma-Hock, Treumann et al. 2009; Mercer, Scabilloni et al. 2013), a pathological response in the pleura upon exposure (Ryman-Rasmussen, Cesta et al. 2009) as well as the development of mesothelioma (Rittinghausen, Hackbarth et al. 2014). In addition to carbon nanotubes, other fibrous nanomaterials have also been assessed (Poland, Byrne et al. 2012) and, from these studies, a strict relationship emerges between the biological reactivity of these fibre-like nanomaterials and their geometry, while chemical composition would have a greater impact on biopersistence rather than on toxicity per se. In particular, most studies indicate that length and aspect ratio of fibres significantly affect their toxic properties (Poland, Duffin et al. 2008; Rotoli, Bussolati et al. 2009; Ji, Wang et al. 2012), with long fibres exerting higher toxicity than shorter ones suggesting the relevance of the FPP to nanofibres. Recent research has shown that some additional determinants in bio-reactivity of ENM should be considered, such as possible contamination with endotoxins especially during manufacturing processes (Esch, Han et al. 2010; Smulders, Kaiser et al. 2012), although the properties of nanomaterials predictive for endotoxin adsorption have not been characterized yet. Whilst the relevance of the FPP to nanofibres is considered of great importance, particularly in relation to the assessment of potential risks arising from exposure, understanding the cellular interactions that underlie the observed respiratory toxicity is also of high interest. A challenge in undertaking such studies is to compare long and

short versions of the same material that differ only in terms of length as opposed to comparing two separate samples obtained from different sources (e.g. batches, process or manufacturer) or modified in other ways such as surface defects by milling (Muller, Huaux et al. 2008). Only few notable exceptions (Hamilton, Wu et al. 2009; Ramkumar, Manjula et al. 2012) have been able to investigate this issue *in vitro*. In this part of the thesis I evaluate the biological effects of two forms of TiO_2 nanofibres (NF), which differ only in terms of length and aspect ratio, investigating in different cell models their cytotoxic and pro-inflammatory effects as well as their capability to impair epithelial monolayers.

Synthesis, dispersion and physico-chemical characterization of NM

Preparation and dispersion of nanomaterials

Pristine nanofibres of titanium dioxide (P-TiO_2 NF), produced by an electro-spinning process, were obtained from Elmarco, Liberec, Czech Republic) and Aeroxide® P25 TiO_2 nanoparticles (TiO_2 NP, 80% anatase, 20 % rutile) from Evonik Degussa GmbH, Germany). UICC Asbestos crocidolite was a generous gift of Prof. Bice Fubini, University of Turin.

For fibre shortening, performed in the laboratory of Dr. Anna Costa (ISTEC CNR, Faenza, Ravenna, Italy), the pristine TiO_2 NF were suspended in distilled water and subjected to ball milling for 15h using ZrO_2 spheres. In order to control the homogenization of size and favor the milling process, grinding media with different diameter were used (50 wt% ZrO_2 spheres with 3 mm diameter or 50 wt% ZrO_2 spheres with 5 mm diameter). Ball-milled TiO_2 nanofibres (BM-TiO_2 NF) were obtained as a colloidal suspension (3 wt% in distilled water, pH = 3.8). Powders of pristine (P) or BM NF were suspended in a sterile-filtered solution of 0.05% Bovine Serum Albumin (BSA, Sigma Aldrich, Milan, Italy) in Phosphate Buffered Saline without calcium and magnesium (PBS) to obtain 10X stock suspensions of the highest concentration tested (1.3 mg/mL, corresponding to 80 µg/cm^2 for cells seeded in 96- and 24-well plates, or 1 mg/mL, corresponding to 80 µg/cm^2 for cells seeded into cell culture inserts with membrane filters for 24-well multitrays). After vortex mixing (30 sec) and water bath sonication (10 min), the stock suspensions were subsequently diluted in the same solvent to obtain 10X stocks of the other doses.

Endotoxin contamination analysis

Materials were suspended in endotoxin-free water at 1 mg/mL and sonicated for 10 min at room temperature (RT) in a bath sonicator (Ultrawave Sonicator QS25, 400W). After 24h incubation in endotoxin free water, samples were centrifuged at 15000g for 15 min. Supernatants were assessed for endotoxin contamination using the Pyrogen Assay according to the manufacturer's instructions (Lonza, Blackley, UK). Endotoxin levels were calculated according to the standard curve obtained, and results were expressed as endotoxin contamination (EU/mL). These analyses were performed by Dr. Craig Poland (Institute of Occupational Medicine, Edinburgh, UK).

Characterization of TiO_2 NF

The investigation of the fibre size distribution was performed by scanning electron microscopy using FE-SEM (Carl Zeiss Sigma NTS, Gmbh Öberkochen, Germany). Nanofibres were dispersed on

a standard aluminum support by simple drop casting of the suspensions. Samples were left to air dry in a dust free atmosphere then placed on a hotplate at 100° C for 5 min to ensure the complete evaporation of water before FE-SEM analysis. Average diameters and lengths of P-TiO_2 NF and BM-TiO_2 NF samples were calculated on more than 100 nanofibres, by analyzing different images (ImageJ, Wayne Rasband, 1997). The specific surface area (SSA) measurements were determined with the Brunauer-Emmett-Teller (BET) method, using N_2 as adsorptive gas Sorpty 1750 (Carlo Erba, Italy). The zeta potential values of P- and BM-TiO_2 NF were evaluated with a Zetasizer nano ZSP (model ZEN5600, Malvern Instruments, UK) in 0.9% NaCl. Zeta potential data were obtained by electrophoretic light scattering (ELS), and the Smoluchowski approximation was applied to convert the electrophoretic mobility to Zeta potential. Zeta potential measurements were performed on 700 µL of NF dispersion (1 g/L) at 25°C, and the measurement duration was set to automatic as well as the attenuator position and the applied voltage. The Zeta potential data were obtained by averaging three measurements. These analyses were performed in the laboratory of Dr. Anna Costa (ISTEC CNR, Faenza, Ravenna, Italy).

Decontamination of BM-TiO_2 NF

For LPS decontamination, an aliquot of the 3% suspension of BM-TiO_2 NF was dried at 45 °C for 3d. The resulting powder was heated at 230 °C for 4h and, once cooled at RT, re-suspended in sterile-filtered solution of 0.05% BSA in PBS. An aliquot of P-TiO_2 NF powder was heated in parallel. After decontamination, both samples were re-suspended in 0.05 % BSA in PBS at the concentration of 1.3 mg/mL.

Results

Characterization of TiO_2 NF

TiO_2 nanofibres (NF) were modified with a "size control" strategy through a ball milling (BM) treatment, which was chosen due to its industrial relevance as well as low cost and easily scalable characteristics. This strategy was applied in order to decrease length and aspect ratio (AR) of the fibres and as an easy remediation step in the manufacturing line. The starting pristine material was found to be very inhomogeneous (diameters ranging from about 200 to 1000 nm) but showed the desired nanostructured morphology, as demonstrated by high specific surface area (SSA= 91.2 m^2/g by BET measurements) and by FE-SEM imaging (Figure 4A). As expected, the milling treatment did not affect the fibre diameter yet produced a clear modification of the average fibre length with, consequently, a significant decrease of aspect ratio in BM TiO_2 NF (Table 2, Figure 4B) and an increase in SSA (118 m^2/g).

Analysis of the test materials for the presence of bacterial endotoxin (LPS) showed that no endotoxin could be detected in both P-TiO_2 NF and in TiO_2 NP (used as a non-fibrous benchmark material, data not shown), whereas crocidolite, used as a fibrous benchmark material, showed the presence of endotoxin contamination (>5 EU/ml). The action of ball milling resulted in a heavy endotoxin contamination of BM NF (>5 EU/ml).

Table 2: Properties of pristine long (P-TiO_2 NF), ball-milled short (BM-TiO_2 NF) TiO_2 nanofibres and benchmark materials (TiO_2 nanoparticles and UICC crocidolite)

Sample	BM Time (h)	Average Length (µm)	Average Diameter (µm)	Average AR	Zeta Potential (mV)[b]
P-TiO_2 NF	0	9.9 ± 5.8	0.3 ± 0.1	29:1	16.0 ± 0.6
BM-TiO_2 NF	15	2.1 ± 2.4	0.4 ± 0.2	5:1	9.2 ± 0.8
TiO_2 NP	-	-	-	-	13.3 ± 1.4
UICC Crocidolite[a]	-	2.5 ± 2.0	0.3 ± 2.1	7.5:1	ND[c]

[a] Data from (Kohyama, Shinohara et al. 1996)
[b] 1g/L in NaCl 0.9%
[c] ND, Not determined

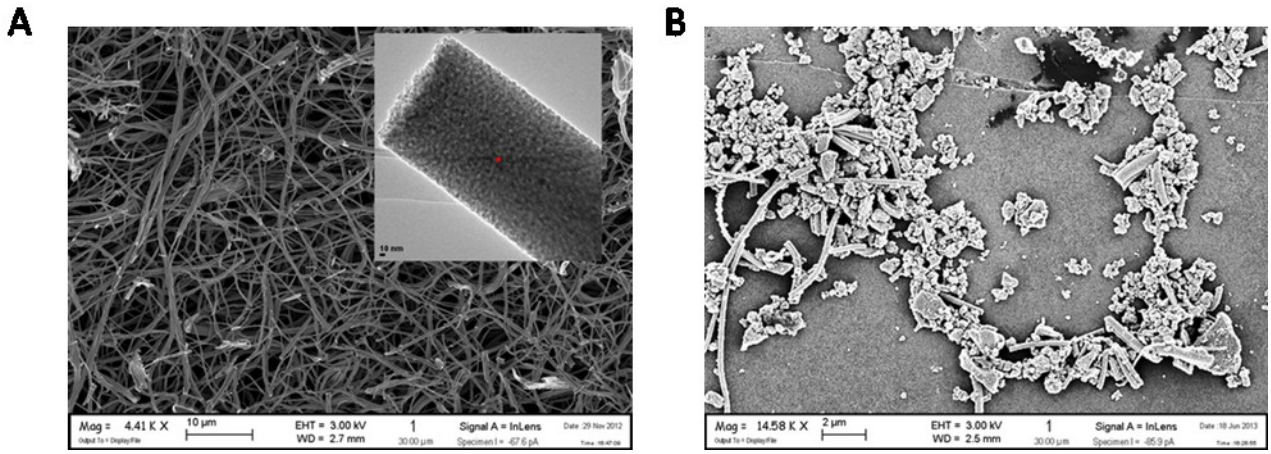

Figure 4. FE-SEM image of TiO_2 nanofibres. (A) P-TiO_2 NF. (B) BM-TiO_2 NF

Cell viability and cytotoxicity

The effects of P-TiO_2 NF (dose range 2.5-80 μg/cm^2) on the viability of Raw 264.7 and A549 cells were tested by resazurin assay after 24, 48 and 72h- exposure (Figure 5). In macrophages (Panel A), P-TiO_2 NF slightly lowered cell viability inducing a maximal decrease of 22% after 72h of incubation at the highest dose tested (80 μg/cm^2). The TiO_2 NP (80 μg/cm^2) sample, used as a low-toxicity benchmark material, did not affect cell viability, while, at the same dose, crocidolite had a modest effect comparable to that of P-TiO_2 NF. In A549 cells (Panel B), P-TiO_2 NF significantly lowered cell viability in a dose-dependent manner with a significant reduction already detectable at 24h. The maximal decrease was detected at 48h (50%, 80 μg/cm^2). TiO_2 NP did not significantly affect cell viability, while Crocidolite markedly lowered cell viability of A549 cells in a time-dependent manner. Cytotoxicity was also tested on each cell type using the LDH assay (not shown). In macrophages, TiO_2 NF did not induce significant cytotoxicity, similarly to TiO_2 NP. Crocidolite induced a dose-dependent increase in cytotoxicity with a maximal LDH release of 32% at the highest dose tested. In A549 cells (not shown), none of the compounds tested significantly induced cytotoxicity except TiO_2 NP at the highest dose.

To assess the lytic action of the materials on cell membranes, they were co-incubated with red blood cells and the level of haemolysis was measured (Figure 6). P-TiO_2 NF was significantly more haemolytic than either TiO_2 NP or crocidolite, with an effect larger than 40% at the maximal dose tested. The haemolytic activity of all the materials was dose dependent.

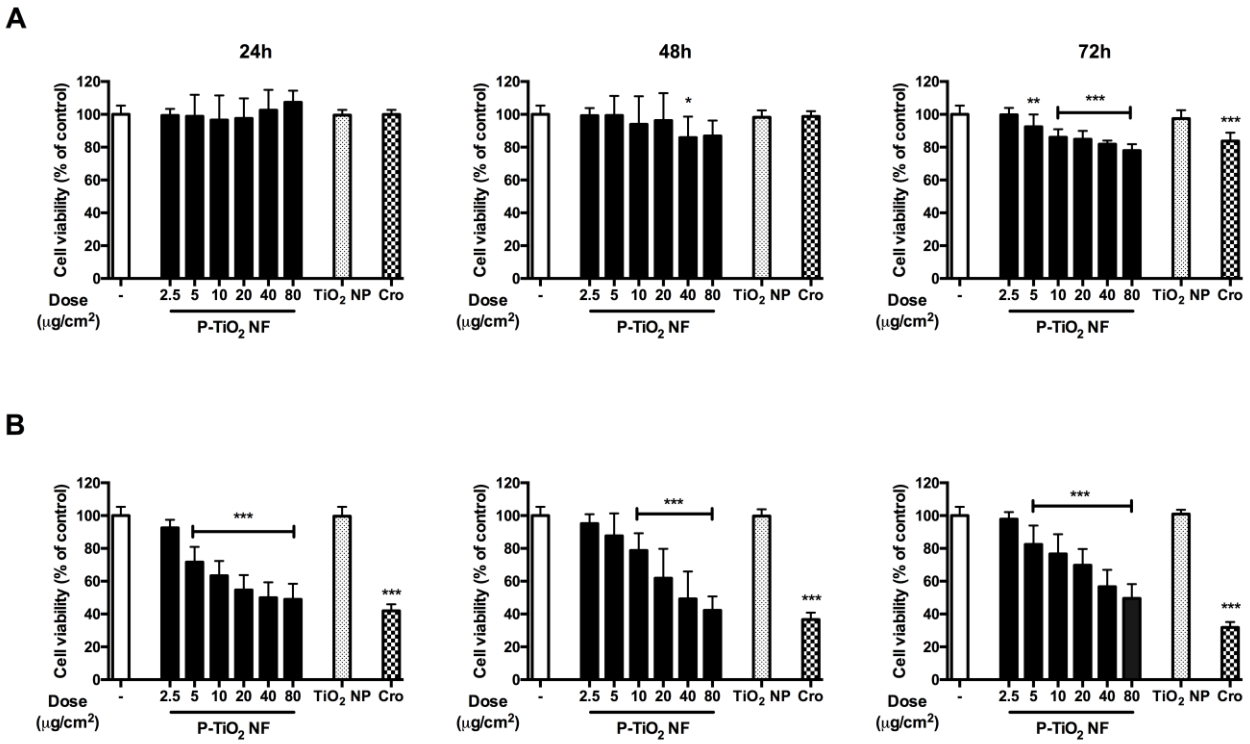

Figure 5. Effect of tested materials on cell viability. Raw 264.7 (A) and A549 (B) cells were treated for up to 72h with or without pristine TiO_2 NF (range dose 2.5-80 μg/cm^2), crocidolite (Cro; 80 μg/cm^2) or TiO_2 NP, and cell viability was assessed with the resazurin assay. Data are means ± SD of twelve independent determinations obtained in three experiments. * $p < 0.05$, ** $p < 0.01$, *** $p < 0.001$ *vs.* control, untreated cultures, as evaluated by One-way ANOVA for multiple comparisons with Tukey correction.

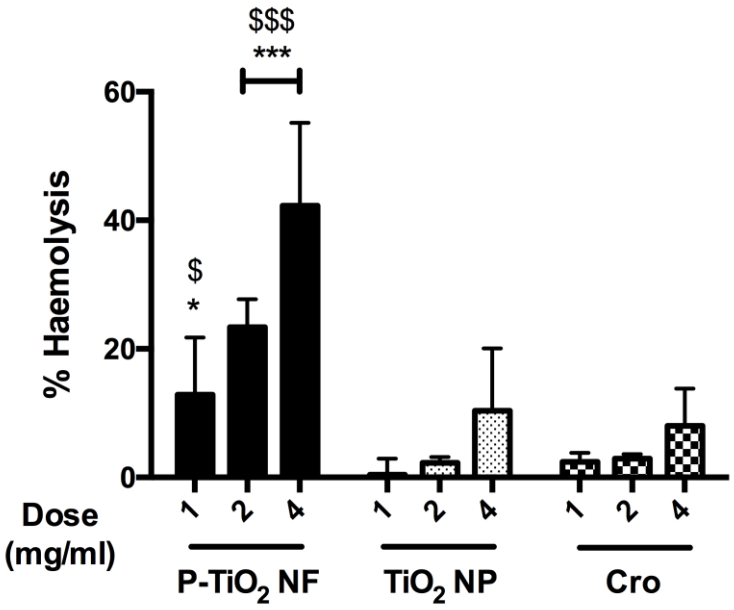

Figure 6. Haemolytic activity of the tested materials. The mean percentage of haemolysis induced by materials (dose range 1 – 4 mg/ml) was determined. Results are expressed as means ± SD with vehicle (negative control) being set at 0% and Triton X-100 (positive control) at 100%. * $p < 0.05$, *** $p < 0.001$ *vs.* the same dose of TiO_2 NP; \$ $p < 0.05$, \$\$\$ $p < 0.001$ *vs.* the same dose of Cro, as evaluated by one-way ANOVA for multiple comparisons with Tukey correction.

ROS production in acellular systems and oxidative stress

The intrinsic activity in terms of ROS production exhibited by the various materials was assessed by co-incubation with a spin trap (Tempone-H) to detect the release of oxygen free radicals (not shown). The results showed that P-TiO_2 NF did induce a small but significant ROS production above vehicle control; however, the effect was comparable with that caused by the same dose of TiO_2 NP. Crocidolite caused very high levels of ROS production (in excess of the positive control, consisting of 100 µM pyrogallol). None of the compounds tested induced a significant oxidative stress in either macrophages or alveolar epithelial cells, as assessed with the DCFH-DA assay (not shown). However, a significant decrease in reduced glutathione (GSH) could be detected when macrophages were treated with P-TiO_2 NF (Figure 7A). In the same cell model, crocidolite significantly decreased cell GSH down to 40%. Conversely, no significant effect on cell GSH could be seen with any of the materials tested in alveolar epithelial cells (Figure 7B).

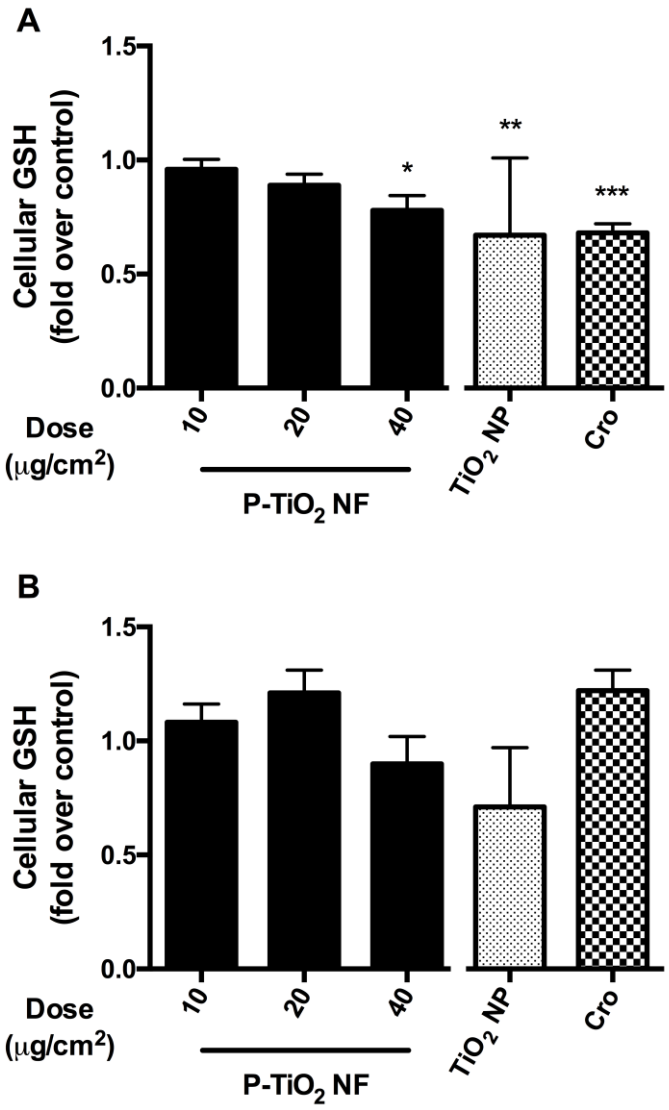

Figure 7. Glutathione levels in macrophages and airway epithelial cells. The cell content of glutathione (GSH) was measured in Raw 264.7 macrophages (Panel A) and A549 (Panel B) cells after 24h of treatment with increasing doses of pristine TiO_2 NF (range dose 2.5 – 40 μg/cm^2), Crocidolite (Cro) (40 μg/cm^2) and TiO_2 NP (40 μg/cm^2). Results are expressed as fold change ± SEM of 9 independent determinations *vs.* control. * $p < 0.05$, *** $p < 0.001$ *vs.* untreated cultures, as evaluated by One-way ANOVA for multiple comparisons with Tukey correction.

Barrier competence of CaLu-3 monolayers

Figure 8 (Panel A) reports the time course of changes in the Trans-Epithelial Electrical Resistance (TEER) of CaLu-3 cells monolayers exposed to increasing doses of P- TiO_2 NF (40-80 μg/cm^2) up to 12d. TEER is a parameter associated with the integrity and the barrier competence of epithelial monolayers (Rotoli, Bussolati et al. 2008). P-TiO_2 NF significantly lowered TEER by 24% after 3d of exposure to the highest dose tested (80 μg/cm^2), with a maximal decrease of 54% at 12d, indicating a clear dose- and time-dependent effect on barrier competence. Crocidolite (80 μg/cm^2) produced a decrease of TEER comparable to that caused by pristine TiO_2 NF. On the contrary, TiO_2 NP did not alter TEER. Figure 8 (Panel B) shows TEER changes after 12d of treatment. Cell viability, monitored at the end of the experiment in the same wells where TEER evaluation was performed, exhibited no significant changes under any experimental condition (Figure 8, Panel C).

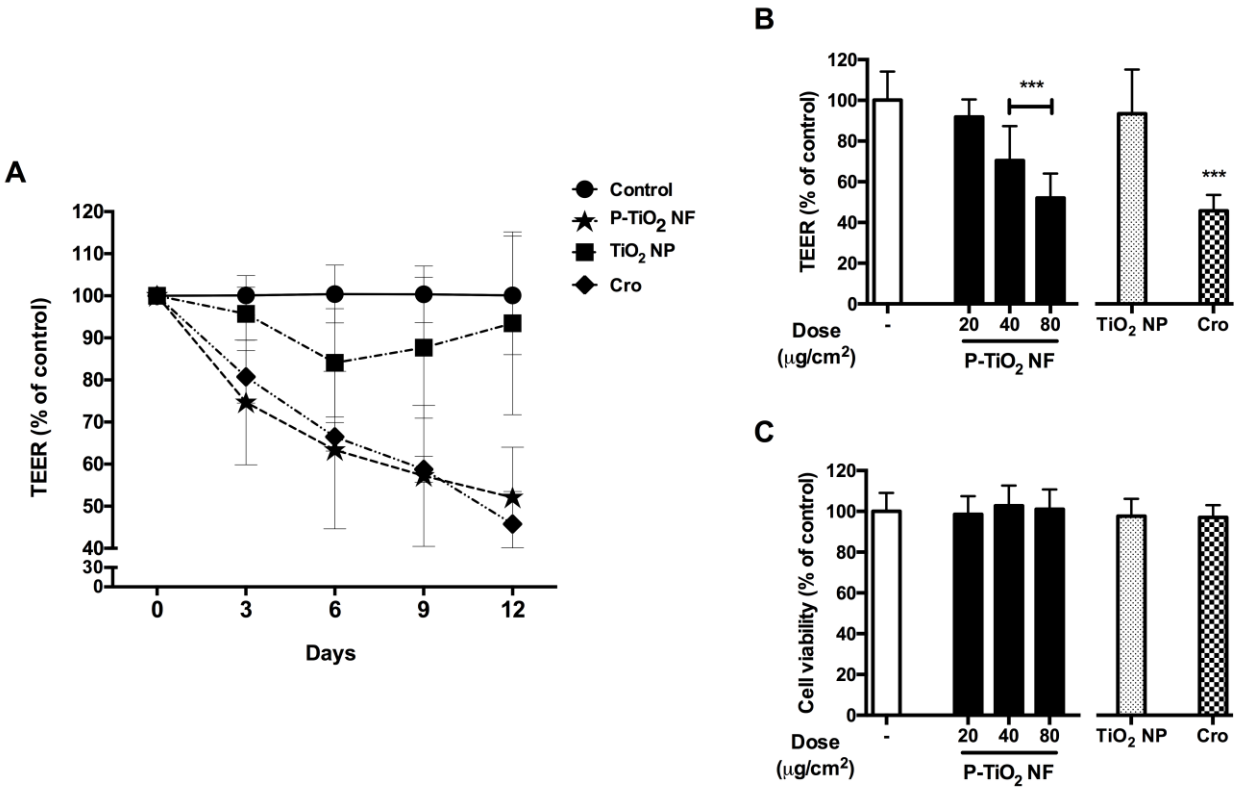

Figure 8. Effect of tested materials on barrier integrity and cell viability of CaLu-3 cell monolayers. The Trans-Epithelial Electrical Resistance (TEER), as a proxy of barrier integrity, and cell viability was assessed in confluent monolayers of CaLu-3 cells after incubation with the indicated materials. (A) TEER (%of control) recorded every 3 d up to 12 d. (B) TEER (% of control) at 12 d. (C) Effect of the materials on cell viability, assessed by resazurin assay at the end of TEER experiments. Data are means ± SD of 8 independent determinations. ***p < 0.001 *vs.* control, untreated cultures, as evaluated by One-way ANOVA for multiple comparisons with Tukey correction.

Expression of pro-inflammatory markers

Figure 9 reports nitric oxide (NO) production, as assessed from nitrite concentration in the culture medium after 48h (Panel A) or 72h (Panel B) of treatment of Raw 264.7 cells with increasing doses of TiO_2 NF (range 10-80 μg/cm^2). In cells treated with P-TiO_2 NF, NO production was increased already at 48h compared with control (2-fold at 80 μg/cm^2), reaching a maximal stimulation after 72h (5-fold at 80 μg/cm^2). TiO_2 NP and crocidolite, both used at 80 μg/cm^2, significantly stimulated NO production after a 72h-treatment. NO production was consistently associated with the induction of Nos2 (Figure 9C). The pro-inflammatory effect of TiO_2 NF was not limited to *Nos2* induction and NO production, but involved also other pro-inflammatory markers such as the expression of *Ptgs2*, which encodes for the inducible form of cyclooxygenase, Cox2, which was also significantly increased by P-TiO_2 NF (5-fold at 80 μg/cm^2, Figure 9D).

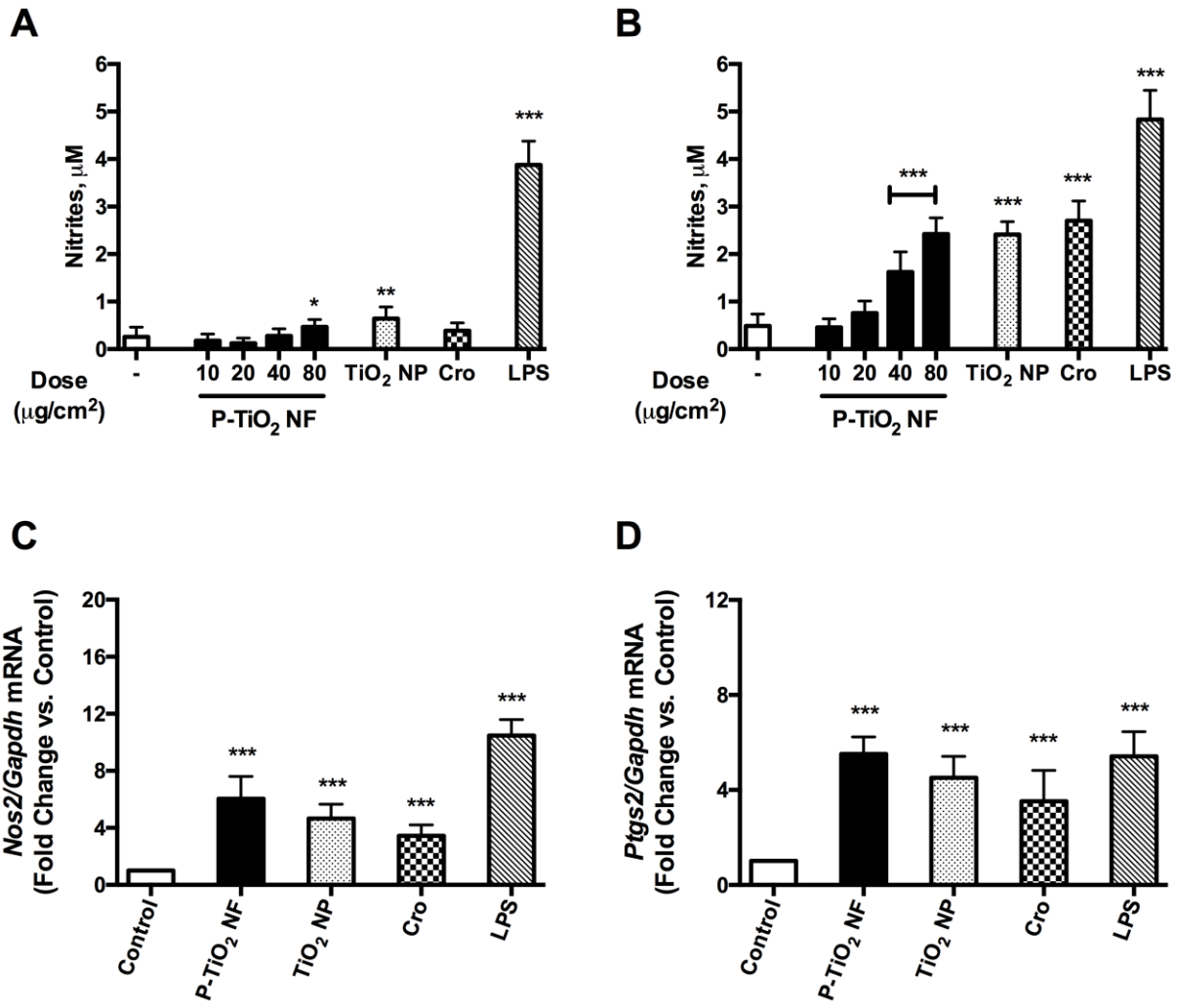

Figure 9. Expression of pro-inflammatory markers in macrophages. Macrophages were treated with the indicated materials up to 72h. (A, B) Effects of TiO_2 NF on NO production after 48h (A) and 72h (B). (C, D) Effects of the indicated materials on *Nos2* (C) or *Ptgs2* (D) gene expression, assessed with RT-PCR after 24h-exposure. Data are means ± SD of a minimum of 3 independent determinations.*$p < 0.05$, ** $p< 0.01$, ***$p < 0.001$ *vs.* control, untreated cultures, as evaluated by two-tailed *t* test for unpaired data.

Comparative biological effects of pristine and ball-milled TiO_2 NF

In Table 3, a summary of the main biological effects of BM-TiO_2 NF, in comparison with the pristine form are summarized. Compared with pristine TiO_2 NF, BM-TiO_2 NF caused a significantly smaller cytotoxic effect in both A549 and Raw 264.7 cells, with IC_{20} values markedly higher than those obtained with P-TiO_2 NF at all the experimental time points (24, 48, 72h). LDH assay did not reveal significant cytotoxicity for both P- and BM-NF. The hemolytic potential, the TEER changes detected in CaLu-3 cell monolayers and the depletion of the cellular anti-oxidant GSH in Raw 264.7 macrophages were all mitigated by aspect ratio reduction. Conversely, BM-TiO_2 NF were much more active than P-TiO_2 NF in promoting the expression of inflammatory markers (NO production, *Nos2* and *Ptgs2* expression, secretion of TNF-α and IL-6).

Table 3. Summary of cellular responses to P-TiO_2 NF and BM-TiO_2 NF

Endpoint	Parameter	Cells	P-TiO_2 NF	BM-TiO_2 NF	BM vs. P	Biological effects (BM vs. P)
Cell viability (resazurin)	IC_{20} (80 µg/cm^2, 24h)	Raw 264.7	5.1	> 80	***	⇓⇓
		A549	6.1	> 80	***	⇓⇓
Haemolytic activity	% (4 mg/ml, 24h)		40	20	*	⇓⇓
Decrease in GSH content	% of control (80 µg/cm^2, 24h)	Raw 264.7	80	NS	*	⇓
		A549	NS	NS		
Barrier competence	TEER, % of control (80 µg/cm^2, 12d)	CaLu-3	50	75	***	⇓⇓
NO production	Medium nitrites, fold change vs. control (80 µg/cm^2, 24h)	Raw 264.7	5	36	***	⇑⇑
Nos2 induction	Fold change vs. control (80 µg/cm^2, 24h)	Raw 264.7	6	34	***	⇑⇑
Ptgs2 induction	“”	Raw 264.7	5	11	***	⇑⇑
TNF-α	Fold change vs. control (80 µg/cm^2, 48h)	Raw 264.7	NS	60	***	⇑⇑⇑
IL-6	“”	Raw 264.7	NS	43	***	⇑⇑⇑

Role of LPS contamination and phagocytosis in the pro-inflammatory activity of BM-TiO_2 NF

Determination of LPS in BM-TiO_2 NF had yielded very high values (>5EU/ml). To ascertain if the high pro-inflammatory activity of BM-TiO_2 NF was due to LPS contamination, P- and BM-TiO_2 NF were decontaminated by thermal treatment (see Methods), and their effects on inflammatory markers were compared (Figure 10). After heating, P-TiO_2 NF stimulated NO production (Figure 10A) in a dose dependent manner with a maximal 7-fold stimulation vs. control at 80 μg/cm^2 (72h) and consistently, *Nos2* gene expression (Figure 10B) was significantly induced. Heat decontaminated BM-TiO_2 NF stimulated both NO production and *Nos2* gene induction at much higher levels and were also much more active than pristine counterparts in promoting the secretion of IL-6 and TNF-*α*, or *Il1b* and *Ptgs2* expression (Figure 10 C-F).

To study further the mechanism underlying the pro-inflammatory role of BM-TiO_2 NF, Raw 264.7 cells were exposed for 48h to the materials (40 μg/cm^2) in the presence or in the absence of the cytoskeletal drug cytochalasin B (5 μg/ml), which prevents actin polymerization and, hence, phagocytosis (Figure 11). Under these conditions, nitrite production was almost completely suppressed. On the contrary, cytochalasin B did not reduce nitrite production in cells exposed either to P-TiO_2 NF or LPS alone (10 ng/ml).

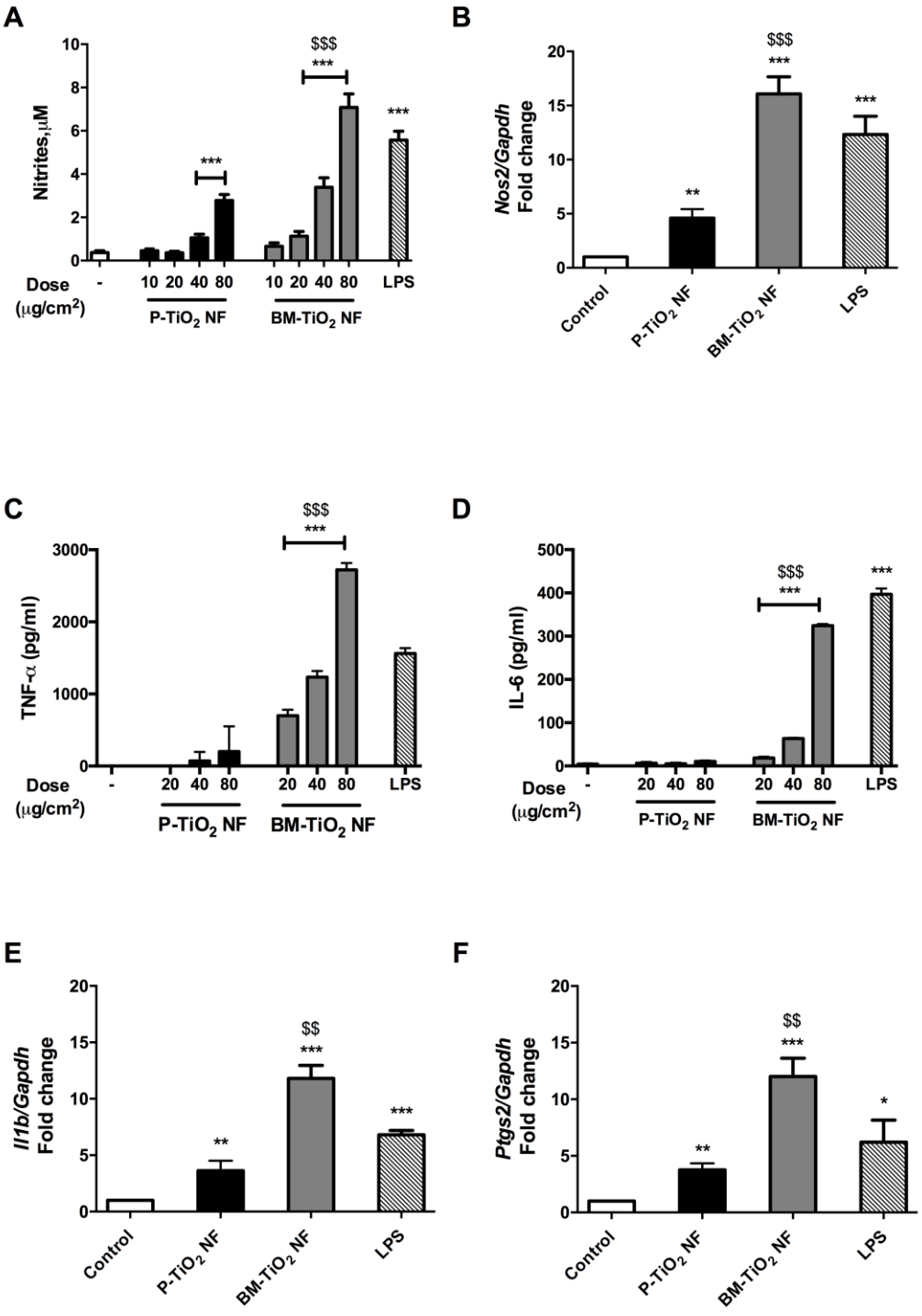

Figure 10. Comparative effects of pre-heated Pristine and Ball-milled TiO_2 NF on the expression of pro-inflammatory markers in Raw 264.7 cells. Macrophages were treated with P-TiO_2 NF or BM-TiO_2 NF (both pre-heated at 230°C for 4h to remove endotoxin) at the indicated doses or with LPS (10 ng/ml). (A) Effects of TiO_2 NF on NO production determined at 72h; (B) Effects of TiO_2 NF on *Nos2* induction assessed at 24h; (C, D) Effects of TiO_2 NF on TNF- α (C) and IL-6 (D) production determined at 48h; the expression of *Il1b* (E) and *Ptgs2* (F) was assessed wit RT-PCR after 24h of treatment with the materials. Data are means ± SD of a minimum of 3 independent determinations.*p < 0.05, ** p< 0.01, ***p < 0.001 *vs.* control, untreated cultures; $$ p < 0.01; $$$ p < 0.001 *vs.* P-TiO_2 NF, as evaluated by Two way ANOVA for multiple comparisons with Tukey correction.

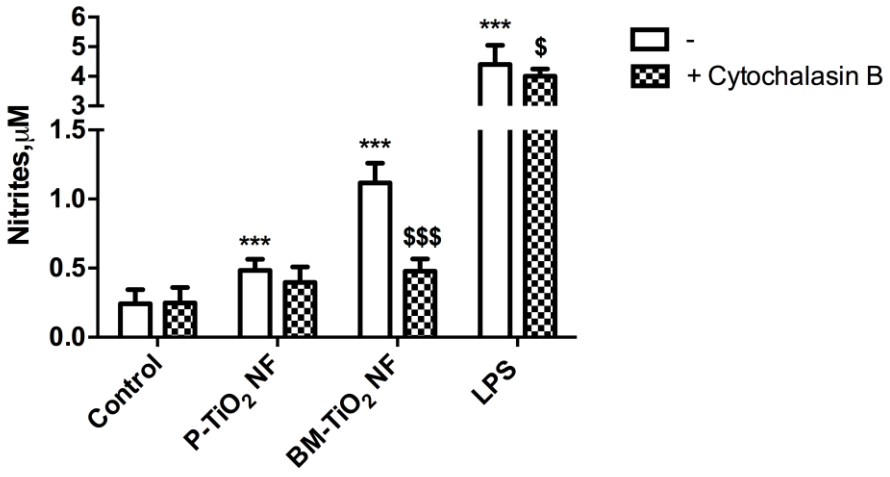

Figure 11. Role of material internalization on NO production in Raw 264.7 cells exposed to pristine and ball-milled TiO_2 NF. NO production by Raw 264.7 cells was measured after 48h after exposure to TiO_2 NF (40 μg/cm^2) or to LPS (10 ng/ml) with or without cytochalasin B (5 μg/ml), used to prevent active particle uptake by the cells. Data are means ± SD of 8 independent determinations in two experiments. *** $p < 0.001$ *vs.* control, untreated cultures; \$ $p < 0.05$; \$\$\$ $p < 0.001$ *vs.* the same condition without cytochalasin, as evaluated by two-tailed *t* test for unpaired data.

Interaction of materials with macrophages

In order to study how cells interact with the various materials tested, macrophages were treated with the materials (all at the dose of 10 μg/cm^2) and observed with confocal microscopy and scanning electron microscopy. Confocal microscopy (Figure 12A and B, Figure 13) was used to study changes in cell morphology/behavior upon the internalization of TiO_2 NF. In cultures exposed to pristine NF, bundles of nanofibres were readily detected (Figure 12A). Cells tended to adhere to the bundles, spreading along the long axis of the bundles, which in some cases appeared partially internalized, while they are able to completely internalize few shorter fibres. On the contrary, most cells incubated with BM-TiO_2 NF (Figure 12B) had internalized the material, some exhibiting a rounded morphology, others a symmetrically elongated morphology, indicating activation. In some cases, large amounts of NF were detected inside the cells yet, even in these cases, no co-localization of the NF with the cytoplasmic marker was observed, suggesting the compartmentalization of the material (Figure 12B). When viewing the cells with a scanning electron microscope, macrophages treated with P-TiO_2 NF spread along the fibres in attempted phagocytosis (Figure 12C) but the fibres were too long to be fully internalized and protruded from the cells (a situation called frustrated phagocytosis (Murphy, Schinwald et al. 2012)). In other cases (Figure 13), fibres were shared by two or more cells, indicating that macrophages were engaging with the material but were unable to engulf it completely. Similar images were detected in cells exposed to crocidolite (Figure 12E). Conversely, when incubated with BM-TiO_2 NF the macrophages presented a more rounded morphology (Figure 12D) with no signs of frustrated phagocytosis. Rounded morphology also characterized most macrophages treated with TiO_2 NP (Figure 12F), although few elongated cells, likely corresponding to cell activation, were also detected (Figure 13).

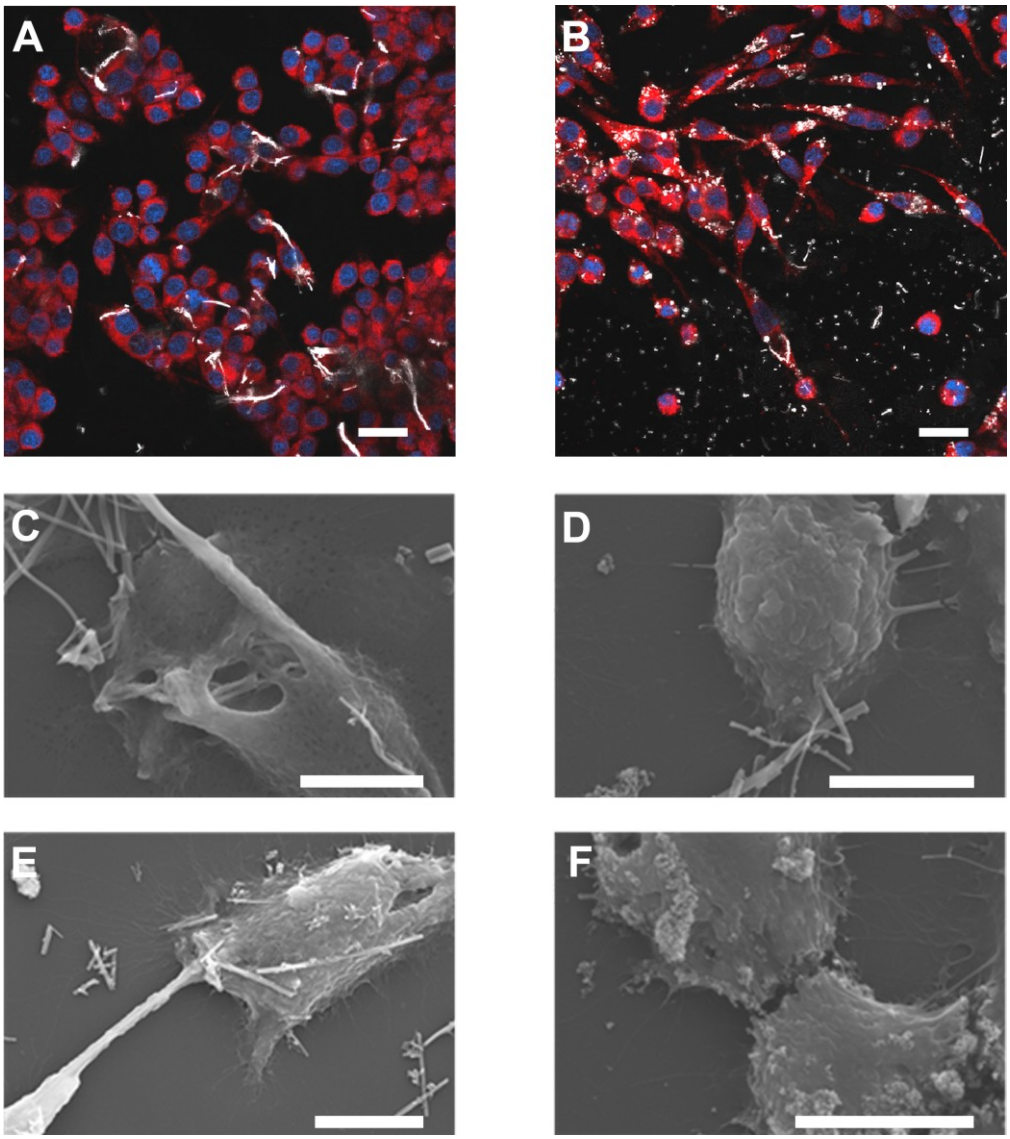

Figure 12. Characterization of particle internalization by macrophages. Raw 264.7 cells were seeded on coverslips and treated for 24h with pristine TiO_2 NF (A, C), ball-milled TiO_2 NF (B, D), crocidolite (E) or TiO_2 NP (F) at a dose of 10 µg/cm^2. Cells were then labeled (see Methods), fixed, mounted and observed in confocal microscopy (A, B) or fixed and dehydrated before being mounted for SEM analysis (C-F). In confocal microscopy (A, B), TiO_2 NF are shown in white, the cytoplasm in red and nuclei in blue. Bars, 20 µm (A, B), 10 µm (C-F).

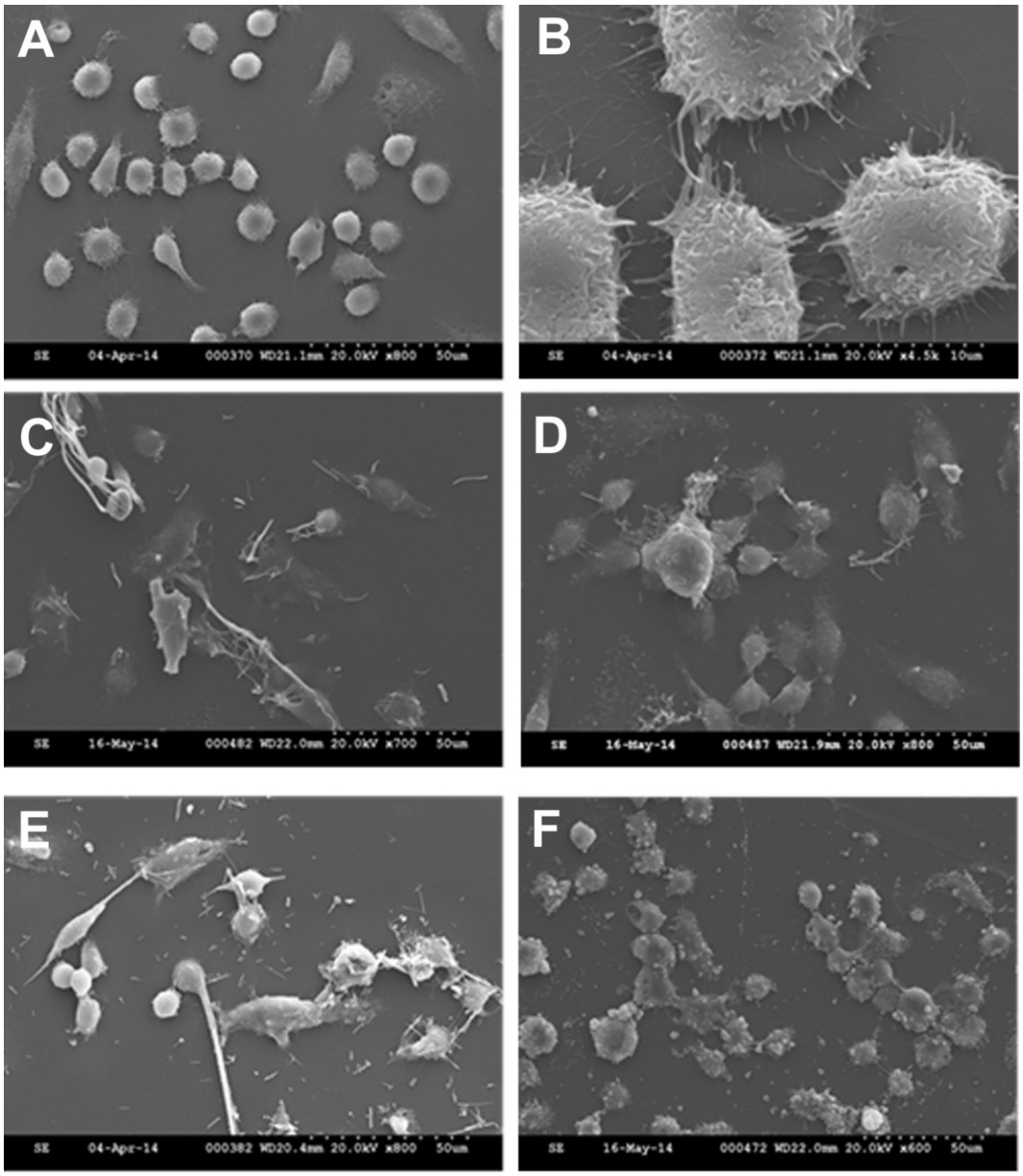

Figure 13. Characterization of macrophage/materials interactions by SEM. Raw 264.7 cells were seeded on coverslips and incubated for 24 in the absence (A, B, untreated control) or in the presence of the following materials at 10 μg/cm^2: P-TiO_2 NF (C), BM-TiO_2 NF (D), crocidolite (E), TiO_2 NP (F). The preparations were fixed and dehydrated before being mounted for SEM analysis (see Methods). Images shown in Panels C, D, E and F are the same fields shown in Figure 12 C, D, E and F, taken at lower magnification.

Discussion

The aim of this part of the thesis was to assess the effects of length/aspect ratio modification of TiO_2 nanofibres on different toxicity endpoints. A key aspect of this approach is the change from a respirable fibre into an elongated particle. Whilst this distinction may seem arbitrary, the definition of a respirable fibre has within it specific dimensional criteria of having a length greater than 5 µm, a diameter less than 3 µm and a length-to-width ratio (its aspect ratio) greater than 3:1 (W.H.O. 1997). Outside this definition, the particle cannot be considered a respirable fibre since it should meet all of these minimum requirements rather than just one (e.g. having a high aspect ratio). Where a particle does not adhere to all of to these criteria, an elongated particle could be seen as a more suitable description of its shape. These dimensional criteria dictate if the fibre is respirable based on its diameter, because the fibre aerodynamic diameter is proportional to the fibre diameter rather than to length and only very slightly to increased aspect ratio (Jones 1993). Therefore, fibres in excess of 3 µm will see a marked decrease in respirability and, conversely, will deposit to a greater extent in the head and upper airways. The minimum length requirement of 5 µm reflects the role that length has in determining fibre-type pathogenicity. This aligns with early observations by Stanton and colleagues who evaluated the outcome of 72 experiments, across a wide variety of respirable minerals ranging in size, chemical and structural attributes, in terms of their ability to cause mesothelioma after being introduced surgically onto the pleural surface of female rats (Stanton, Layard et al. 1981). This analysis showed that thin fibres shorter than 4 µm were low in mesothelioma potential whilst those longer than 4 µm increased in carcinogenic activity. As this definition of a fibre is so closely aligned to the presentation of dose (respirability) and ability to elicit a fibre-type toxicological response, the same criteria should be applied to nanofibres. Here the name “nano” would naturally imply that the diameter criterion is met although the length criterion should also be met to define it as a true fibre rather than a high aspect ratio elongated nanoparticle.

Within this study, before undergoing size modification, the pristine nanofibres met the requirements (low diameter, high surface area, high aspect ratio (29:1) and, crucially, a length in excess of 5 µm). The action of ball milling was successful in mitigating the presence of true fibres by reducing their length. When considering the toxicological results of these materials, it is useful to note at this point that both samples meet the diameter and the aspect ratio criteria of a respirable fibre while only the pristine sample meets the length criterion.

These particles were assessed *in vitro* for their toxicity towards *in vitro* models of macrophages and alveolar epithelial cells, which represent key target cells within the lung, the organ of primary concern for exposure to fibrous materials. The doses selected encompassed a large range (2.5-80 µg/cm2) with the primary aim of covering either the low dose range, which is of the greatest relevance to occupational exposure, or the higher dose range, where subtler differences in toxicity may become more apparent (although the practical relevance of such effects at high doses must always be considered). To place this dose range into context, a partner of our lab, Dr. Craig Poland (Institute of occupational Health, UK) calculated an estimated human equivalent dose (HED) by scaling the *in vitro* dose per cm^2 to the retained dose taking into account clearance halftime (representing the steady state equilibrium obtained during chronic exposure) based on human alveolar surface area. This was then used to calculate a deposited dose rate followed by the inhaled dose rate and finally an estimation of the human exposure (mg/m^3), which would give rise to this equivalent retained dose. The deposited dose rate was based on a deposition efficiency of 9% in the alveolar region in humans, calculated using MPPD (V2.11) software and based on published particle aerodynamic parameters. Specifically, these parameters were a mass median aerodynamic diameter (MMAD) of 800 µm, a geometric standard deviation (GSD) of 1.4 µm at an aerosol concentration of 33 mg/m^3 (Baisch, Corson et al. 2014) and a true density by helium pycnometry of 4.2213 g/cm^3 (Anjilvel and Asgharian 1995). Using this approach it has been estimated that the human equivalent (chronic) exposure at the low *in vitro* doses are high, but plausible levels of 7.3, 14.7 and 29.3 mg/m^3 for *in vitro* doses of 2.5, 5 and 10 $\mu g/cm^2$, respectively.

As summarized in Table 3, the evaluation of cytotoxicity indicated a dual differential of long vs. short TiO_2 nanofibres but also of macrophage vs. epithelial cell sensitivity. The IC_{20}, which indicates the toxic threshold effect concentration, was significantly higher for the BM-TiO_2 NF sample (>80 $\mu g/cm^2$) than for the long fibre P-TiO_2 NF sample (5.1-6.1 $\mu g/cm^2$) in either Raw 264.7 macrophages or A549 alveolar epithelial cells, indicating a length effect. This effect was also noted when looking at the barrier competence of a different epithelial cell line, CaLu-3, which similarly showed a smaller reduction after treatment with short compared to both P-TiO_2 and crocidolite fibres. The difference in sensitivity to the materials between macrophages and epithelial cells may reflect the different specialized function typical of these cell types: a relatively passive epithelial cell, in terms of particle interaction, as opposed to macrophages which seek out and engulf particles thereby accumulating dose.

The haemolytic potential of the particles shows a difference among the long P-TiO_2 NF, the short BM-TiO_2 NF and the TiO_2 NP used as a benchmark. However, whilst the ball milled fibres show significantly lower activity as compared to the long fibre sample (20.2% vs. 42.3% at 4 mg/ml, respectively, $P<0.05$), they were slightly more active than the TiO_2 nanoparticle control, although the difference was not statistically significant. Surface charge is known to be a prominent driver of haemolytic activity with strongly positive particles causing perturbation and rupture of the negatively charged RBC lipid membrane (Cho, Duffin et al. 2012). However, P-TiO_2, BM-TiO_2 NF as well TiO_2 NP, despite all possessed a positive charge, they are endowed with completely different behavior indicating that surface charge was not the primary driver of membrane rupture in this instance and, from this, it can be concluded that the difference in activity was due to aspect ratio, with the long fibres causing more damage than the short ones. This is supported by the fact that, whilst the UICC crocidolite sample, which contained long fibres as well as elongated particles, had an average length of 2.5±2.0 μm and, hence, was somewhat shorter than the P-TiO_2 NF (9.9±5.8 μm), it was more in line with the BM-TiO_2 (2.1±2.4 μm), which showed a similar level of haemolytic activity.

In relation to the LDH assay results, the positive fibre benchmark, UICC crocidolite, induced a dose-dependent increase in cytotoxicity up to 32% at 40 μg/cm^2, and these results are in agreement with the literature showing that crocidolite could increase cell damage at doses ≥ 10 μg/cm^2 (Hahon, Vallyathan et al. 1986; Castranova, Pailes et al. 1994). In contrast with the crocidolite sample and the resazurin assay results, the long P-TiO_2 NF did not induce significant cytotoxicity in macrophages, even at 40 μg/cm^2. This discrepancy between the LDH and the resazurin assay may reflect their different biological targets, specifically, metabolic capacity of cells as an indicator of cell viability in the case of the resazurin assay, versus membrane destabilization/rupture, leading to release of the cytosolic enzymes, for LDH. This also reflects a challenge when interpreting results based on outputs from multiple assays using separate principles for a given endpoint as recommended by ISO/TR 16197:2014 (ISO/TR16197:2014 2014). The observation of the differential cytotoxicity reflects the results of the 2009 study by Hamilton *et al*., (Hamilton, Wu et al. 2009), who exposed primary alveolar macrophages from C57BL/6 mice to short and long TiO_2 nanobelts and similarly found that only the long nanobelts were significantly cytotoxic at higher (100-200 μg/ml) concentrations. They proposed that the mechanism of long-fibre toxicity was attributable to lysosomal destabilization resulting in the release of destructive enzymes, such as cathepsin B, into the cytoplasm (Hamilton, Wu et al. 2009).

When investigating the oxidative stress potential of the short and long nanofibres, both materials displayed similar significant increase in ROS production as assessed by EPR, which was similar to the level produced by the TiO_2 nanoparticle control. As the intrinsic production of ROS is a factor of particle composition/surface properties, modification of shape would not be expected to alter such reactivity as confirmed by these results. The intrinsic reactivity measured by EPR did not transpire to cellular oxidative stress, as assessed using the DCFH-DA assay, yet incubation with the long but not short fibres did lead to a significant reduction in the cellular anti-oxidant GSH in macrophages. A GSH decrease was also noted after treatment with TiO_2 nanoparticles, which is commensurate with the observations of others (Jugan, Barillet et al. 2011). The fact that TiO_2 nanoparticles caused a larger depletion than the BM-TiO_2 NF at the same mass dose is not clearly explainable. If GSH depletion were driven purely by the intrinsic production of ROS, the key dose modifier would be particle surface area, yet the surface area of the BM TiO_2 NF measured here (118 m^2/g) is higher than that of TiO_2 nanoparticles (57 m^2/g (Rushton, Jiang et al. 2010)). The enhanced reduction of GSH by the long fibres may suggest a role for shape rather than just composition in oxidative stress. The reason behind this, and also why a greater reduction of cellular GSH was noted for macrophages rather than for A549 cells, could reflect the presence of oxidative burst, a component of frustrated phagocytosis (see below), which is characterized by the generation of superoxide free radicals, which can also form H_2O_2 through the action of superoxide dismutase (SOD). These observations on GSH depletion resulting from exposure to long TiO_2 NF agree with the study of Ramkumar et al. (Ramkumar, Manjula et al. 2012), who used TiO_2 nanofibres of similar diameter and length as those used within this study. However, whilst Ramkumar and colleagues did note significant, dose dependent increases in oxidative stress and lipid peroxidation, this study did not, despite the higher dose range used.

Loss of epithelial barrier competence and monolayer integrity are important parameters correlated to penetration of the nanomaterials in the bronchial wall, alterations of epithelial functions and nanomaterial bio-persistence (Banga, Witzmann et al. 2012). P-TiO_2 NF, but not to BM-TiO_2 NF, cause a clear cut epithelial barrier impairment, indicated by the decrease in TEER. Similar effect were observed in the same cell model upon exposure to long, needle-like, but not tangled, Multi-walled Carbon NanoTubes (MWCNT) (Rotoli, Gatti et al. 2015). In the case of MWCNT, loss of barrier integrity is due to focal damage to the epithelial cell monolayer, attributable to the interaction with nanomaterial agglomerates. Although this issue has not been specifically addressed here, absence of loss in cell viability at the whole population level suggests

that a similar mechanism may underlie P-TiO_2 NF effect. Interestingly, similar to what observed here for TiO_2 NF, also for MWCNT length appears an important structural determinant for epithelial barrier damage (Rotoli, Bussolati et al. 2009).

In contrast with parameters associated with cytotoxicity, oxidative stress or barrier competence, all the inflammatory endpoints (NO production, *Nos2* and cytokine gene induction) are higher in cells treated with short BM-TiO_2 NF compared with macrophages incubated with long P-TiO2 NF (Table 3). In their assessment of short and long TiO_2 nanobelts (Hamilton, Wu et al. 2009), Hamilton *et al.* noted that only the long TiO_2 nanobelts (after LPS priming) led to a significant increase in IL-1β release, whilst treatment with the short and particulate TiO_2 did not. The apparent difference between Hamilton's results and those obtained in this thesis may derive from the different mechanisms of stimulation of the pro-inflammatory responses, as highlighted by an important experimental observation made by those authors. They reported, indeed, that differential effects in the release of IL-1β (a proxy measure for the NALP3 inflammasome formation) between long and short fibres was noted in alveolar macrophages but not in Raw 264.7 murine macrophages (used also in this study), which are known to have a scarce ability to form the NALP3 inflammasome (Pelegrin, Barroso-Gutierrez et al. 2008; Hamilton, Wu et al. 2009). However, it should be stressed that the inflammatory parameters studied here do not require inflammasome but depend on NF-κB activation. Therefore, the peculiarities of the selected cell type and the different transduction mechanims involved in the effects lead to the conclusion that the results reported here are not in contrast with the responses noted by Hamilton *et al*.

The analysis of LPS contamination indicated that BM-, but not P-TiO_2 NF, had been contaminated by endotoxin, likely during the milling treatment. LPS contamination is a frequently encountered, and often overlooked, problem in nanotoxicology (Esch, Han et al. 2010; Smulders, Kaiser et al. 2012). Moreover, in another part of this thesis I will show that TiO_2 NP synergize the pro-inflammatory effects of LPS, thus suggesting that the effects on inflammatory parameters of BM-NF observed in macrophages could derive from the LPS adsorbed to the material. However, the results obtained after heat treatment of both P- and BM-NF (Figure 10) indicate that the pro-inflammatory effects of BM-NF persisted even after fibre decontamination from LPS, pointing to a greater ability of shorter nanofibres to activate macrophages. The higher activating capability of BM- compared with P-NF is at least in part attributable to a more efficient phagocytosis. Indeed, the inhibition of this active mechanism of uptake by the cytoskeletal drug cytochalasin B severely

hampers the pro-inflammatory effects of BM-TiO_2 NF, thus supporting the hypothesis that an intracellular site is involved in this pathway and highlighting the relevance of length in determining the outcome of the interaction between nanofibres and innate immunity cells. All the inflammatory parameters tested (NO production, induction of inflammatory genes and TNF-α/IL-6 secretion) are related to the M1 activation type (Mills, Kincaid et al. 2000; Murray, Allen et al. 2014) and are, therefore, associated with increased phagocytosis and predictive of enhanced clearance ability in the context of an acute inflammatory reaction.

The analysis of cellular interactions by confocal microscopy showed that most cells incubated with BM-NF internalized the material and displayed a nearby-normal rounded morphology or a symmetrically elongated morphology, indicative of cell activation, but no distortion or stretching, indicating mild perturbation of cell shape by internalized particles. This cellular morphology was also noted with SEM, although the presence of the ball milled fragments inside the cells could not be observed with this surface scanning technique. Incubation with long fibres caused cell adhesion to the fibres, which in some cases appeared partially internalized. The SEM image revealed some consequences of internalization, with some cells markedly stretched along the fibre surface and, in some cases, several cells penetrated by the same fibre. This situation of attempted, partial or failed phagocytosis due to the physical limitations of the cells in relation to the fibre length is indicative of frustrated phagocytosis, and similar observations have been already reported for other materials (Hamilton, Wu et al. 2009; Sweeney, Grandolfo et al. 2015). The implication of this situation is likely to be impaired movement due to the presence of a large penetrating fibre, as demonstrated by others. For example, Schinwald et al. (Schinwald, Chernova et al. 2012) investigated the threshold length for fibre-induced reduced mobility in macrophages and pulmonary inflammation by treating bone marrow derived macrophages in culture with nanofibres of different lengths. Treatment of the macrophages with fibres as short as 5 µm did lead to slight inhibition of macrophage mobility, which was assessed using the wound healing assay; however, treatment with fibres of 14 µm or longer led to substantial retardation of macrophage mobility (Schinwald, Chernova et al. 2012). Based on such results and the observation of frustrated phagocytosis by confocal as well as scanning electron microscopy, the short ball-milled TiO_2 NF would unlikely cause severe difficulties in macrophage mobility (at least in non-overload conditions), while the longer, pristine fibres would be expected to affect mobility and, as such, hinder effective, macrophage-mediated clearance from the lung.

In conclusion, these findings demonstrate that long TiO_2 nanofibres cause frustrated phagocytosis, cytotoxicity, hemolysis, oxidative stress and epithelial barrier perturbation. All these effects are mitigated by fibre shortening through ball-milling. However, short TiO_2 NF exhibit enhanced ability to activate acute pro-inflammatory effects in macrophages, an effect dependent on phagocytosis. Therefore, aspect ratio reduction mitigates toxic effects and enhances macrophage activation rendering the NF prone to phagocytosis (Figure 14). Thus, under in vivo conditions, short NF would be associated with acute inflammatory reaction, but would undergo a relatively rapid clearance, while long NF, although associated with a relatively smaller acute activation of innate immunity cells, are not expected to be removed efficiently and, therefore, may be associated to chronic inflammatory responses.

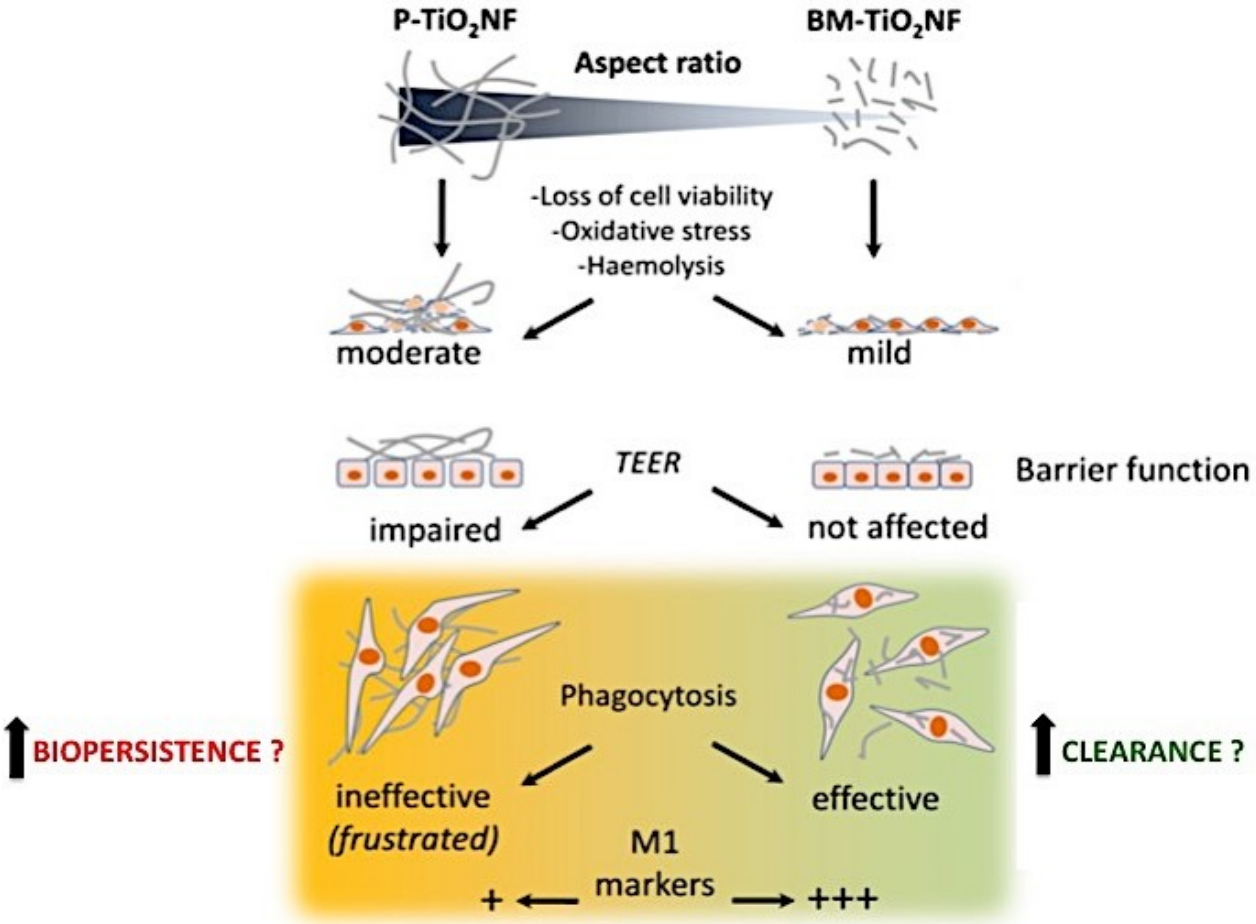

Figure 14. **Differential biological effects of pristine and ball-milled TiO_2 nanofibres.**

Investigation of the synergistic effect of LPS and TiO_2 NP on the expression of inflammatory markers and the role played therein by TLR-4

Abstract

Although causing moderate cytotoxicity and inflammatory effects, TiO_2 nanoparticles (NPs) are considered relatively safe materials. However, it is known that TiO_2 NPs bind bioactive environmental contaminants, such as bacterial lipopolysaccharide (LPS, endotoxin), and it is possible that this interaction leads to increased biological activity. In this part of the thesis I have investigated the pro-inflammatory responses of Raw264.7 murine macrophages exposed to two preparations of TiO_2 NPs, co-administered with LPS. The simultaneous exposure to NPs and LPS produced marked increases in *Nos2* mRNA, Nos2 protein and medium nitrite concentration (an indicator of NO production) well beyond the levels observed with LPS or TiO_2NP alone. TiO_2 NPs also synergized LPS effects on *Ptgs2* expression and cytokine secretion. The cytoskeletal drug cytochalasin B lowered the amount of NPs internalized by the cells and suppressed the synergy between TiO_2 NPs and LPS in NO production and cytokine secretion. Pre-treatment with the TLR-4 inhibitors polymyxin B and CLI-095 eliminated the synergy that was also partially hampered by the inhibition of p38 MAPK, but not of ERK1/2. Moreover, p38 phosphorylation was synergistically enhanced by the combined treatment at 6 h of incubation. It is concluded that TiO_2 NPs enhance macrophage activation by LPS *via* a TLR-4-dependent mechanism that involves p38 and is mainly triggered from an intracellular site. These findings suggest that the simultaneous exposure to LPS and TiO_2 NPs may exacerbate the inflammatory response *in vivo*.

Background

Lipopolysaccharides (LPS, endotoxins) are large, heat-stable molecules (molecular weight: 200 to 1000 kDa) from the outer membrane of Gram-negative bacteria, consisting of a polysaccharide part (O domain) and a bioactive lipid part, known as lipid A, responsible for their toxicity. LPS are Pathogen-Associated Molecular Patterns (PAMPs), acting as strong macrophage activators, and their effects range from airway disease, to fever, hypotension, septic shock, depending on the administration route and dose. In mammals, including man, most of the toxic/inflammatory effects of LPS and, in particular, all those based on transcriptional mechanisms, are mediated by the TLR-4 signaling pathway (Tan and Kagan 2014). The activation of innate immune cells such as monocytes and macrophages by LPS through TLR-4 is a major step of the defensive inflammatory reaction against bacteria and is initiated in different cellular locations, triggering distinct transduction pathways, first at the plasma membrane and later in an endosomal compartment (Gangloff 2012). LPS-stimulated cells produce a variety of inflammatory factors, such as tumor necrosis factor-α (TNF-α) and interleukin-6 (IL-6), and secrete nitric oxide (NO), a short-lived free radical, which mediates many biological functions such as host defense, neurotransmission, neurotoxicity and vasodilation.

The biological effects of TiO_2 NP have been deeply investigated in the recent years in several animal models and many authors report a significant toxic effect of this material (Shi, Magaye et al. 2013).

The interaction between LPS and TiO_2 NP may modify NP toxicity in vivo. For instance, Moon et al. (Moon, Park et al. 2010) have demonstrated that TiO_2 NP are able to induce acute inflammation in mice causing more evident effects if animals were primed by a treatment with LPS. Possible interactions between LPS and nanomaterials are not limited to TiO_2 NP since other engineered nanomaterials may be contaminated with bacterial endotoxin or other PAMPs. For instance, LPS may enhance the oxidative stress induced by amorphous silica NPs to initiate cytotoxicity (Shi, Yadav et al. 2010), and carbon nanotubes promote NLRP3 inflammasome activation in synergy with toll-like receptor (TLR) ligands (Yang, Flavin et al. 2013).

Biological effects of TiO_2 NP have been also investigated in a number of *in vitro* studies. Several reports have demonstrated that TiO_2 NP generate ROS (Bhattacharya, Davoren et al. 2009; Shukla, Sharma et al. 2011; Saquib, Al-Khedhairy et al. 2012) and induce genotoxicity (Bhattacharya,

Davoren et al. 2009; Saquib, Al-Khedhairy et al. 2012) but only mild, although clear cut, acute cytotoxicity in macrophages and airway epithelial cells (Fenoglio, Greco et al. 2009; Rotoli, Bussolati et al. 2012).

The possibility that the assessment of NP toxicity in vitro may be influenced by their contamination with bio-active molecules, and, in particular by LPS, has been debated (Oostingh, Casals et al. 2011). Indeed, previous studies performed with fine, micrometric TiO_2 particles and LPS suggested that the material was able to bind LPS and that the interaction enhanced the biological effects of the endotoxin (Ashwood, Thompson et al. 2007; Hirayama, Tamaki et al. 2011). LPS binding to nanosized TiO_2 is expected to be much higher due to higher surface area of NP compared to fine particles. In a recent study, Jiang reported that the binding between TiO_2 NP and LPS is relatively strong and does not involve the lipid A but the polysaccharide moiety (Jiang 2011). As a consequence, the interaction between LPS and TiO_2 NP should not prevent the binding between the endotoxin and the receptor. This hypothesis is consistent with the findings by Smulders et al. (Smulders, Kaiser et al. 2012) who, while he was evaluating different test methods to detect nanomaterial contamination with LPS, have reported a synergistic TLR-4-activation by LPS and several types of NP, and in particular of TiO_2 NP, in a TLR-4-transfected mammalian cell model.

Using Raw264.7 cells, a macrophage line endowed with high endogenous TLR-4 expression and widely adopted in the nanotoxicological field, the present study investigates the synergistic effect of LPS and TiO_2 NP on the expression of inflammatory markers and the role played therein by TLR-4.

Synthesis, dispersion, physico-chemical characterization of NM and experimental treatments

Preparation and dispersion of nanomaterials

Experiments presented in this part of the thesis were performed with Aeroxide® P25 NP (anatase/rutile 83/17, produced through the flame hydrolysis Aerosil® process), purchased from Evonik Degussa GmbH, Germany. Selected experiments were also performed with a colloidal suspension of TiO_2 NP (NAMA41®, 6 wt%, anatase/brookite 84/16, obtained through dispersion in water),18 provided by Colorobbia Holding S.p.A., Italy. Before experiments, Aeroxide® P25 NP were heated at 230°C for 3h to ensure endotoxin elimination (Muller, Huaux et al. 2005). NP were then suspended in a sterile-filtered solution of 0.05% Bovine Serum Albumin (Sigma Aldrich, Milan, Italy, cat. A9418) in Phosphate Buffered Saline without calcium and magnesium to obtain 100X stock suspensions of the highest dose tested (80 μg/cm^2, corresponding to 128 μg/ml). For the preparation of NAMA41® stock solution, the percent of BSA in PBS was corrected in order to reach a final concentration of 0.05%. After vortexing (30 s), sonication (10 min), and a further brief vortexing the stocks were subsequently diluted in the same solvent to obtain the other 100X stocks. The stock solutions were made fresh for each experiment.

Characterization of TiO_2 NP

The physico-chemical characterization of the TiO_2 NP when interacting with the biological environment were carried out adopting the same set parameters used for the in vitro cellular tests reported below (e.g., time, temperature, dose and culture medium). Particle size distribution was evaluated by dynamic light scattering (DLS) assessing the hydrodynamic diameter of the dispersed NPs. Similarly, a laser scattering technique was used to assess the ζ (zeta) potential as expression of surface charge of TiO_2 NPs and of their colloidal stability in the selected aqueous medium. For both DLS and ζ potential measurements, the stock solutions (10 mg/ml) were sonicated for 15 minutes and diluted to 128 μg/ml, both in deionized water and in complete medium (Dulbecco's modified Eagle's medium (DMEM), Euroclone, code n° ECB7501L, Pero, Milan, Italy). Standard polystyrene cuvette and folded capillary cell DTS 1070 were used for size and zeta potential measurements, respectively. Particle size and ζ potential of dispersed particles were measured by applying DLS and Laser Doppler Velocimetry (LDV) techniques, respectively, using ZetasizerNano ZS (Malvern Instruments, UK). For the evaluation of particle size, data were recorded at 25 ± 1°C,

in a backscattering detection mode (scattering angle of 173°). Each result corresponds to the average of five consecutive measurements and each measurement is the average of 15 analyses. The instrument measures the hydrodynamic diameter that is a diameter that includes the coordination sphere and the species adsorbed on the particle surface such as stabilizers, surfactants and so forth. DLS analysis provides also a polydispersity index (PDI), which is a number ranging from 0 to 1 useful to quantify the colloidal dispersion degree: samples with PDI close to 0 are considered monodispersed. Size data are calculated directly from correlation function (Cumulants analysis for z-average diameter and polydispersity index; CONTIN analysis for intensity size distribution). For the evaluation of ζ potential the system records light scattered at an angle of 13°, determining an electrophoretic mobility. The Smoluchowski approximation was applied to calculate ζ potential from the mobility. The specific surface area (SSA) was determined by BET single point method (Sorpty 1750, Carlo Erba, Milano, Italy). For spherical shape particles it is possible to correlate specific surface area to diameter by a simple geometric relationship (German and Park 2008).

$$d = \frac{6}{\rho X SSA}$$

Where:

SSA= Specific Surface Area (m^2/g)

d= particle mean diameter (µm)

ρ= powder density (g/cm^3)

Applying this relationship it was possible to calculate the particle mean diameter from SSA and to compare it with hydrodynamic diameter obtained by DLS. The physico-chemical characterization of TiO_2 NF was performed in the laboratory of Dr. Anna Costa (ISTEC CNR, Faenza, Ravenna, Italy)

Experimental treatments

Raw264.7 cells were seeded in complete growth medium in 96-well plates, at a density of 30×10^3 cells/well or in 24-well plates at a density of $15x10^4$ cells/well. Cell growth medium was replaced, 24h after cell seeding, with fresh medium supplemented with TiO_2 NP at the doses indicated for each experiment in the presence or in the absence of LPS (from *E.coli*, O55:B5 serotype, Sigma-Aldrich, Milan, Italy) at a concentration of 1 ng/ml or 10 ng/ml (from 100X stock solutions in DMEM). In all the experiments, vehicle (PBS + BSA) was added to the control. For experiments in which inhibitors of macrophage activation were used, compounds were added 1h before the

exposure to LPS and/or NP and maintained throughout the experiment. The selected inhibitors were: Ethyl (6R)-6-[N-(2-Chloro-4-fluorophenyl)sulfamoyl]cyclohex-1-ene-1-carboxylate (CLI-095, 1 µg/ml, from a stock solution of 10 µg/ml in DMEM, InvivoGen, San Diego, CA, USA); polymyxin B (50 µg/ml, from a stock solution of 500 µg/ml in DMEM, InvivoGen); cytochalasin B (5 µg/ml, from a stock solution of 50 µg/ml in DMEM; Sigma-Aldrich), 1,4-diamino-2,3-dicyano-1,4-bis[2-aminophenylthio] butadiene (U0126, 1 µM, from a stock solution of 10 mM in DMSO, Calbiochem, Merck Millipore, Darmstadt, Germany); 4-(4-fluorophenyl)-2-(4-methylsulfinylphenyl)-5-(4-pyridyl)-imidazole (SB203580, 2 µM, from a stock solution of 10 mM in DMSO, Calbiochem).

Results

Physico-chemical characterization of TiO_2 NP

Physico-chemical properties of NAMA41® (spray dried) and Aeroxide® P25 are summarized in Table 4 whereas results of wet characterization (pH, ζ potential and mean hydrodynamic diameter by intensity) of their dispersions in deionized water and complete culture medium are reported in Table 5. TiO_2 samples are comparable in phase distribution and density, although NAMA41® SSA BET exceeds approximately two and a half times that of Aeroxide® P25, suggesting a bigger primary particle diameter for the latter preparation. Both the samples showed a broad size distribution and a low colloidal stability, especially for Aeroxide® P25 NP that possess a lower ζ potential value in comparison to NAMA41® in all the dispersions tested. Sample stability strongly decreased passing from water dispersion at natural pH to culture medium, likely due to the increase of pH towards the isoelectric point that is 6.0-7.0 for titania (Preocanin, Cop et al. 2006). In order to discriminate between the influence of pH and medium components on final colloidal stability, ζ potential and mean hydrodynamic diameter of samples at natural pH, medium pH (around 7.5) and medium are compared (Table 5). The results showed that a strong destabilizing effect occurred at neutral pH. This behavior, more evident for NAMA41®, is explainable by considering that uncoated TiO_2 NPs, passing from natural to neutral pH, cross the isoelectric point and reverse ζ potential sign from positive to negative, with an expected destabilization of the sample as demonstrated by the significant size increase and absolute ζ potential value reduction. This trend is confirmed in complete medium, even if TiO_2 NP appeared to aggregate more in water at neutral pH than in biological medium probably due to protein corona stabilizing effect (Gebauer, Malissek et al. 2012). In water dispersion, at the same pH of cell culture medium, both TiO_2 samples showed slightly negative ζ potentials which, in cell culture media, levelled off around values of BSA and other serum protein at same pH (BSA isoelectric point ≅ 5) (Song, Yang et al. 2012). Thus, considering and comparing data obtained from the different TiO_2 NP dispersions tested, the lower size increase and the levelling of ζ potentials occurring in culture medium seems to be consistent with protein absorption on NP surfaces. In order to discriminate between the contributions of medium components adsorbed onto TiO_2 NP surfaces or freely dispersed in the medium, samples were assessed after ultrafiltration and re-dispersion in water. ζ potential values remained approximately the same (around -10 mV, data not shown), confirming that TiO_2 NP surfaces were coated by protein components, as suggested by the protein corona paradigm (Cedervall, Lynch et al. 2007). Table 6 reports the amount of BSA (0.05% BSA concentration)

normalized for the surface area of TiO_2 samples (at a dose of 80 μg/cm^2) derived from BET analysis and, hence, corresponding to the maximal theoretical free surface (see Table 5). The BSA amount normalized over powder surface area corresponds to 25.4 mg/m^2 and 65.1 mg/m^2 for NAMA41 and P25, respectively. These data are consistent with the formation of BSA coating, since in all cases they are much higher than the minimum amount of BSA leading to surface saturation of TiO_2 NP under comparable conditions (0.04 mg/m^2,(Song, Yang et al. 2012)). Analogously, Table 6 reports the amount of LPS (at a concentration of 1 ng/ml) normalized for the surface of TiO_2 samples, which is in both cases much lower than the saturation threshold reported in literature (0.3 mg/m^2) (Jiang 2011).

Table 4. Physico-chemical properties of NAMA41® (spray dried) and Aeroxide® P25.

TiO_2 NP	XRD phase distribution		Density (g/cm^3)	SSA_{BET}* (m^2/g)	d_{BET}** (nm)
	Anatase (%)	Brookite (%)			
NAMA41®	84	16	3.98	154	10
Aeroxide® P25	83	17	4.10	60	24

Table 5. Mean size distribution by intensity and ζ potential for 0.125 mg/ml of NAMA41® and Aeroxide® P25 dispersed in deionized water and complete culture medium.

TiO_2 NP	Deionized water $_{natural\ pH}$				Complete culture medium				Deionized water$_{medium\ pH}$			
	pH	Size (d. nm)	PdI#	ζ pot. (mV)	pH	Size (d. nm)	PdI#	ζ pot. (mV)	pH	Size (d. nm)	PdI#	ζ pot. (mV)
NAMA41	3,9	45	0,48	41,2	7,3	1962	0,98	-10,9	7,3	9864	0,76	-15,9
SD		1	0,09	0,0		147	0,03	0,5		2390	0,30	0,4
AeroxideP25	6,5	286	0,30	37,4	7,7	532	0,53	-10,8	7,7	3425	0,36	-11,0
SD		4	0,04	0,9		16	0,11	0,4		226	0,10	0,1

PDI: Polydispersity Index

Table 6. Amount of BSA and LPS present in test samples, normalized for the TiO_2 NP surface area.

TiO_2 NP	SSA (m^2/g)	BSA/TiO_2* (mg/m^2)	LPS/TiO_2 (mg/m^2)**
NAMA41®	154	25.4	0.00005
Aeroxide P25®	60	65.1	0.00013

* referred to a BSA concentration of 0.05%

** referred to a LPS concentration of 1 ng/ml

Synergistic effects of TiO_2 NP and LPS on the expression of pro-inflammatory markers in macrophages

The effects of TiO_2 NP (dose range 10-80 μg/cm^2), alone or in combination with LPS (1 or 10 ng/ml), on the viability of Raw264.7 cells were tested by resazurin assay after a 48h-exposure. TiO_2 NP, alone or in the presence of LPS (1 ng/ml), did not significantly affect cell viability even at the highest dose tested (not shown). In the presence of 10 ng/ml LPS a modest, but significant, reduction of cell viability (< 15%) was detected only at the highest dose of TiO_2 NP (80 μg/cm^2).

Figure 15A reports *Nos2* mRNA expression after 24h of treatment of Raw264.7 cells with 80 μg/cm^2 of TiO_2 NP alone or in combination with LPS (1 or 10 ng/ml). In cells treated with TiO_2 NP alone the messenger was much less induced compared with 1 or 10 ng/ml LPS (2-fold induction vs. 5-fold induction with LPS 1 ng/ml and 30-fold induction with LPS 10 ng/ml). However, the simultaneous exposure to both LPS and TiO_2 NP induced *Nos2* at a much higher level than LPS alone (16-fold with LPS 1 ng/ml and 55-fold with LPS 10 ng/ml).

The time dependency of the effect was studied at mRNA level (Figure 15B). After 6 h of exposure, a small increase in *Nos2* expression was detected in cells treated with TiO_2 NP alone, while *Nos2* mRNA was already markedly induced in cells treated with LPS or, simultaneously, with LPS and NP. *Nos2* expression increased in cells treated with TiO_2 NP up to 24h exposure, while it decreased between the 12h- and the 24h-time points in cells treated with LPS + TiO_2 NP or, more evidently, with LPS alone. Under this latter condition, *Nos2* was only slightly induced after 24h exposure compared with untreated cells (3-fold). On the contrary, at the same experimental time point, *Nos2* was still markedly induced compared with untreated control (19-fold increase) in cells treated with LPS and NP. The synergistic effect of TiO_2 NP and LPS on *Nos2* gene expression was confirmed at protein level after a 48h exposure (Figure 15C). The effect here is typically a dose-dependent response for both absence and presence of LPS (1 ng/ml). In the absence of LPS, the lowest dose of NP able to induce Nos2 was 20 μg/cm^2, while 10 μg/cm^2 of TiO_2 NP were able to increase the expression of the protein in the presence of LPS (1 ng/ml).

The stimulation of *Nos2* expression was associated with the increase in NO production, as assessed from nitrite concentration in the medium (Figure 15D). Nitrite concentration was significantly enhanced after a 48h-exposure to TiO_2 NP (80 μg/cm^2) or LPS, with an evident synergistic effect. The maximal stimulation was recorded in the presence of 10 ng/ml LPS + TiO_2 NP, where a 33-fold increase in medium nitrites was detected compared with the matching control. Comparable effects were observed with another murine macrophage line, MH-S, derived

from alveolar macrophages (data not shown). The synergy between TiO_2 NP and LPS was not limited to *Nos2* but involved also other inflammatory markers. *Ptgs2*, a pro-inflammatory LPS target gene which encodes for the inducible form of cyclooxygenase, Cox2, was only slightly induced by TiO_2 NP (80 μg/cm^2) alone, while LPS produced a 3-fold and 21-fold increase of *Ptgs2* mRNA at 1 ng/ml or 10 ng/ml LPS, respectively (Figure 16A). The effect was much larger in cells co-treated with LPS and NP, with a 6- fold and a 43-fold induction at, respectively, 1 or 10 ng/ml.

The secretion of TNF-α (Figure 16, Panel B) was detectable also in control, untreated Raw264.7 cultures and was significantly stimulated by TiO_2 NP (2-fold) or LPS alone (2-fold or 4.5-fold at 1 ng/ml or 10 ng/ml, respectively) and, at higher levels, by TiO_2 NP + LPS (4.5 or 7.5 at 1 or 10 ng/ml/ml of LPS, respectively). Instead, IL-6 secretion (Panel C) was undetectable in untreated cells and in cells treated with TiO_2 NP alone but was readily stimulated by LPS at either 1 ng/ml (47±5 pg/ml) or, much more markedly, at 10 ng/ml (1100±40 pg/ml). Co-treatment with TiO_2 NP and LPS caused a further increase in secretion when compared with cells treated with LPS alone, either at 1 or at 10 ng/ml.

In the experiments described in Figure 17, the effects of Aeroxide P25® were compared with those of a different preparation of titania of industrial origin (NAMA41®). Also these NP are predominantly anatase but are synthesized through a different process (see Experimental). The effects on nitrite concentration in culture medium (Panel A), *Nos2* expression (Panel B), and cytokine secretion (Panel C) were comparable for both TiO_2 NP preparations. The effects of LPS and NAMA41® on NO production were clearly synergistic, as demonstrated with two-way ANOVA (Figure 17A). Thus, the biological activity of the two titania in the presence of the endotoxin was similar, as expected by their comparable capacity to bind LPS. These data indicate that enhancement of LPS effects is not a peculiar feature of Aeroxide P25® TiO_2 NP.

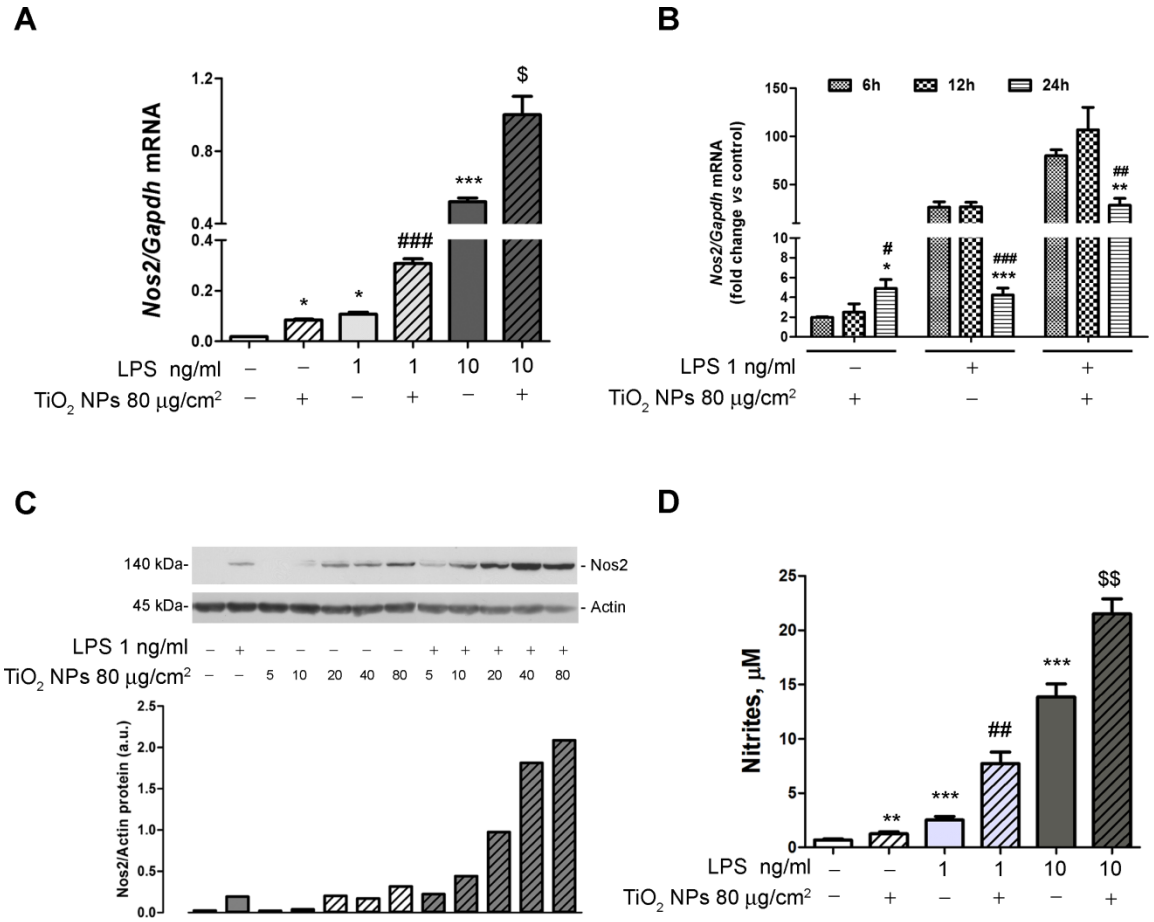

Figure 15. Effects of TiO_2 NP and LPS on *Nos2* expression and NO production in Raw264.7 cells. Growth medium was replaced 24h after cell seeding with medium supplemented with the indicated doses of TiO_2 NP and/or LPS. (A) After 24h of treatment, mRNA was extracted and the expression of *Nos2* evaluated as described in Experimental. Data are means ± S.D. of four independent determinations in two separate experiments. *p < 0.05 *vs.* control, untreated cultures; ### p < 0.001 *vs.* cultures treated with LPS 1 ng/ml alone; $p<0.05 *vs*. LPS 10 ng/ml alone. (B) At the indicated times, cells were lysed and the expression of *Nos2* mRNA was evaluated through RT-PCR. Data are expressed as fold stimulation *vs.* control, untreated cells and are means of 4 determinations ± S.D. obtained in two separate experiments. *p< 0.05, **p < 0.01, ***p < 0.001 *vs.* the same experimental condition at 6h of treatment; # p < 0.05, ## p < 0.01, ### p < 0.001 .*vs.* the same experimental condition at 12h of treatment. (C) After 48h of treatment, cells were extracted, and the expression of the protein Nos2 was evaluated through Western Blot. A representative blot is shown, with actin expression used for loading control (upper panel). In the lower panel the densitometric analysis of Nos2 protein is shown. (D) After 48h of treatment, nitrite concentration was determined in the culture medium. Data are means of eight independent determinations ± S.D. in two separate experiments. **p < 0.01, ***p < 0.001 *vs.* control, untreated cultures; ## p < 0.001 *vs.* cultures treated with LPS 1 ng/ml alone; $$ p < 0.01 *vs*. LPS 10 ng/ml alone. Two-tailed *t* test for unpaired data has been used for the statistical analysis

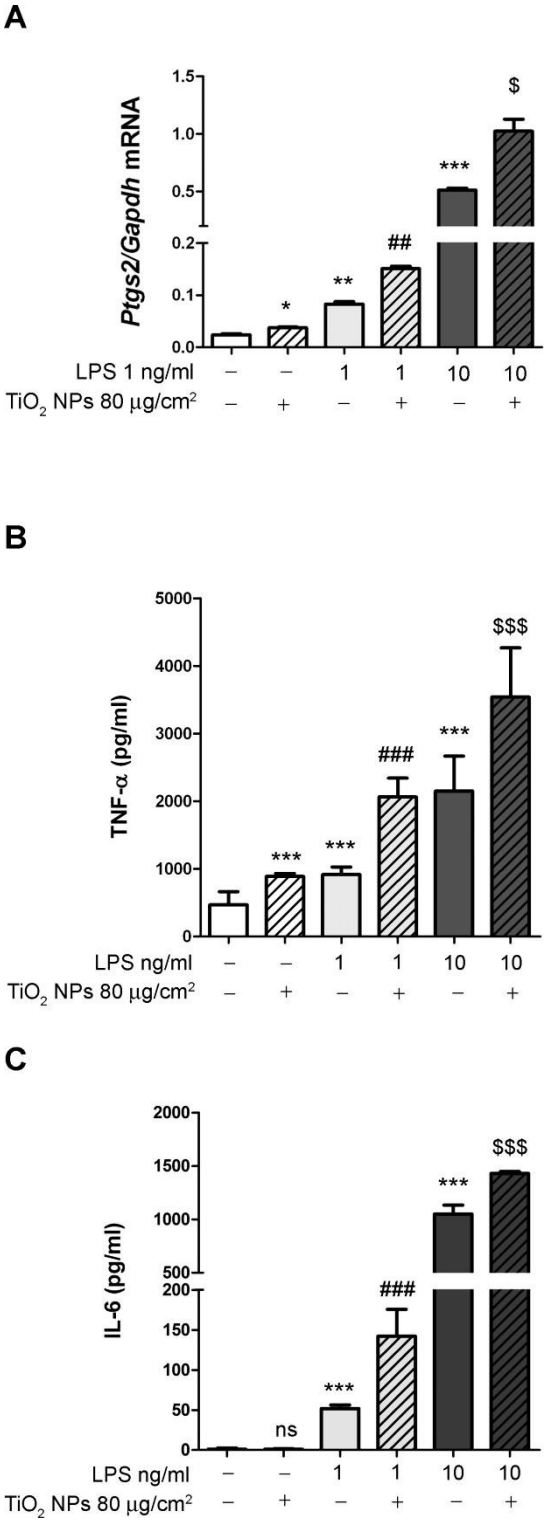

Figure 16. Synergistic effects of TiO_2 NP and LPS on the expression of inflammatory markers. (A) Growth medium was replaced 24h after cell seeding with medium supplemented with the indicated doses of TiO_2 NP and/or LPS. A. After 24h of treatment, mRNA was extracted and the expression of *Ptgs2* was analyzed with RT-PCR. Data are means of 4 independent determinations in two separate experiments with S.D. indicated. B, C. After 48h of treatment, TNF-α (B) and IL-6 (C) were determined in the extracellular medium, as described under Experimental. Data are means of 3 independent determinations ± S.D. For A, B, and C *p < 0.05, ***p < 0.001 *vs.* control, untreated cultures; ## p < 0.01, ### p < 0.001 *vs.* cultures treated with LPS 1 ng/ml alone; $ p < 0.05, $$$ p < 0.001 *vs*. LPS 10 ng/ml alone. Two-tailed *t* test for unpaired data has been used for the statistical analysis.

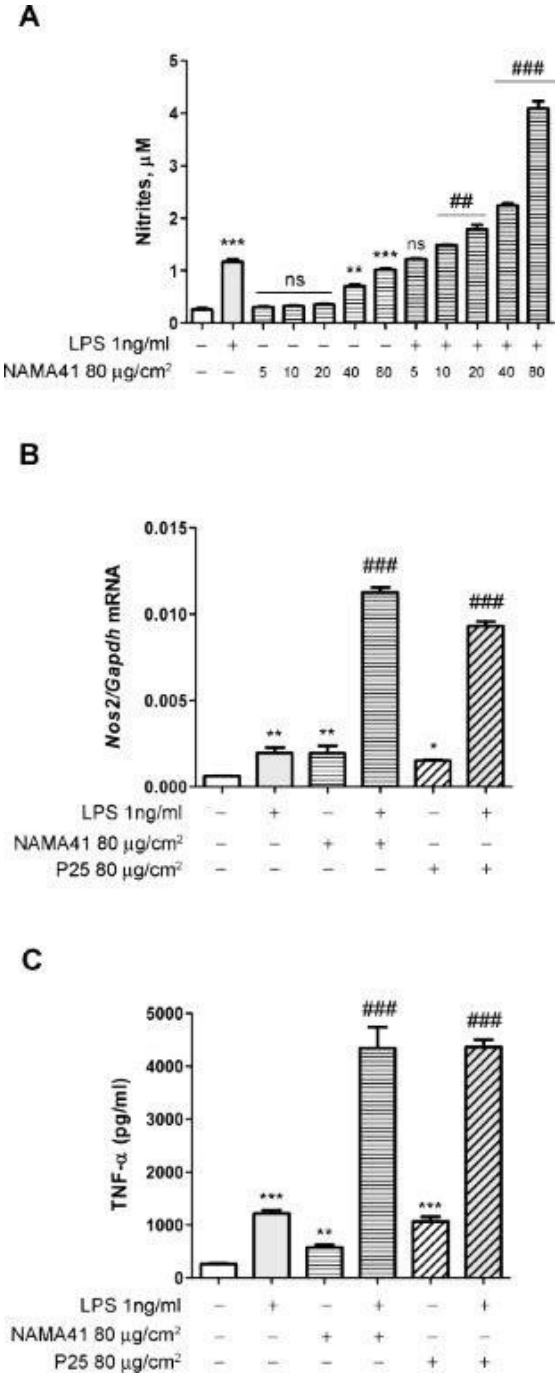

Figure 17. Effects of two preparations of TiO_2 NP on inflammatory markers in Raw264.7 cells. Growth medium was replaced 24h after cell seeding with medium supplemented as indicated with the indicated additives. A. After 48h of treatment, nitrite concentration was determined in the culture medium. Data are means of eight independent determinations ± S.D. in two separate experiments. **p < 0.01, ***p < 0.001 vs. control, untreated cultures; # p < 0.05, ### p < 0.001 vs. cultures treated with LPS 1 ng/ml alone, as evaluated by two-way ANOVA for multiple comparisons with Tukey correction. B. After 24h of treatment, mRNA was extracted and the expression of *Nos2* evaluated as described in Experimental. Data are means ± S.D. of four independent determinations in two separate experiments. *p < 0.05, **p < 0.01 vs. control, untreated cultures; ###p<0.001 vs. cultures treated with LPS 1 ng/ml alone, as evaluated by two-tailed *t* test for unpaired data. C. After 48h of treatment, TNF-α was determined in the extracellular medium, as described under Experimental. Data are means of 3 independent determinations ±± S.D. **p < 0.01, ***p < 0.001 vs. control, untreated cultures; ### p < 0.001 vs. cultures treated with LPS 1 ng/ml alone, as evaluated by two-tailed *t* test for unpaired data.

Sensitivity to cytoskeletal disorganization of LPS-dependent stimulation of NO production in the absence or in the presence of TiO_2 NP

The relevance of cytoskeletal integrity in the stimulation of NO production by LPS and TiO_2 NP was investigated in the experiments recounted in Figure 18. Although cytochalasin is known to inhibit LPS-dependent stimulation of NO production, interfering with Nos2 assembly on actin cytoskeleton (Webb, Harvey et al. 2001); the inhibition was not significant at 1 ng/ml of LPS, while the drug lowered NO production by roughly 30% in cells stimulated with 10 ng/ml of LPS. The inhibition was much more evident in cells treated with both LPS and TiO_2 NP, where cytochalasin lowered NO production by 60% (at LPS 1 ng/ml) or over 70% (at LPS 10 ng/ml). Therefore, while the simultaneous exposure to TiO_2 NP caused a marked increase in LPS-dependent stimulation of NO production in the absence of cytochalasin, the cytoskeletal drug completely suppressed the effect at 1 ng/ml LPS and severely lowered it at 10 ng/ml LPS (from +136% to +42%). Consistently, cytochalasin almost completely suppressed the synergistic effect of LPS (1 ng/ml) and TiO_2 NP on TNF-α secretion (from 4,525 ± 32 pg/ml to 1,424 ± 114 pg/ml; control 625 ± 120 pg/ml; n =3). The effect of cytochalasin on the uptake of P25 TiO_2 NP by Raw264.7 cells, incubated in the presence of LPS, was assessed in confocal microscopy (Figure 18, Panels B and C). In the absence of cytochalasin (Panel B) several cells exhibited large amounts of internalized NP, clustered in large agglomerates localized in discrete subcellular regions. NP were scarcely detectable in the extracellular space. Cytochalasin (Panel C) severely hampered TiO_2 NP internalization, and most TiO_2 NP were visualized outside the cells, in some cases close to the cell surface. Under both conditions, signals of internalized NP and cytoplasmic markers did not co-localize, suggesting that NP were sequestered in an intracellular compartment distinct from cytoplasm.

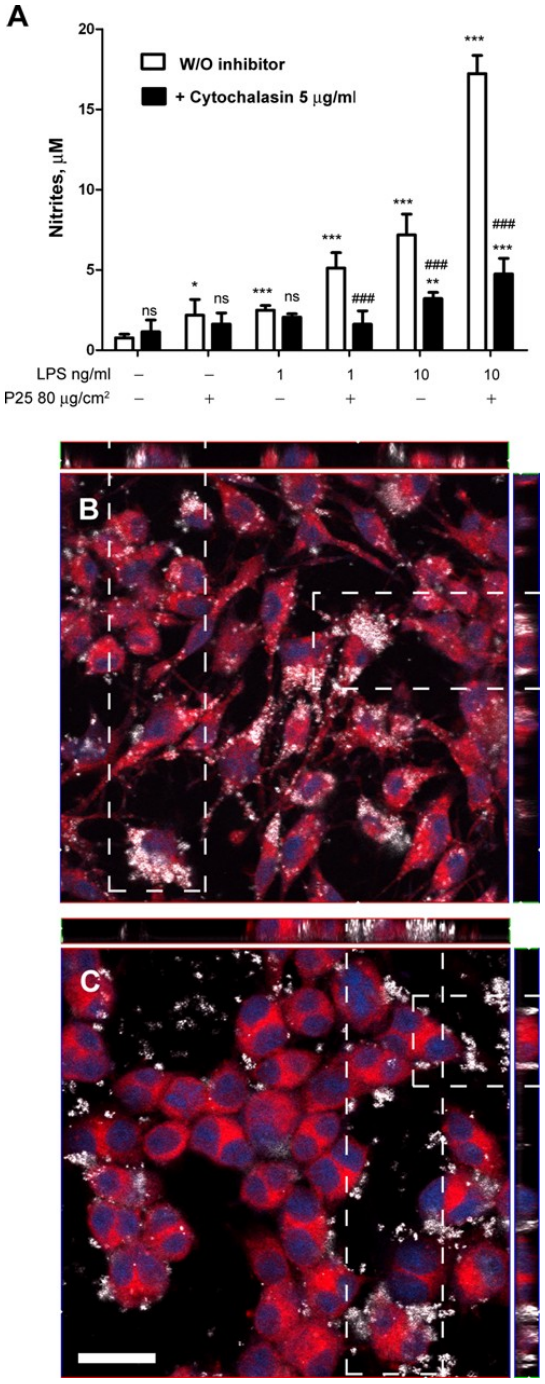

Figure 18. Effects of cytochalasin B on NO production and NP internalization by Raw264.7 cells treated with TiO_2 NP and LPS. Cells were treated as described in Figure 1D. One hour before exposure to TiO_2 NP (80 µg/cm2) and/or LPS (1 ng/ml or 10 ng/ml), cytochalasin B (5 µg/ml) was added to the medium, as indicated, and maintained throughout the experimental treatment. (A) After 48h, nitrite concentration was determined in the extracellular medium, as described under Experimental. Data are means of four independent determinations ± S.D. *p < 0.05, **p < 0.01,***p < 0.001 *vs.* control, untreated cultures; ###p<0.001 *vs.* cultures treated under the same conditions without the inhibitor, as evaluated by two-tailed *t* test for unpaired data. (B, C) Parallel cultures were seeded on coverslides and incubated for 24h with TiO2 NP (10 µg/cm2) in the presence of LPS (1 ng/ml), without (B) or with (C) cytochalasin B. At the end of the experiment cells were labelled and fixed as detailed under Experimental. For either condition, a single horizontal confocal section is shown along with two orthogonal projections. Dashed lines highlight the orthogonal projections of single cells. White, TiO_2 NP; Blue, nuclei; Red, cytoplasm. Images report representative fields. Bar = 20 µm.

Role of MAPK activation in the effects of LPS and TiO_2 NP

Given that MAPK have been repeatedly involved in *Nos2* induction and NO production triggered by LPS in macrophages (Chen and Wang 1999; Rao, Meighan et al. 2002; Jones, Adcock et al. 2007), their role in the synergistic effect of LPS and TiO_2 NP has been investigated (Figure 19). U0126, which prevents the activation of ERK 1/2 by suppressing the activity of the MAP Kinase Kinase MEK1/2 (DeSilva, Jones et al. 1998), inhibited the increase in NO production caused by exposure to LPS (Panels A and B) but did not hinder, but rather increased the effect of the combined exposure to LPS and TiO_2 NP (Panels C and D). On the contrary, SB203580, which inhibits p38 MAPK catalytic activity by binding to the ATP-binding pocket (Kumar, Jiang et al. 1999), was without effect on the stimulation of NO production caused by LPS but partially inhibited the combined effect of TiO_2 NP and LPS. Neither U0126 nor SB203580 affected the slight stimulation of NO production by TiO_2 NP (not shown). Thus, the ERK1/2 branch appears essential for the stimulation of macrophage NO production by LPS but not by LPS + TiO_2 NP, while, conversely, p38 seems more involved in the combined effect. Neither ERK1/2 nor p38 are indispensable for the stimulation of NO production by TiO_2 NP.

The role of p38 phosphorylation in the combined effect was directly investigated in the experiment shown in Figure 20. After a short (3h) incubation in the presence of LPS and/or TiO_2 NP, a definite activation of p38 (Panel A) and ERK1/2 (Panel C), but the simultaneous exposure to the two compounds showed no additive effect for p38 or a less-than-additive effect for ERK1/2. Conversely, after 6h of treatment, cells co-treated with LPS and TiO_2 NP showed a level of phosphorylated p38 much higher than the cells incubated with either compound alone (Panel C), while ERK1/2 phosphorylation was comparable in cells treated with LPS or LPS + TiO_2 NP (Panel D).

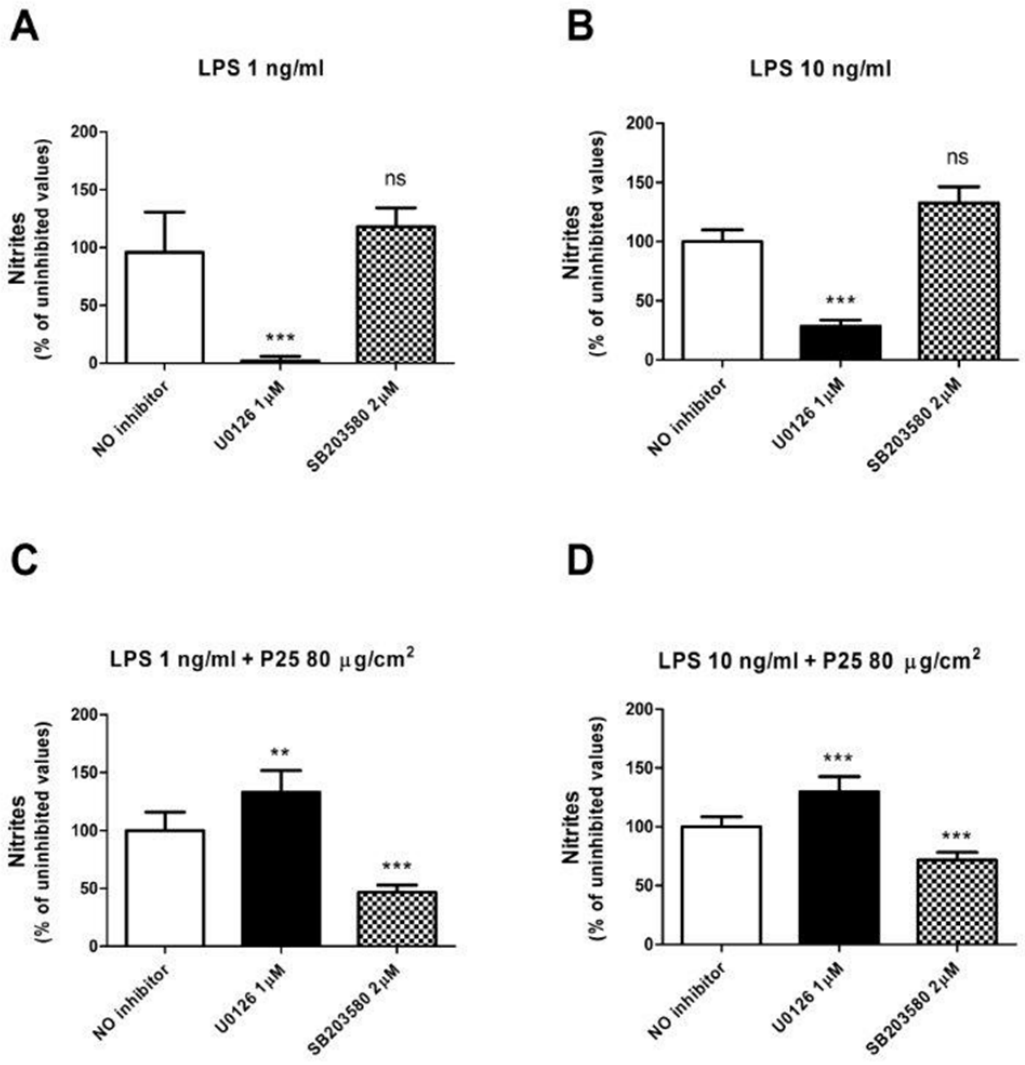

Figure 19. Differential effects of MAPK inhibitors on NO production promoted by TiO_2 NP and LPS. Cells were treated as described in Figure 1D. A, B, C, D. One hour before the exposure, the MAPK inhibitors U0126 or SB203580 were added to the medium, as indicated, and maintained throughout the experimental treatment. After 48h of treatment, nitrite concentration was determined in the extracellular medium, as described under Experimental. Data are expressed as percent of the value obtained under the indicated conditions in the absence of inhibitors and are means of eight independent determinations ± S.D. Statistical analysis was performed on the absolute values. For all the panels, **p < 0.01 and ***p < 0.001 *vs.* cultures incubated with the same doses of LPS and TiO_2 NP in the absence of inhibitors, as evaluated by two-tailed *t* test for unpaired data.

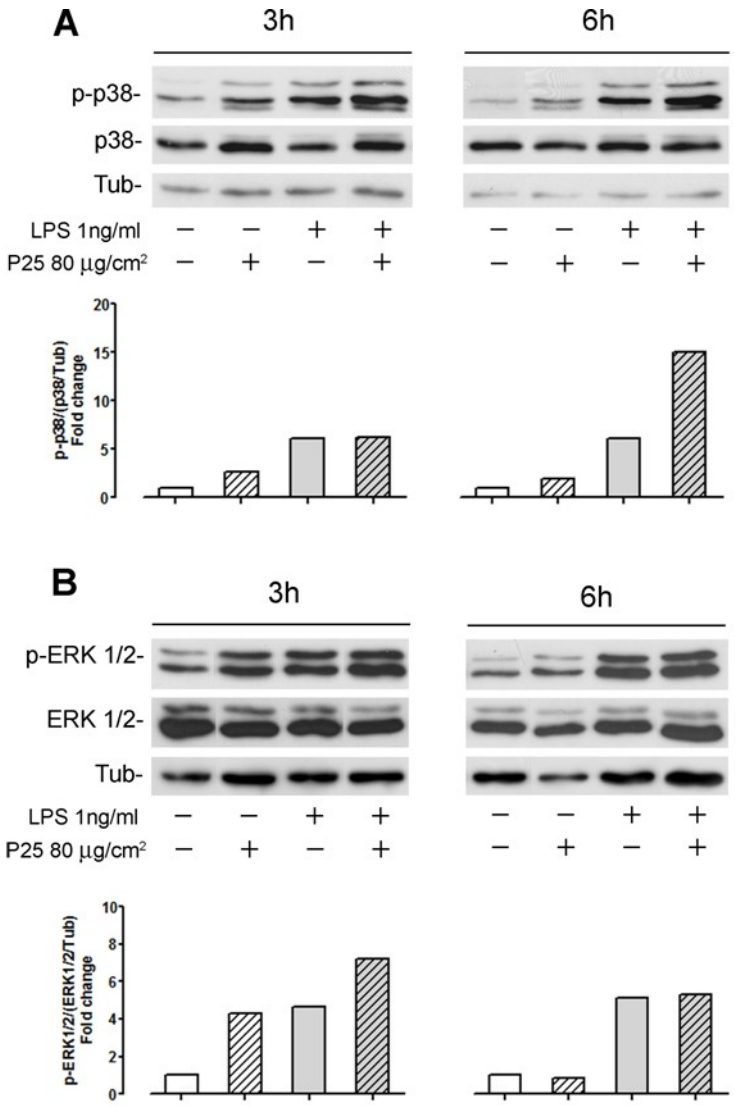

Figure 20. The synergistic effect of LPS and TiO_2 NPs on p38 phosphorylation. Cells were incubated for 3h or 6h in the presence of LPS and/or TiO_2 NP. At the indicated times cells were lysed and the expression of the phosphorylated isoform and of total p38 (Panels A and B) or ERK1/2 (Panels C and D) was assessed. Tubulin was used as loading control. In the lower part of each panel the densitometric analysis is shown. The experiment was performed twice with comparable results.

The combined effects of TiO_2 NP and LPS are suppressed by TLR-4 inhibition

The dependence of the effects of NP and LPS on TLR-4 is shown in Figure 21. Polymyxin B, an antibiotic derived from *Bacillus polymyxa*, binds the lipid A moiety of LPS with very high affinity, thus preventing its interaction with TLR-4 (Moore, Bates et al. 1986). The antibiotic almost completely inhibited the stimulation of NO production (Panel A) or Nos2 protein expression (Panel B) in macrophages treated with TiO_2 NP and LPS, used either alone or together. Polymyxin B had comparable effects on TNFα secretion (Panel C), which was completely suppressed either in cells treated with TiO_2 NP, LPS, or both. Also CLI-095, which blocks the signalling mediated by the intracellular domain of TLR-4 (Ii, Matsunaga et al. 2006), almost completely suppressed the effect, individual or combined, of TiO_2 NP and LPS on NO production (Panel D). Interestingly, polymyxin did not significantly affect the production of NO elicited by treatment with 40 or 80 μg/cm^2 of NAMA41® (see Figure 17), indicating that the material was not contaminated with LPS (not shown).

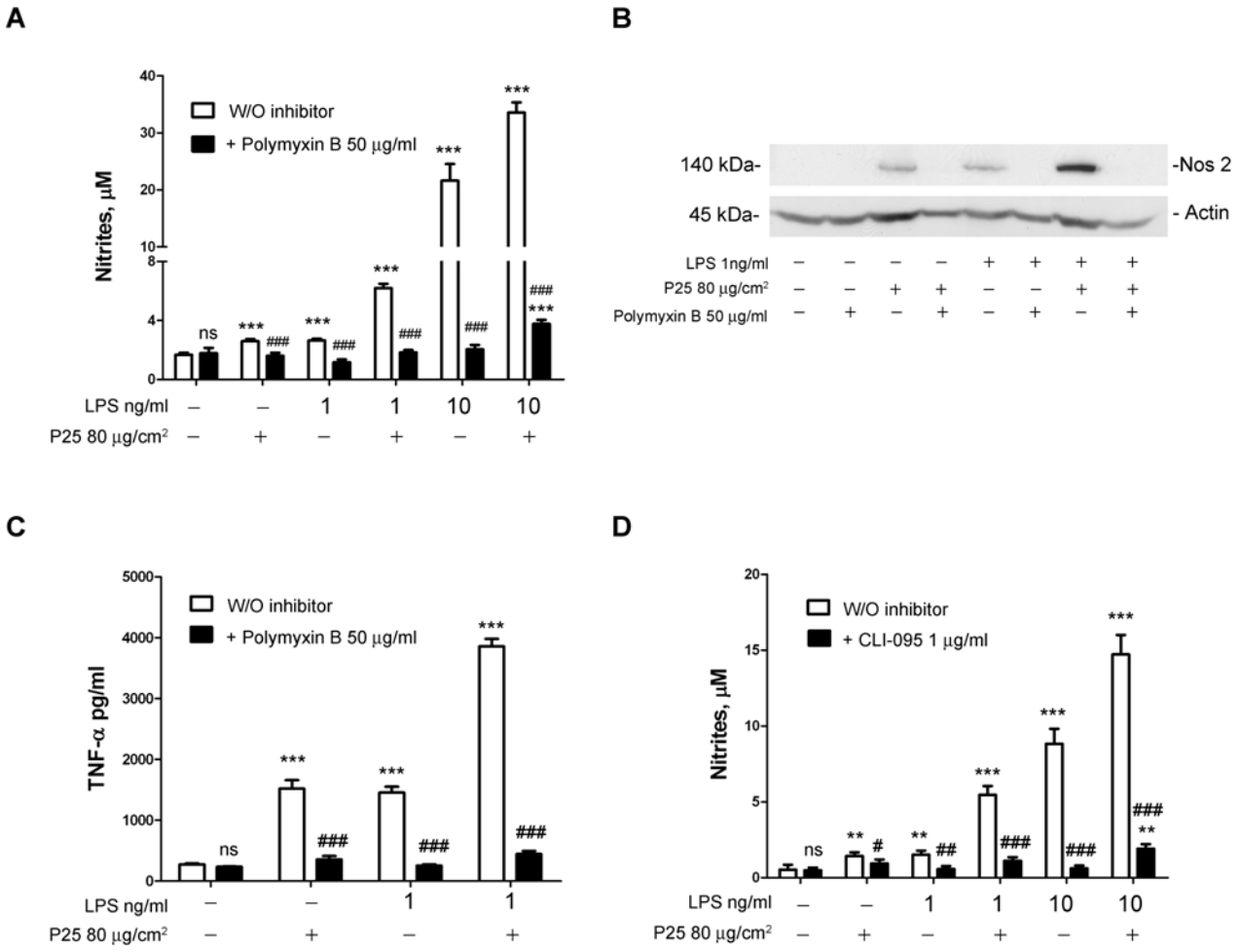

Figure 21. Effects of TLR-4 inhibitors on NO and TNF-α production by Raw264.7 cells treated with TiO_2 NP and LPS. Cells were treated as described in Figure 2. One hour before exposure to TiO_2 NP (80 μg/cm^2) and/or LPS (1 ng/ml or 10 ng/ml), polymyxin B or CLI-095 were added to the incubation medium, as indicated, and maintained throughout the experimental treatment. After 48h, the concentration of nitrites (Panels A and D), the expression of Nos2 (Panel B) and the secretion of TNF-α (Panel C) were determined, as described under Experimental. For B, a representative experiment is shown, performed twice with comparable results. Data are means (n = 4 for A and D, n = 3 for C) ± S.D. in a representative experiment. *p < 0.05, **p < 0.01,***p < 0.001 *vs.* control, untreated cultures; # p < 0.05, ## p < 0.01, ### p < 0.001 *vs.* cultures treated under the same conditions without the inhibitor, as evaluated by two-tailed *t* test for unpaired data.

Discussion

In this part of the thesis, the effects of the simultaneous exposure of macrophages to TiO_2 nanoparticles and LPS have been studied. From the data reported in Table 6, the amount of LPS available for the surfaces of the two TiO_2 NP preparations is more than one-thousand-fold lower than the saturation level under the experimental conditions adopted. Thus, even if agglomerated in culture medium (Table 5), it is likely that TiO_2 NP bind most if not all the LPS available. Therefore, although it should be expected a higher reactivity for the sample endowed with an higher surface area (NAMA41®), which should be able to drag an higher amount of LPS, the agglomerated state of both materials is expected to decrease the free surface area at comparable levels, and should therefore justify a comparable capacity to adsorb LPS (and, hence, to activate macrophages), consistently with the results obtained.

The endpoints investigated in this part of the thesis, and found to be synergistically stimulated by TiO_2 NP and LPS, are the increase in NO production and the enhanced secretion of pro-inflammatory cytokines. These effects are also involved in the toxic effects elicited by TiO_2 NP *in vivo*. For instance, excess of NO production is responsible increase is responsible for the impairment of microvascular reactivity observed in rats exposed to titania through inhalation (LeBlanc, Cumpston et al. 2009; Knuckles, Yi et al. 2012). Changes in NO production are also of pivotal importance in respiratory pathophysiology: while *Nos2* is constitutively expressed in the human airway epithelium, its expression, along with NO production (Liu, Zhang et al. 2010), is increased by exposure to TiO_2 NP in lung macrophages *in vivo*. Interestingly, recent research supports the use of the non-invasive determination of NO in exhaled breath of workers handling TiO_2 nanopowders as a biomarker of inflammatory effect (Wu, Liao et al. 2014). Sustained increase in cytokine production is observed during lung inflammation caused by TiO_2 after intratracheal instillation (Gustafsson, Lindstedt et al. 2011) or oropharyngeal aspiration (Delgado-Buenrostro, Medina-Reyes et al. 2015). The increased secretion of pro-inflammatory cytokines is also observed after exposure to TiO_2 NP *in vitro.* In particular, the exposure to nanosized TiO_2 stimulates TNF-α secretion in rat alveolar macrophages (Scherbart, Langer et al. 2011) and in murine macrophages (Xiong, George et al. 2013), as well as the secretion of IL-6 in human THP-1 cells, where the co-treatment with LPS potentiate the effect of TiO_2 NP (Morishige, Yoshioka et al. 2010).

TiO_2 NP are increasingly used for industrial purposes and their production is in the order of hundreds of tons per year, although they are considered as relatively non-toxic at the levels

detected in occupational environments. On the other hand, the inflammogenic potential of TiO_2 NP *in vivo* has been identified since several years (Oberdorster, Finkelstein et al. 2000; Kobayashi, Naya et al. 2009; Ma-Hock, Burkhardt et al. 2009) and it is known that not only TiO_2 NP (Moon, Park et al. 2010), but also carbon-based nanomaterials significantly exacerbate respiratory inflammation induced by LPS in vivo (Inoue 2011). Those data and the results presented here suggest that, in an occupational setting, a significant part of the inflammatory effects observed may be due not only to nano-structured materials themselves but also to airborne and ground molecules adsorbed therein or in environmental particulate (Long, Suh et al. 2001; Soukup and Becker 2001).

The synergistic effect of LPS and TiO_2 NP on NO production and cytokine secretion as well as NP internalization, are significantly hampered by cytochalasin D. These data indicate that cytoskeletal integrity and phagocytic activity are required for the effect and point to the involvement of an intracellular site of signalling. On the contrary, consistent with previous literature data (Eswarappa, Pareek et al. 2008), the effects of LPS alone on NO production are mostly independent on cytoskeleton, indicating a surface site of signalling.

The MAPK transduction pathway is differently involved in the effects of TiO_2 NP alone or in the presence of LPS. The ERK1/2 branch appears essential for the stimulation of NO production by LPS but not by LPS + TiO_2 NP, while, conversely, p38 seems more involved in the combined effect (Figs. 19 and 20). Interestingly, neither ERK1/2 nor p38 are indispensable for the stimulation of NO production by TiO_2 NP. Previous studies showed that LPS treatment of Raw264.7 cells causes the activation of all the three MAPK pathways, ERK1/2, p38, and JNK (Sanghera, Weinstein et al. 1996; Akira and Takeda 2004). Moreover, one of the preparations of TiO_2 NP used here, P25, triggers MAPK phosphorylation in lung tissue and alveolar macrophages *in vivo*, an effect enhanced by previous priming with LPS (Moon, Park et al. 2010). However, it is known that the contribution of the three MAP kinases to *Nos2* induction and NO production by activated macrophages can vary depending upon the macrophage type and the experimental conditions adopted (Chen and Wang 1999; Rao, Meighan et al. 2002; Jones, Adcock et al. 2007). It is therefore, possible, that the simultaneous presence of NP and LPS modulates the MAPK activation pattern, as demonstrated by Liu et al. (Liu, Li et al. 2012) for gold NP and LPS in the same cell model used here. In our case, the different sensitivity of the combined and LPS-specific effects to MAPK inhibitors and the clear cut synergy in p38 phosphorylation, observed at 6h of treatment, suggest that the intracellular signals

elicited by LPS alone or by LPS and TiO_2 NP are, at least in part, distinct and different. Moreover, the effects of TiO_2 NP and LPS on *Nos2* induction have also different time courses. Indeed, while the effect of LPS is fairly rapid and is markedly lowered when the treatment is prolonged from 12 h to 24 h, the effect of TiO_2 NP is characterized by a latency of few hours and is larger at 24h than at 6h of treatment. However, in the presence of TiO_2 NP, LPS effect is prolonged, and gene induction is still very evident after 24h of treatment (Figure 15B). Also the experiment presented in Figure 20 indicates that the synergy, as far as p38 phosphorylation is concerned, requires prolonged times of incubation. Both the effect of LPS alone and the combined effect are abolished if the binding of LPS to TLR-4 is prevented by polymyxin B, or the transduction of the TLR-4 signal is suppressed by CLI-095. Overall, the data presented in this contribution suggest that TiO_2 NP enhance the biological activity of LPS in murine macrophages though a mechanism that depends on TLR-4, involves the p38 rather than the ERK1/2 branch of the MAPK cascade, and is, at least prevalently, triggered in an intracellular, phagocytosis-dependent compartment. These features are recounted in a model depicted in the chart shown in Figure 22. According to this model, TiO_2 NP would behave as a Trojan horse, able to facilitate the entry of LPS in the endosomal compartment. Thus, when exposed simultaneously to LPS and TiO_2 NP, macrophages would be mainly stimulated through TLR-4 in the endosomal compartment, triggering a sustained signal transduction that leads, eventually, to enhanced effects.

The findings described in this part of the thesis demonstrate that the macrophage activation by LPS *in vitro* is markedly enhanced by the simultaneous exposure to TiO_2 NP. The doses of LPS adopted are well below the binding capacity of the TiO_2 NP (Table 6) and suggest that most, if not all the LPS is bound. Therefore, the overall message is that, when bound to TiO_2 NP, LPS exerts a much more powerful inflammatory effect. This effect may explain why the inflammatory changes observed *in vivo* after exposure to LPS are exacerbated by TiO_2 NP (Moon, Park et al. 2010). On the other hand, they also suggest that the inflammatory changes observed upon exposure to TiO_2 NP may be due, at least in part, to their capability to bind LPS and, possibly, other TLR agonists, and to enhance their biological activities. As a consequence, the inflammatory effects of TiO_2 NP may be of particular concern for individuals with respiratory conditions, where increased levels of such compounds are expected.

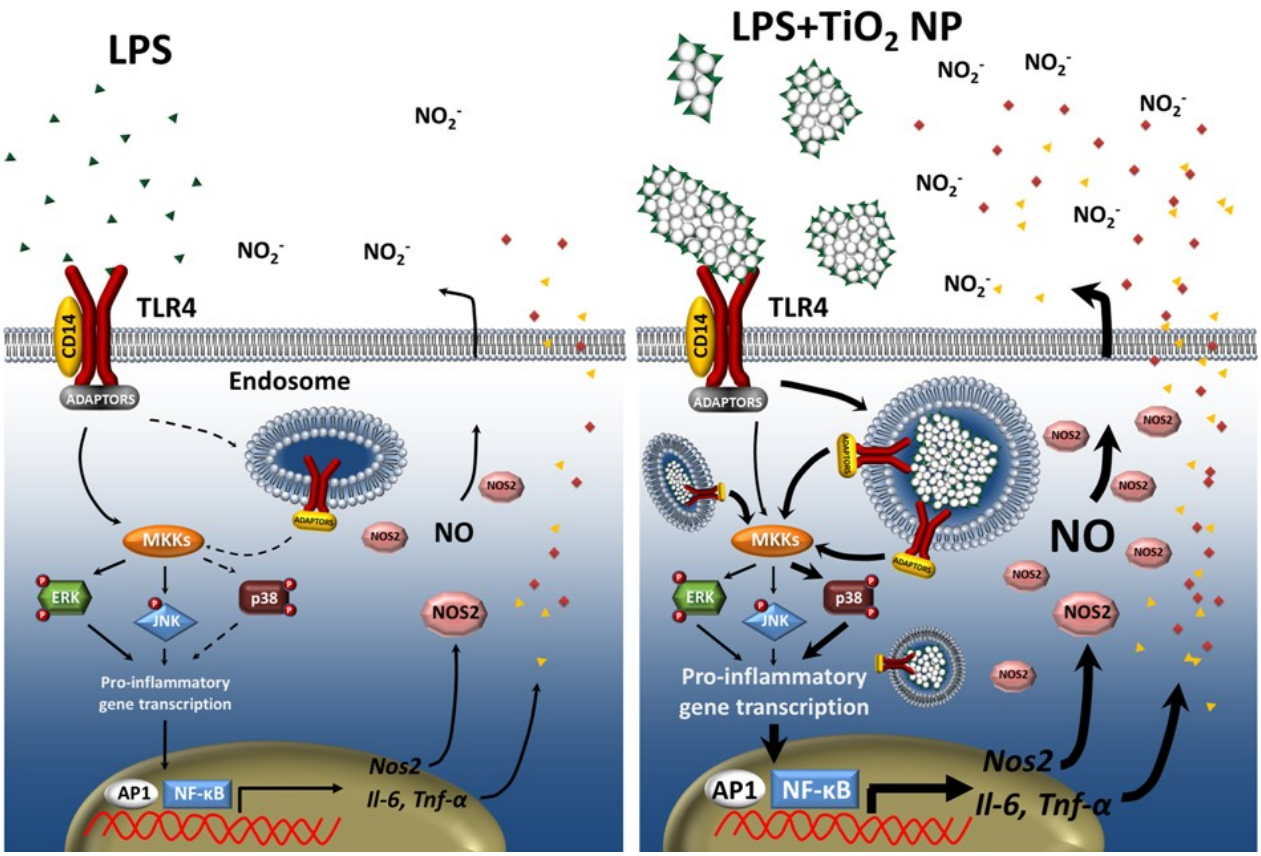

Figure 22. A comparison between the transduction pathways triggered by LPS alone (left) and by LPS + TiO_2 NP (right). See text for further explanations.

Figures from 15 to 22 and text from page 72 to page 94 have been adapted (by permission of the Royal Society of Chemistry) from a manuscript in which I am first co-author: Bianchi, MG., **Allegri, M**. et al. (2015) Titanium dioxide nanoparticles enhance macrophage activation by LPS through a TLR4-dependent intracellular pathway. ***Toxicol. Res.***, 2015,**4**, 385-398. **DOI:** 10.1039/C4TX00193A.

pubs.rsc.org/en/content/articlelanding/2014/tx/c4tx00193a#!divAbstract

Toxicity determinants of Multi-Walled Carbon Nanotubes: the relationship between functionalization and agglomeration

Abstract

The elucidation of toxicity determinants of Multi-Walled Carbon Nanotubes (MWCNTs) is still incomplete. Functionalization with carboxyl groups is, however, commonly used to mitigate MWCNT toxicity, although the rationale for the mitigating effect has not been fully clarified yet. In this part of the thesis, two optimized chemical vapor deposition methods were employed to obtain MWCNTs of comparable length but different diameter, which were subsequently functionalized. For MWCNT of diameter larger than 40 nm, no detrimental effects on cell viability of macrophages were observed, while a mild cytotoxicity was recorded for diameters between 15 and 40 nm, with a mitigating effect of functionalization. To investigate the factors responsible for the mitigating effect, we used the thinnest MWCNT preparation on different cell models, evaluating several endpoints, such as viability, production of nitric oxide (NO), expression of pro-inflammatory markers, modification in the Trans-Epithelial Electrical Resistance (TEER), and clonogenic activity. Substantial mitigation was observed not only with carboxyl-, but also with amino-functionalized MWCNT. Different biological reactivity of the three MWCNT preparations (pristine or functionalized) was associated with differences in their agglomeration tendency, correlated to their different capability of interacting with culture media proteins. In particular, functionalized preparations exhibited a stronger tendency to agglomerate that was strictly dependent on the presence of proteins, suggesting that the formation of larger agglomerates in biological media contributed to the mitigated toxicity of functionalized MWCNT preparations. These data demonstrate that surface chemistry, in particular surface charge, influences the protein adsorption onto the MWCNT surface, allowing to the formation of different protein coronae, which lead to different MWCNT bio-reactivity.

Background

Toxicity determinants of CNTs

Although many contributions focused on the biological effects *in vivo* and *in vitro* of CNTs, the toxicological characterization of these materials is far from being complete and the identification of the structural determinants of toxicity is still on-going. Arguably, controversy and lack of comparability among the different preparations exist about CNT bio-safety, as some preparations appear to be highly hazardous, while others seem harmless (Flahaut, Durrieu et al. 2006; Pulskamp, Diabate et al. 2007; Cheng, Muller et al. 2009; Park, Zahari et al. 2014). Thus, toxicity evaluation of these materials has to be taken on a case-by-case study, because CNTs cannot be regarded as a simple chemical substance. As a consequence, the investigation of their nanotoxicity has to be designed according to their specific features and cannot adopt the same strategy of the conventional toxicology studies applied for general chemical compounds (Meng, Xia et al. 2009). However, CNT toxicity studies have yielded divergent results, due to the use of materials with different degree of purity and structural features (Wick, Manser et al. 2007), as well as, for in vitro studies, the different cell culture media (Zhu, Ran et al. 2006) and different cell types used for the assay (Kostarelos, Lacerda et al. 2007). Thus, despite of several excellent reviews on the knowledge advancement about CNT toxicity (Donaldson, Aitken et al. 2006; Lam, James et al. 2006; Aschberger, Johnston et al. 2010; Cui, Vashist et al. 2010; Pacurari, Castranova et al. 2010; Lanone, Andujar et al. 2013; Toyokuni 2013), the current understanding of toxicity determinants is still an unsettled issue (Jacobs, Ellenbecker et al. 2014). In general, the toxicity of CNTs is attributed to their physico-chemical characteristics, such as length, diameter, shape, purity, surface area and surface chemistry, which, in turn, are remarkably influenced by the synthetic route. The impact of residual catalyst metals that are present in the interior structure of CNTs is also important.

The role of surface area and surface chemistry

Among the various determinants known to influence the biological activity of CNTs, also functionalization with carboxylic and amino groups has been considered and investigated in several studies, despite contrasting results have been reported. Functionalization enhances toxicity in airway epithelial BEAS-2B cells (Chatterjee, Yang et al. 2014; Ursini, Maiello et al. 2015), while, on the contrary, it has been demonstrated to suppress bioactivity in other epithelial models (Liu, Dong et al. 2014) and in macrophages (Hamilton, Wu et al. 2013). Also in vivo models have

yielded diverging data, with mitigating (Jain, Thakare et al. 2011; Sager, Wolfarth et al. 2014) or enhancing (Urankar, Lust et al. 2012) effects reported for different endpoints.

When suspended in biological media, MWCNTs adsorb macromolecules that form a corona and modify the properties of the material (Marchesan and Prato 2015). Protein adsorption is heavily influenced by surface curvature and surface area. Surface curvature is directly related to the outer diameter (Raffaini and Ganazzoli 2013; Gu, Yang et al. 2015), while surface area is influenced by outer diameter, pore volume and surface chemistry. In particular, surface chemistry influenced the adsorption of macromolecules to CNTs depending on (Cho, Huang et al. 2011) 1) the available specific surface area (functionalized CNTs may present higher or lower surface area values according to the functional groups which are attached on their sidewalls); 2) solution pH, in relation to CNT pKa value (increased adsorption at pH below pKa); 3) ionic strength in the solution (increased adsorption increasing the ionic strength).

In this part of the thesis, I investigate the combined influence of two characteristics, i.e. diameter and surface chemistry, on the biological effects of MWCNT in different cell models. Four MWCNT preparations, of comparable length but different diameter, have been examined (three synthesized in an associate laboratory via CVD method and one commercial). For each preparation, both pristine and functionalized MWCNT were investigated. The toxicological profile of the samples was compared with that of a benchmark CNT preparation obtained from the JRC repository.

Synthesis, dispersion, physico-chemical characterization of NM and experimental treatments

Supply and synthesis of carbon nanotubes

A Thermal Chemical Vapor Deposition (T-CVD) reactor was used to synthesize MWCNTs. The reactor consists of a horizontal quartz tube with 3.4 cm inner diameter and 100 cm length housed in a three-zone 80 cm long cylindrical furnace. Synthesis of CNTs was performed by two approaches. In the first case, camphor and ferrocene were used as carbon source and catalyst, respectively, while acetylene as carbon source and iron particles supported on Al_2O_3 substrate as catalyst were used in the latter.

A Thermal Chemical Vapor Deposition (T-CVD) reactor was used to synthesize MWCNTs. The reactor consists of a horizontal quartz tube with 3.4 cm inner diameter and 100 cm length housed in a three-zone 80 cm long cylindrical furnace. Synthesis of CNTs was performed by two approaches. In the first case, camphor and ferrocene were used as carbon source and catalyst, respectively, while acetylene as carbon source and iron particles supported on Al2O3 substrate as catalyst were used in the latter.

More specifically, for the preparation of the CNT1 sample (see Table 7), a Pyrex flask containing the reagent mixture, which consisted of camphor (96% purity in weight, Sigma-Aldrich, Athens, Greece) as carbon precursor and ferrocene (98% purity in weight, Sigma-Aldrich, Athens, Greece) as catalyst, in a 20/1 mass ratio, was connected to the tube nearby the nitrogen inlet. Nitrogen gas flow was used to carry the gas mixture of precursors towards the center of the furnace, where pyrolysis took place at 850 ^{o}C, and CNTs were grown. For the preparation of CNT2 and CNT3 samples, the catalyst particles were placed on a ceramic boat inside the quartz tube and in the middle of the isothermal zone of the reactor. Firstly, a constant nitrogen flow rate was passed through the quartz tube to remove the air from the system, and then the reactor was heated at 700 ^{o}C under nitrogen flow. Subsequently, nitrogen was replaced by a mixture of acetylene/nitrogen.

Commercial MWCNTs were obtained from Nanothinx S.A. (Patra, Greece). In particular, two types of commercial nanotubes were used in this study: NTX1 (pure MWCNTs, REF) and NTX5 (MWCNTs functionalized with –COOH groups, O-REF). The physical characteristics of these nanomaterials (according to the technical datasheet) are presented in Table 7. Additionally, a TEM image of the NTX1 nanomaterial is presented in Figure 23A.

The NM-401 MWCNT preparation was obtained from the JRC Nanomaterials Repository hosting representative industrial nanomaterials (Ispra, Varese, Italy). This nanomaterial is classified as a Representative Test Material (RTM) and includes a (random) sample from one industrial production batch sub-sampled into vials under reproducible (GLP) conditions, with the stability of the sub-samples monitored. A detailed physico-chemical characterization of this material is provided in the JRC Reports (Rasmussen, Mast et al. 2014).

Carbon nanotubes purification and functionalization process

After the synthesis, the raw products were milled and exposed at atmospheric air flow at 400 ^{o}C for 1h, aiming at the removal of amorphous carbon. Afterwards, they were purified with constant boiling of 5M HCl in a Soxhlet extractor in order to remove the remaining metal particles. Finally, the purified CNTs were washed with distilled water and dried in oven. To activate the CNT surface with –COOH groups (O-CNT1, O-CNT2 and O-CNT3), an acid solution mixture of 6 M HNO_3:H_2SO_4 in a ratio of 1:3 was used. Then, the CNTs/acid mixture (0.15 g CNTs/10 ml acid solution) was stirred for 48h at 80 ^{o}C. The suspension was filtered, and the black powder was washed with ethanol, acetone and distilled water and, eventually, dried in oven.

For the preparation of –$CONHCH_2CH_2NH_2$ functionalized (amino) MWCNTs (A-REF), MWCNT-COOH (O-REF) were stirred in a 20:1 mixture of thionyl chloride ($SOCl_2$) and dimethylformamide (DMF) at 70 ^{o}C for 1 day. After the acyl-chlorination, MWCNTs were centrifuged and washed with anhydrous tetrahydrofuran (THF) for five times. The remaining solid was dried under vacuum. The produced acyl-chlorinated MWCNTs reacted with ethylenediamine solution at 100 ^{o}C for 2 days. After cooling at room temperature, the MWCNTs were washed with ethanol to remove excess diamine. Finally, the material was dried overnight at room temperature and under vacuum (Ramanathan, Fisher et al. 2005).

Characterization techniques

X-ray diffraction: The measurements were performed at room temperature with a Bruker D8 Advance Twin Twin X-ray diffractometer (Bruker Corporation, The Woodlands, TX 77381, USA) equipped with a Cu Ka radiation source (wavelength = 1.5418 Å).

Thermogravimetric analysis: The TGA experiments were conducted in oxidative atmosphere (atmospheric air flow: 120mL/min, heating rate: 5°C/min) with a Netzsch 409EP instrument (NETZSCH-Gerätebau GmbH, 95100 Selb, Deutschland).

Scanning electron microscopy: The morphology of CNTs was determined using a Nova NanoSEM 230 (FEI Inc., Hillsboro, OR, USA) microscope with W (tungsten) filament.

Transmission electron microscopy: TEM measurements were performed with a Tecnai G2 Spirit Twin 12 microscope (FEI Inc., Hillsboro, OR, USA) after the dispersion of CNTs in distilled water.

Fourier transform infrared spectroscopy: FT-IR analysis was performed by using a ThermoScientific Nicolet 6700 Fourier Transform Infrared Spectrometer (Thermo Fisher Scientific Inc., Waltham, MA, USA).

Surface area analysis: Brunauer, Emmett and Teller (BET) analysis was performed with a Micromeritics TriStarII 3020 instrument. The specific area was determined by a 5-point BET measurement with UHP nitrogen as the adsorbate and liquid nitrogen as the cryogen.

Characterization of MWCNT Suspension Stability Index

A kinetic analysis of suspension stability was performed by monitoring the absorbance of the suspension at 550 nm for different times, using an UV-Vis DU650 spectrophotometer (Beckman Coulter SpA, Milano, Italy). Typically, 1 mL of the MWCNT suspension at 128 μg/mL was prepared, and absorbance readings were taken at 5 min intervals for 35 min.

Analysis of adsorbed proteins

To analyze proteins adsorbed to MWCNT, two aliquots of each preparation (REF, O-REF, A-REF) suspended at 1.28 mg/ml in PBS + 0.05% BSA were diluted 1:10 in DMEM + 10% FBS or in plain DMEM. After a 1h-incubation at 37°C under continuous stirring, samples were rapidly centrifuged at 12,000 RPM and the pellets were washed three times in bi-distilled water. The pellets were then suspended in 30 μl of sample buffer (31.25 mM Tris–HCl, pH 6.8, 3% SDS, 10% glycerol100 mM, DTT, 0.02% bromophenol blue) and boiled for 10 min. Aliquots of 20 ml were used for SDS-PAGE. After the electrophoresis, gels were washed in water and stained with silver staining (Cosmo Bio Co., Ltd., Tokyo, Japan, Cat. No. 423413) according to manufacturer's instructions.

In parallel, the pellets of other two aliquots, also incubated in DMEM + 10% FBS or in plain DMEM, were suspended in water, and proteins quantified with a modified micro-Lowry procedure (Bianchi, Franchi-Gazzola et al. 2012).

Dispersion of NM and experimental treatments

For treatments, cells were seeded in 96-well dishes at a density of $1.5x10^4$ cells/well for viability experiments and in 24-well dishes at a density of $1x10^5$ cells/well for nitrite determination. MWCNTs were added from stock solutions (2.56 mg/mL) prepared according to a modified Nanogenotox protocol (http://www.nanogenotox.eu/files/PDF/web%20nanogenotox%20dispersion%20protocol.pdf) in which water was replaced with Ca- and Mg-free PBS, in order to maintain the physiological osmolality. Doses of materials were expressed in $\mu g/cm^2$ of monolayer; a fixed proportion was maintained between the culture surface and the volume of incubation, so as to maintain the relationship between doses in $\mu g/cm^2$ and doses in $\mu g/mL$ (dose in $\mu g/cm^2$ x 1.6 = doses in $\mu g/mL$) fixed.

No surfactant agent was employed, since it has been decided to allow aggregation so as to characterize CNT toxicological properties under conditions resembling a real-life, exposure.

Results

MWCNT characterization

After the synthesis, purification and functionalization of MWCNTs, their structure, chemical composition and purity were investigated in the Laboratory of Prof. Constantinos Charitidis (National Technical University of Athens (NTUA), Greece). Table 7 summarizes the features of the MWCNT preparations tested. In Figure 23, TEM images of selected MWCNT samples are shown. Hollow filamentous structures were revealed for all samples and their specific characteristics were found to vary according to the different production method. In particular, the diameter of MWCNTs ranges between 20 to 100 nm depending on the experimental conditions adopted for synthesis. In all cases, the length of CNTs ranges between 10 and 30 μm. Iron particles could be seen mostly encapsulated within the core of the MWCNTs, so that their interaction with the culture medium is expected to be negligible.

SEM images of the CNT preparations produced in the laboratory of Prof. Charitidis (NTUA, Greece), is depicted in Figure 24, along with a representative EDS analysis, XRD diagram and TGA graph of the CNT3 sample. In Figure 24A, 24B, 24C and 24D the SEM images and the corresponding EDS analysis revealed uniform diameter distribution and high purity. The main features of XRD patterns of CNTs were close to those of graphite (Figure 24E); a typical XRD pattern consisted of bands located near the (002), (100) and (110) reflections of graphite. The first peak at $2\theta \sim 26^{o}$ can be attributed to the (002) reflection of graphite while an asymmetric diffraction peak at $2\theta \sim 43^{o}$ was assigned to the (100) reflection of graphite, which is typically observed for MWCNTs (Peigney, Laurent et al. 1998; Philippe, Caussat et al. 2009). TGA was used in order to evaluate the thermal stability and the purity degree of the produced CNTs (Figure 24F). The initial weight loss of 1.5%, observed at temperatures up to 480 ^{o}C, could be attributed to the burning of amorphous carbon material. The residual weight at the end of the thermal oxidative curve (5.7%) corresponded to the iron catalyst particles. The differential thermogravimetric analysis (DTA) curve showed only one narrow peak at 560 ^{o}C indicating the high thermal stability in air atmosphere and the uniform graphitized structure of the CNTs produced. The overall purity of CNT3 was around 92.8%. There were no substantial differences among the various raw MWCNT preparations for EDX and XRD results (not shown). Table 7 includes the TGA data for all the MWCNT preparations.

The functionalization process was studied via FT-IR spectroscopy and TG analysis. Specifically, FTIR spectra of pristine MWCNTs (REF), MWCNTs-COOH (O-REF) and MWCNTs-amino (A-REF) are shown in Figure 25A. Comparing the pristine MWCNTs and MWCNTs–COOH, some new peaks

appeared in the spectrum of MWCNTs-amino. In particular, the C=O stretching frequencies shifted from 1704 cm^{-1} (MWCNTs–COOH) to 1660 cm^{-1} (MWCNTs-amino) and a new peak appears at 1564 cm^{-1}, which could be assigned to N–H in plane. These bonds pointed to the existence of a secondary amine on the sidewalls of MWCNTs-amino.

Thermogravimetric analysis was applied to quantify the functionalization degree of O-REF and A-REF samples (Chronopoulos, Kokotos et al. 2015). From Figure 25B, it is clear that the thermal degradation of the modified CNTs is a multistage process. The weight loss occurs at temperatures up to 160 – 200 °C (~1.3% for O-REF and ~4.7% for A-REF) and is associated with the release of moisture which is physically or chemically absorbed. CNTs-COOH (O-REF) and CNTs-amino (A-REF) samples exhibit a first weight loss at 180–450 °C (~4.4%) and 200–400 °C (~8.7%) corresponding to the burning of the carboxyl and -$CONHCH_2CH_2NH_2$ groups, respectively. The second loss (temperatures above 400 – 450 °C) is attributed to the CNT burning (Datsyuk, Kalyva et al. 2008; Zhao, Yang et al. 2013; Chronopoulos, Kokotos et al. 2015). The approximate molar % functional groups on CNTs were estimated (Zhao, Yang et al. 2013) equal to ~1.3 mole % for both cases, indicating the high conversion of the functionalization process.

Overall, the three CNT preparations do not present significant differences in their specific area. BET analysis revealed the following results: 104 m^2/g (REF), 119 m^2/g (O-REF) and 105 m^2/g (A-REF). It can be observed that after –COOH functionalization, MWCNTs showed a slight increase in their specific area. This may be attributed to the oxidation treatment that creates sidewall openings and defects. On the other hand, the attachment of amino functional groups does not lead to a comparable increase, since the groups added are more bulky than –COOH ones, blocking CNT pores (Carabineiro, Pereira et al. 2011; Birch, Ruda-Eberenz et al. 2013).

The Suspension Stability Index was determined for REF, O-REF and A-REF at the maximal concentration used in the biological experiments (128 μg/mL, corresponding to a monolayer exposure of 80 $\mu g/cm^2$) according to the method described by Wang et al (Wang, Xia et al. 2010). The results (Figure 26) indicate that the suspension of pristine MWCNT (REF) was less stable than carboxyl- (O-REF) or amino-functionalized MWCNT (A-REF) dispersed in PBS (Panel A). However, this pattern was reversed upon the addition of proteins, since REF suspension was more stable than O-REF and A-REF suspensions in either PBS + BSA or medium (DMEM) + 10% FBS. These data suggest that, in protein-rich media, larger agglomerates are formed by O-REF and A-REF MWCNTs. The stability of REF and A-REF samples was roughly comparable in the two protein-rich suspension media, while O-REF suspensions were less stable in PBS + BSA than in medium + FBS.

Table 7. Sample specifications and characteristics

Code	Supplier	Production method	Functionalization	Diameter (nm)	Length (μm)	Purity (%)	SSA (m^2/g)
CNT1	Laboratory of Prof. Charitidis (NTUA, Greece)	CVD Carbon source: camphor Catalyst: ferrocene	-	60-100	10-30	88-90	37
O-CNT1[a]	Laboratory of Prof. Charitidis (NTUA, Greece)	CVD Carbon source: camphor Catalyst: ferrocene	–COOH	60-100	10-30	>90	-
CNT2	Laboratory of Prof. Charitidis (NTUA, Greece)	CVD Carbon source: acetylene Catalyst: Fe particles	-	40-60	10-30	92-94	58
O-CNT2[a]	Laboratory of Prof. Charitidis (NTUA, Greece)	CVD Carbon source: acetylene Catalyst: Fe particles	–COOH	40-60	10-30	>95	-
CNT3	Laboratory of Prof. Charitidis (NTUA, Greece)	CVD Carbon source: acetylene Catalyst: Fe particles	-	20-40	10-30	92-94	96
O-CNT3[a]	Laboratory of Prof. Charitidis (NTUA, Greece)	CVD Carbon source: acetylene Catalyst: Fe particles	–COOH	20-40	10-30	>95	-
REF	Nanothinx (NTX-1)	CVD	-	15-35	10-30	97	104
O-REF[a]	Nanothinx (NTX-5)	CVD	–COOH	15-35	10-30	97	119
A-REF[b]	Nanothinx (NTX-5)	CVD	$–CONHCH_2$ CH_2NH_2	15-35	10-30	97	105
NM-401[c]	JRC	CVD	-	40-90	2-6	75-89	140

[a] O-CNT1,2,3 and O-Ref indicate the oxidized forms (COOH functionalized) of the corresponding CNT preparations

[b] A-REF was amino-functionalized in Charitidis laboratory starting from O-REF

[c] From data reported in (Rasmussen, Mast et al. 2014)

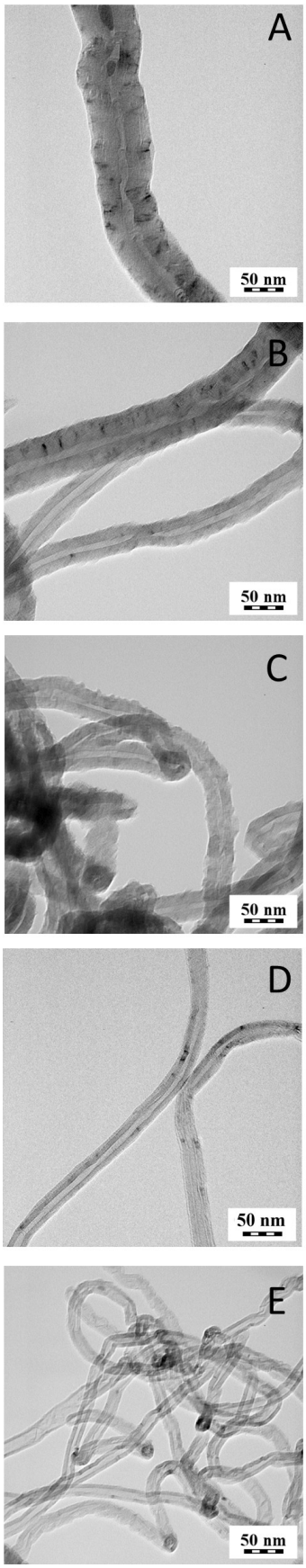

Figure 23. TEM images of O-CNT1 (a), CNT2 (b), O-CNT2 (c), CNT3 (d), REF (e).

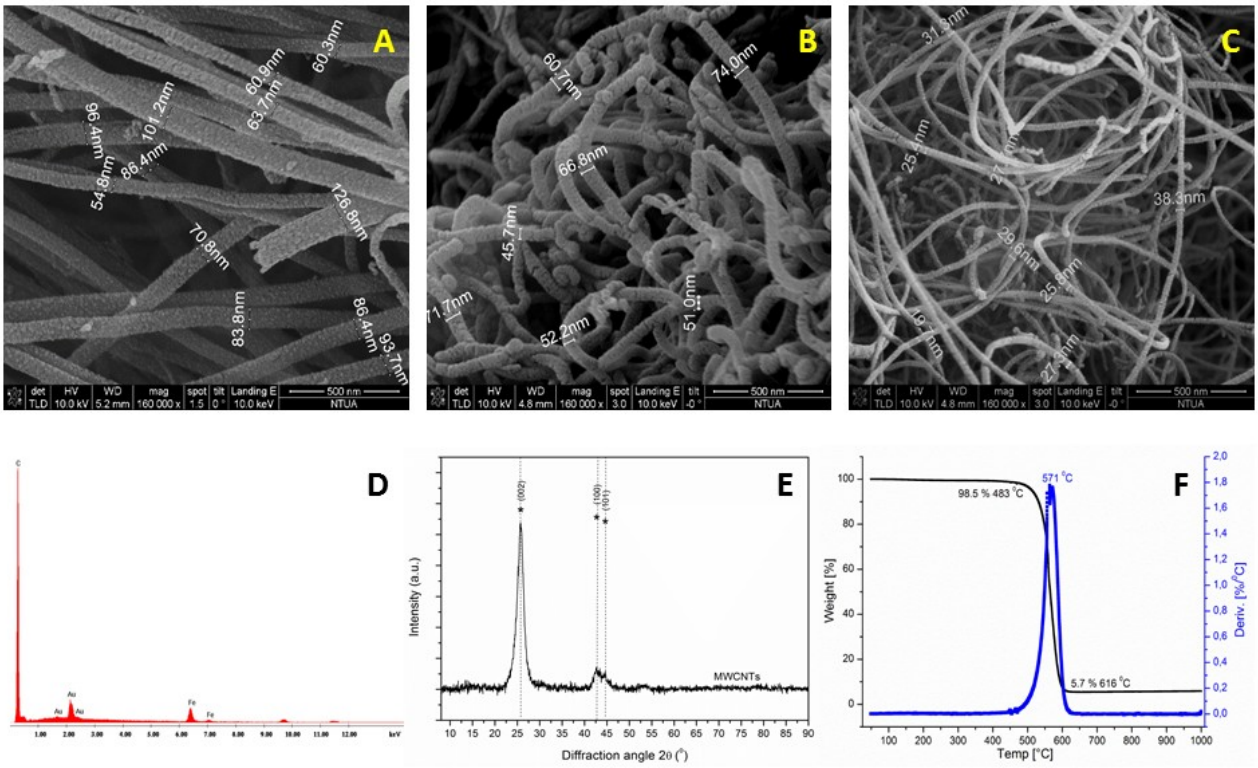

Figure 24. SEM images of (A) CNT1, (B) CNT2 and (C) CNT3; (D) EDS analysis, (E) XRD diagram and (F) TGA graph of CNT3.

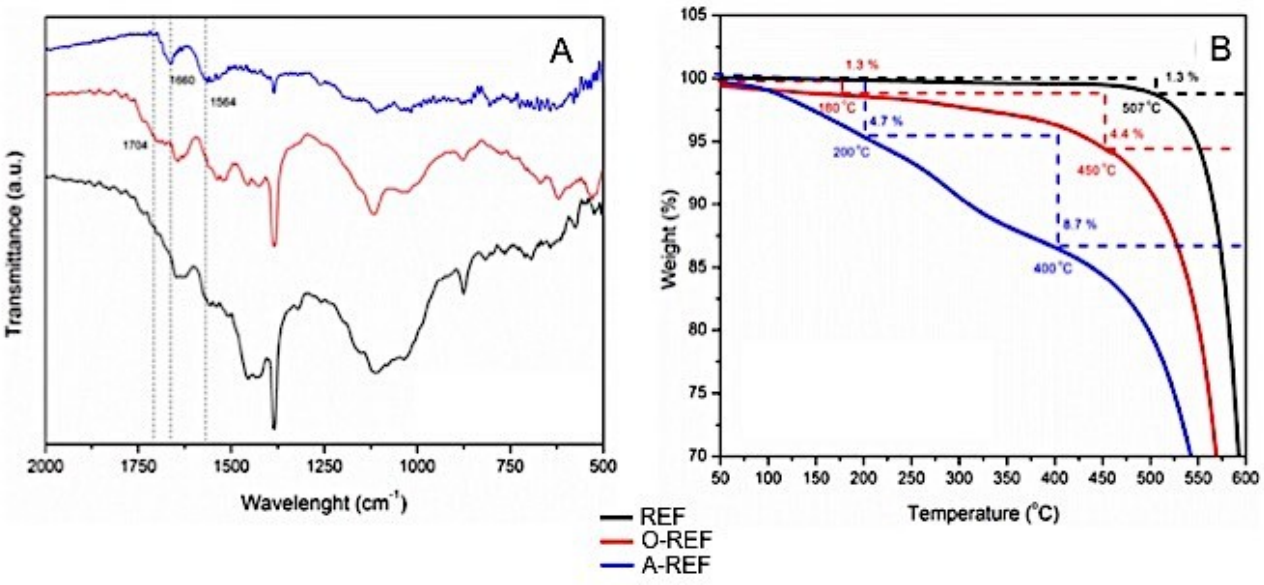

Figure 25. FTIR spectra (A) and TGA graphs (B) of pristine MWCNT (REF), MWCNT–COOH (O-REF) and MWCNT-amino (A-REF) samples.

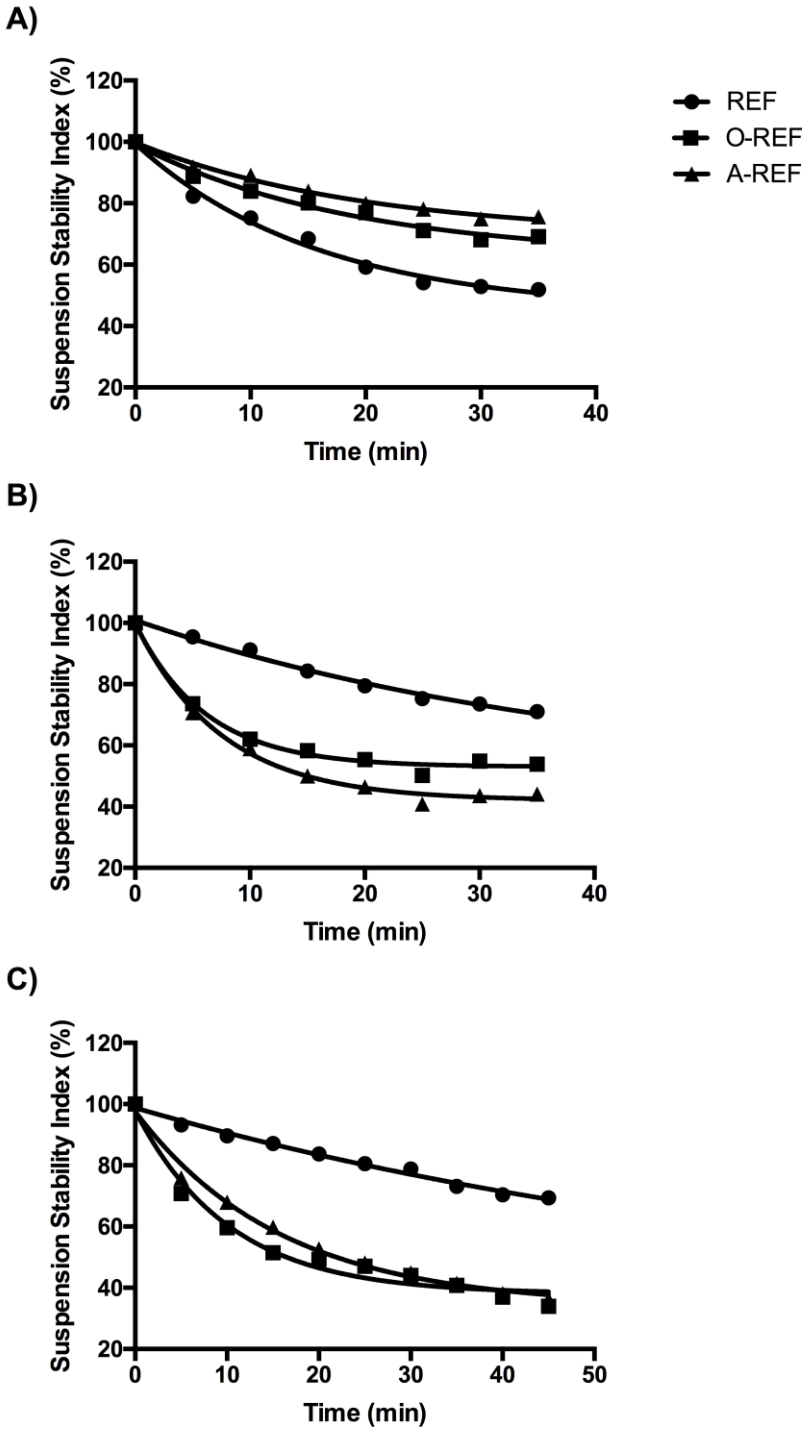

Figure 26. Suspension Stability index of the three preparations of MWCNT. The Suspension Stability Index of the three MWCNT preparations at 128 μg/mL was expressed as the % of the initial absorbance at the indicated times. The absorbance measurements were carried out as described in Materials and Methods. Panel A, MWCNTs were suspended in PBS (Ca- and Mg-free). Panel C, MWCNTs were suspended in growth medium (phenol-red free DMEM) supplemented with 10% FBS. The figure shows a representative experiment, repeated twice with comparable results.

Interaction of MWCNTs with proteins

In order to evaluate the binding of serum proteins with MWCNTs, REF, O-REF and A-REF were incubated with culture medium supplemented with 10% FBS. Proteins adsorbed to MWCNTs were then quantified with a colorimetric method or detected with silver staining after polyacrylamide gel electrophoresis (Figure 27). Quantification of adsorbed proteins (Panel A) evidenced that, although all the three MWCNT preparations bound serum proteins, the amount of adsorbed proteins was significantly higher for functionalized MWCNTs than pristine counterpart (A-REF > O-REF > REF). Moreover, the adsorbed protein pattern was different for the three MWCNTs preparations, with few bands clearly more abundant and other absent in each of the three materials (Panel B).

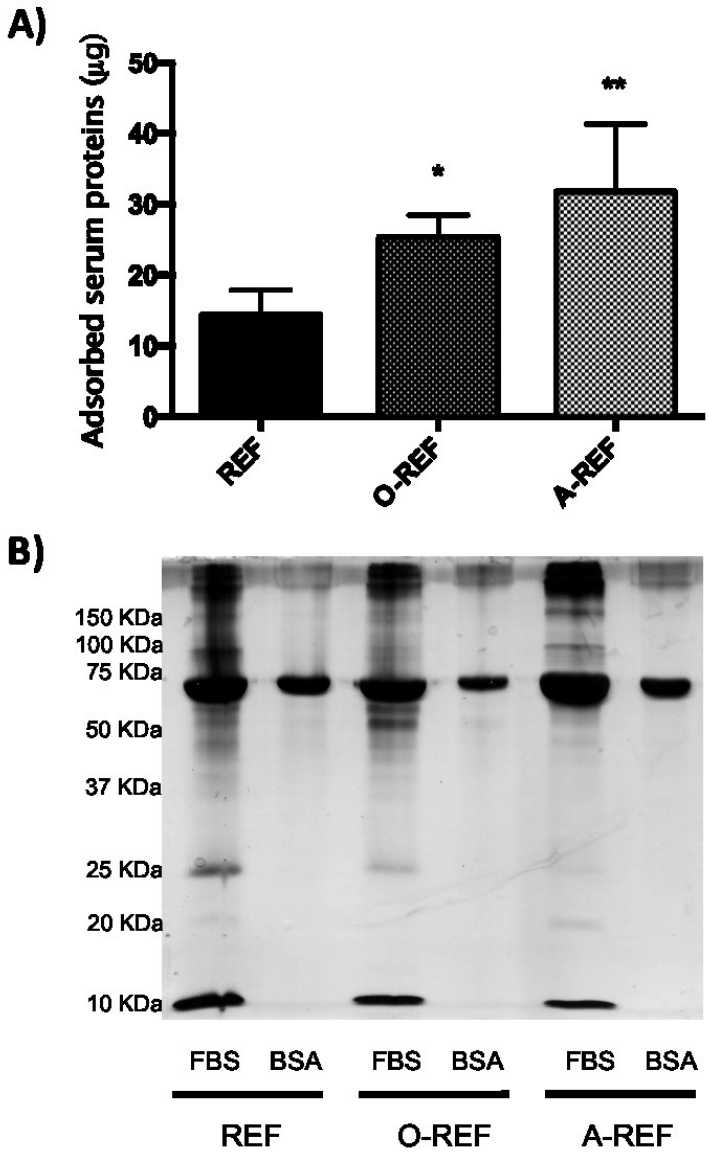

Figure 27. Protein adsorption on MWCNTs. MWCNT preparations, dispersed in 0.05 wt% BSA, were incubated at the concentration of 128 µg/ml for 1h in culture medium with or without 10% FBS. At the end of the incubation, the suspensions were centrifuged, and adsorbed proteins quantified (A) or separated and stained (B) as described before. For (A), data are means ± SD of 4 independent determinations. *$p < 0.05$, ** $p < 0.01$ *vs.* REF, as evaluated by one-way ANOVA for multiple comparison with Tukey correction. For (B) a representative experiment, performed twice with comparable results is shown.

Cell viability

The effect of the different MWCNT preparations (dose range 2.5-80 μg/cm^2) on the viability of Raw264.7 macrophages was tested with the resazurin assay after a 72h-exposure to the materials (Table 8). NM-401 MWCNT, which have been found to be endowed with marked cytotoxic effects towards Raw264.7 macrophages (unpublished results), were used as a benchmark. While NM-401 produced a clear cut dose-dependent decrease of cell viability, only mild effects were observed for the other MWCNT. In particular, no decrease in viability was observed with MWCNT wider than 40 nm. On the other hand, MWCNT preparations with diameters between 15 and 40 nm produced only mild decrease in viability, although no material, but the benchmark NM-401, caused a viability loss larger than 50%. The direct comparison among the IC_{20} values obtained with pristine MWCNTs of different diameter indicated that toxicity was roughly inversely proportional to diameter (REF = CNT3 > CNT2 = CNT1). Given that NM-401 are long, needle-like, while our samples are even longer, but entangled, we can speculate that toxicity is also associated with MWCNT shape, although this issue has not been further investigated.

Functionalization with COOH groups did not change substantially MWCNT effects on cell viability although IC_{20} values of the functionalized O-CNT3 and O-REF were larger than those obtained for the corresponding pristine preparations CNT3 and REF, indicating a modest mitigating effect.

To further investigate the effects of functionalization on MWCNT toxicity, the human airway epithelial cells A549, a cell model widely adopted in toxicological studies, have been used. Unpublished results from our laboratory had indicated that these cells are more sensitive than macrophages to MWCNT toxic effects. On these cells, three preparations (pristine, carboxyl-functionalized and amino-functionalized) of the thinnest MWCNT (listed in Table 7) have been studied. The results (Figure 28) revealed that the pristine REF determined a clear-cut dose dependent decrease of cell viability up to 35% at the maximal dose (80 μg/cm^2). A much slighter, but still significant decrease was instead observed in the case of the COOH-functionalized preparation O-REF (up to 7% at the maximal dose). On the contrary, the amino functionalized A-REF did not show a significant cytotoxic effect even at the highest dose tested (80 μg/cm^2). As expected, the benchmark NM-401, used at the dose of 80 μg/cm^2, determined a marked decrease (around 50%) of cell viability. Thus, when assessed in epithelial cells, MWCNT toxicity seemed to be inversely related to the CNT diameter, while functionalization with either COOH or amino groups mitigated the toxic effect.

To deepen the investigation of the effect of functionalization on cell viability, the different MWCNT preparations (2.5 - 5 μg/cm^2) were studied with a CFE assay on A549 (Figure 29). Only the pristine REF preparation determined a significant decrease of colony number at the highest dose tested of 5 μg/cm^2, while the other MWCNTs did not produce significant effects. The benchmark material NM-401 induced a significant dose dependent decrease of colony number up to 45% at the highest dose tested of 5 μg/cm^2.

Table 8. Effect of MWCNTs on cell viability of Raw264.7 macrophages

Code	IC_{50} ($\mu g/cm^2$)	IC_{20} ($\mu g/cm^2$)
CNT1	>80	>80
O-CNT1	>80	>80
CNT2	>80	>80
O-CNT2	>80	>80
CNT3	>80	23.9
O-CNT3	>80	46.9
REF	>80	29.1
O-REF	>80	39.2
A-REF	ND	ND
NM-401	26.4	9.9

ND, Not determined

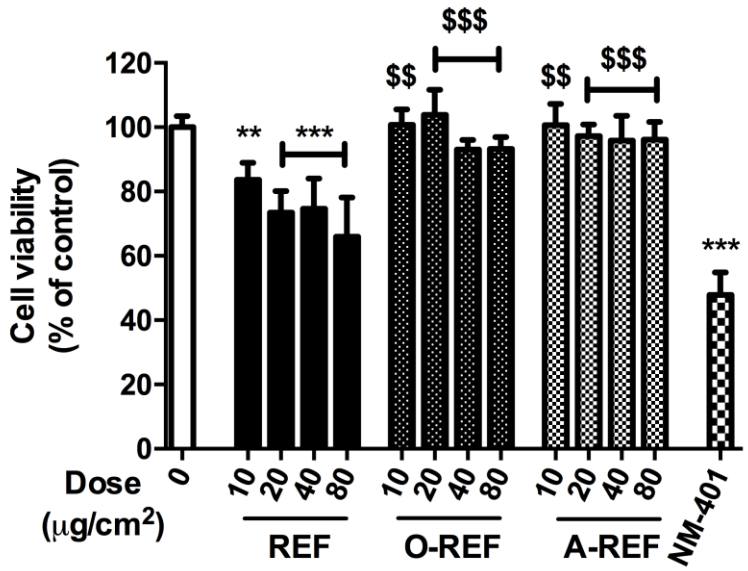

Figure 28. Cell viability of A549 cells exposed to MWCNTs. Cells were treated with increasing doses of MWCNT (range dose 10-80 μg/cm^2 for REF, O-REF and A-REF; 80 μg/cm~~2~~ for NM-401). After 48h cell viability was determined with the resazurin assay. 0, control untreated cells. Data are means ± SD of 6 indipendent determinations obtained in two separate experiments. ** $p < 0.01$, *** $p < 0.001$ vs. control, untreated cells (0); $$ $p < 0.01$, $$$ $p < 0.001$ vs. equivalent doses of REF, as evaluated by one-way ANOVA for multiple comparisons with Tukey correction.

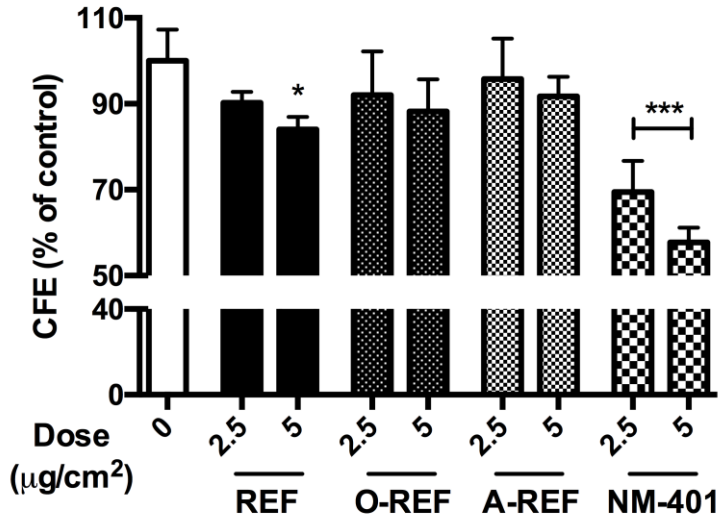

Figure 29. Colony forming efficiency of MWCNT-treated A549 cells. Cells were seeded at a concentration of 100 cells/plate and treated as described in Materials and Methods. Data are means of 4 indipendent determinations. * $p<0.05$, *** $p<0.001$ *vs*. control, untreated cultures, as evaluated by one-way ANOVA for multiple comparisons with Tukey correction.

Macrophage activation

Macrophages play a pivotal role in determining the final outcome of the interaction between nanomaterials and the organism. In particular, if the exposure to the nanomaterial leads to macrophage activation, this triggers an inflammatory response.

Figure 30 reports data on the production of NO, a major inflammatory mediator produced by activated macrophages, and on the expression of pro-inflammatory genes in Raw264.7 cells exposed to MWCNTs. Panels A and B report data on NO production, assessed from the nitrite concentration in the medium after 48h (A) or 72h (B) of treatment of Raw264.7 cells with increasing doses of REF, O-REF and A-REF (range 20-80 μg/cm^2). The NM tested induced dose- and time-dependent increases in NO production with different potencies. In detail, the pristine REF determined the strongest macrophage activation with a rank of pro-inflammatory activity REF > O-REF ≅ A-REF. This rank was also observed for the stimulation of NO production in a different model, the alveolar murine macrophages MH-S, which have a lower basal NO output than Raw264.7 cells. In these cells, nitrite medium concentration in untreated cells was 0.18 μM ± 0.16 and increased by 12-fold ($p < 0.001$) with REF, 3-fold (not statistically significant) with O-REF, and 2-fold (not statistically significant) for A-REF. This rank was maintained also for the induction of a related pro-inflammatory marker, the *Nos2* gene, which encodes for the inducible form of nitric oxide synthase (Nos2) (Panel C). The higher effect of REF on macrophage activation was not limited to NO production and *Nos2* induction but involved also the expression of other three important pro-inflammatory genes: *Ptgs2* (Panel D), which encodes for the inducible form of cyclooxygenase, *Il6*, the gene for the inflammatory cytokine interleukin-6 (Panel E), and *Il1b (*Panel F*),* the gene for IL-1β.

Figure 31 reports phase contrast and confocal images of Raw264.7 cells treated with 80 μg/cm^2 of MWCNTs. In the case of REF (Panel B), MWCNTs appear to be more dispersed with smaller agglomerates than those observed with O-REF (Panel C) and A-REF (Panel D). In all cases, macrophages appear to adhere to the MWCNT agglomerates, to climb on the material, as indicated by the orthogonal projections, and to become markedly elongated, a morphological hallmark of activation. The smaller size of REF agglomerates facilitated macrophage phagocytic activity, as demonstrated by the more diffuse presence of intracellular MWCNTs in this preparation. On the contrary, large agglomerates were not internalized by macrophages.

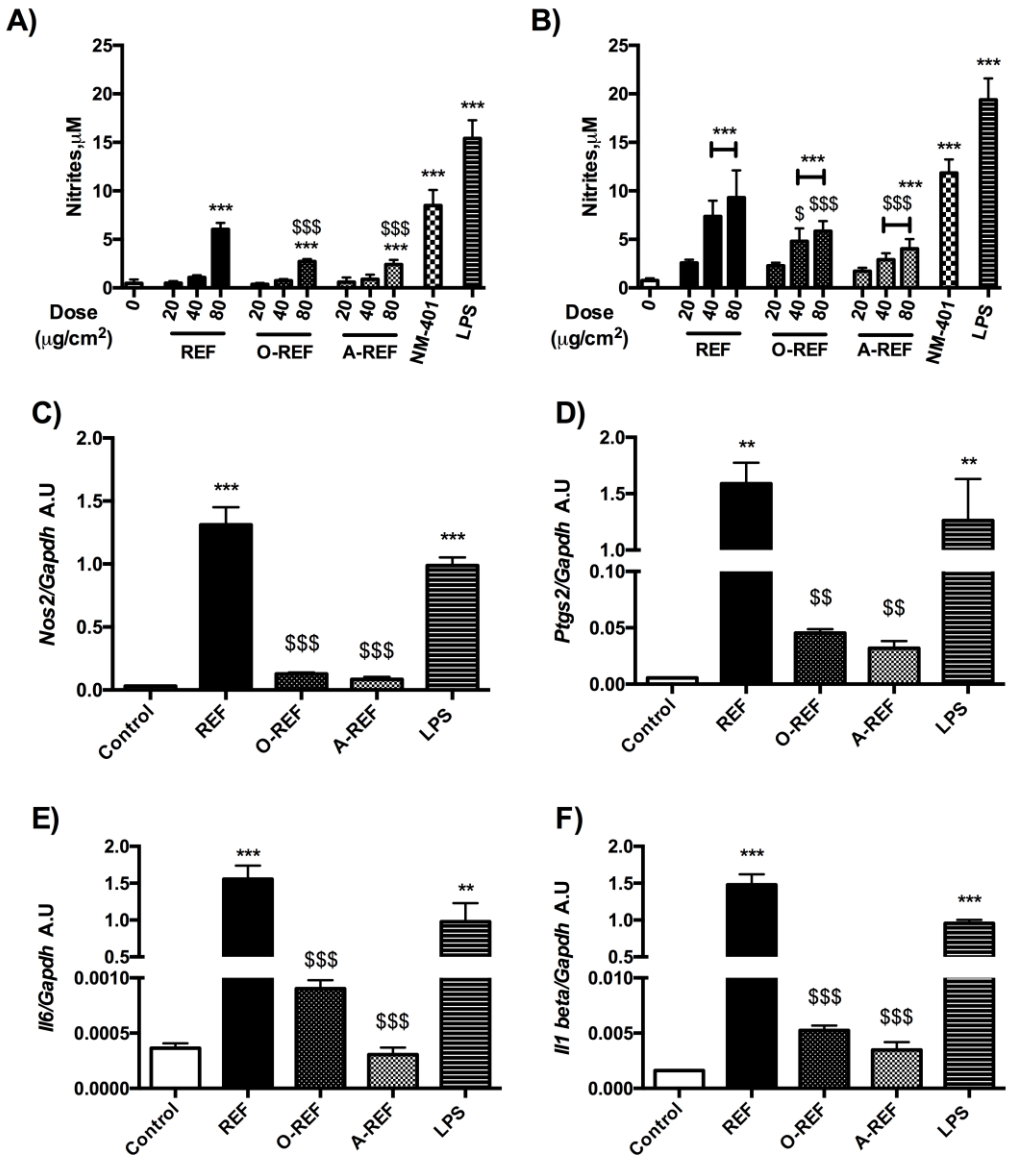

Figure 30. **Expression of pro-inflammatory markers in Raw264.7 exposed to MWCNTs**. Panels A and B. Nitrite concentration in cell culture medium of Raw264.7 cells exposed to MWCNTs. Raw264.7 cells were treated with MWCNTs (REF, O-REF, A-REF: range dose 20-80 μg/cm^2 , NM-401: 80 μg/cm^2). After 48h (Panel A) or 72h (Panel B), the nitrite concentration was determined in the cell culture medium. Lipopolysaccharide (LPS, 10 ng/ml) was used as a positive control. Data are means ± SD of 8 independent determinations obtained in two experiments. Panels C, D, E and F. Expression of *Nos2* (Panel C), *Ptgs2* (Panel D*), Il6* (Panel E) and *Il1 beta* (Panel F), in cells treated with MWCNTs. Raw264.7 cells were treated with the indicated materials at the dose of 80 μg/cm^2. After 18h mRNA was extracted and gene expression was analyzed with RT-PCR. Data are means of 3 independent determinations.
**, *** p< 0.01, p <0.001 *vs.* control, untreated cells. $, $$, $$$ p< 0.05, p< 0.01, p< 0.001 *vs.* REF at the same dose, as evaluated by one-way ANOVA for multiple comparisons with Tukey correction.

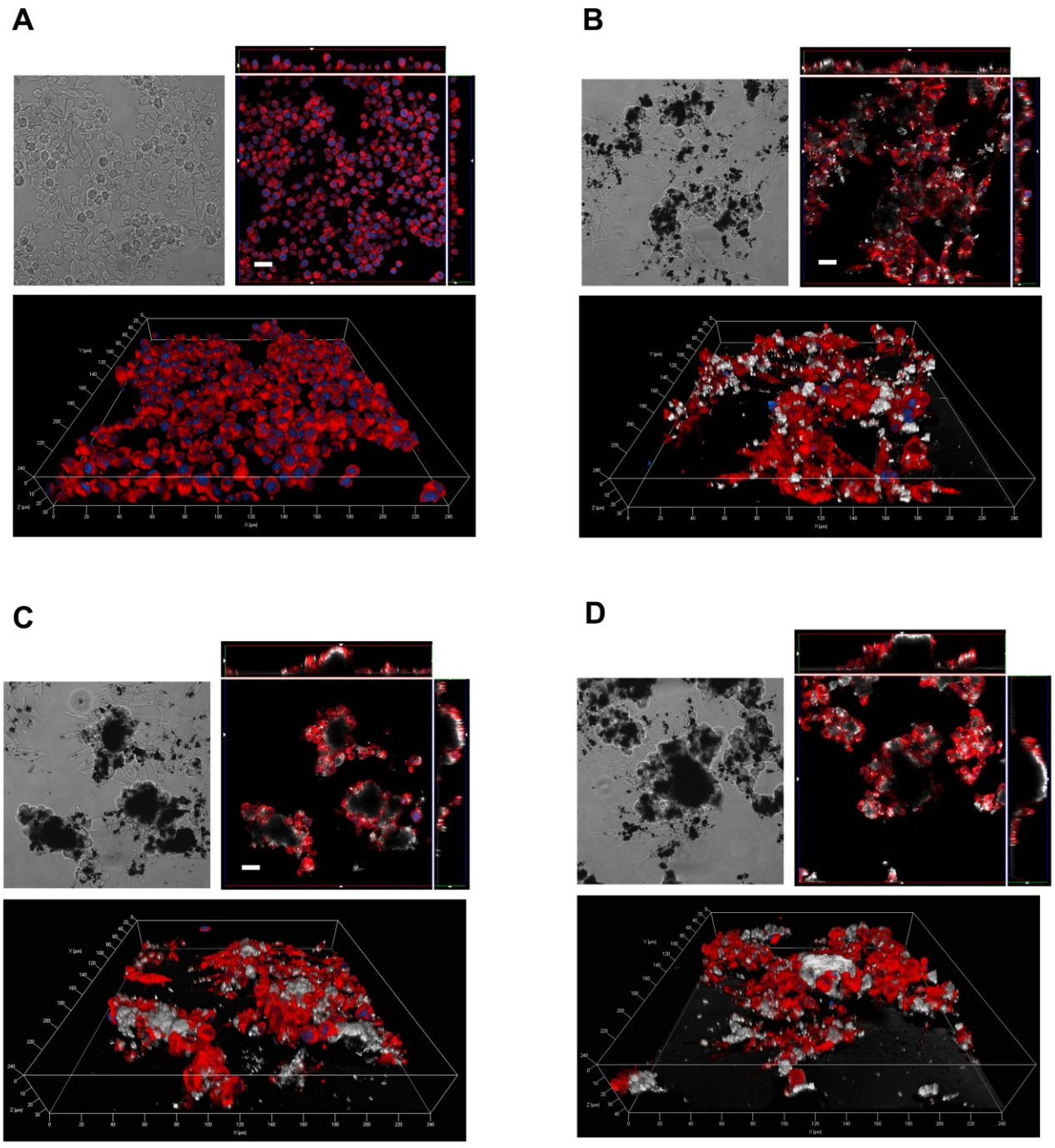

Figure 31. Contrast phase (top left) and confocal images (top right and bottom) of Raw264.7 cells exposed to REF (Panel B), O-REF (Panel C) and A-REF (Panel D) MWCNTs. Cells were treated with 80 µg/cm^2 of each MWCNT preparation for 24h and labelled as described in Methods. The same representative fields are shown in contrast phase (left) and confocal microscopy (right). For each condition, a single horizontal confocal section is shown along with two orthogonal projections. White, MWCNTs (reflectance mode); blue, nuclei; red, cytoplasm. Bars = 20 µm.

Epithelial barrier competence

Figure 32 (Panel A) reports the time course of changes in the Trans-Epithelial Electrical Resistance (TEER) of CaLu-3 cell monolayers exposed to MWCNTs (80 μg/cm^2) up to 12d. TEER is a parameter associated to the integrity and the barrier competence of epithelial monolayers (Rotoli, Bussolati et al. 2008; Banga, Witzmann et al. 2012). REF significantly lowered TEER at 12d with a decrease of 20% compared to control monolayers. Conversely, O-REF and A-REF did not produce any significant effect, while the benchmark material NM-401 produced the largest decrease in TEER (>30% at 12d of treatment). Cell viability, monitored with resazurin assay in the same wells where TEER evaluation was performed, exhibited no significant changes under any experimental condition (Panel C).

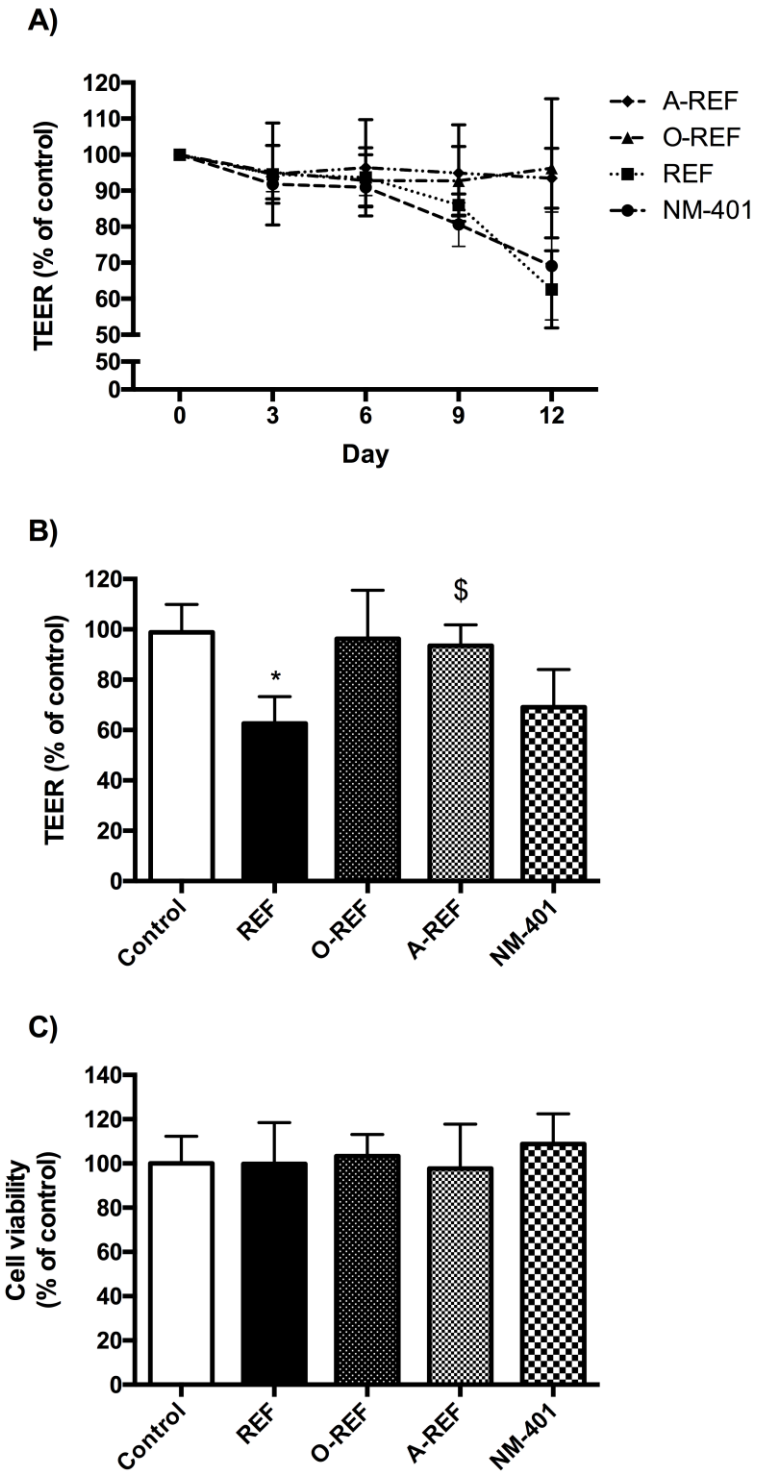

Figure 32. TEER and cell viability of CaLu-3 cell monolayers. Calu-3 cells were seeded on permeable filters as described in Materials and Methods. After a tight monolayer had formed, MWCNTs (80 µg/cm^2) were added to the apical compartment, and exposure prolonged for up to 12 days. At the indicated times, TEER was determined, as described under Methods. (A) TEER (% of control) recorded every 3d up to 12 d. (B) TEER (% of control) at day 12. (C) Cell viability was assessed in the same wells used for TEER determinations with the resazurin assay. For all panels, data are means ± S.D of 4 independent determinations. * $p < 0.05$ vs. control, untreated cultures. The experiment was performed twice with comparable results, as evaluated by one-way ANOVA for multiple comparisons with Tukey correction.

Discussion

Although relatively less studied than the toxicological properties of SWCNTs, also MWCNT toxicity has been repeatedly investigated *in vitro* and *in vivo*. According to the literature, various factors influence the toxicity of MWCNTs and have the potential to modulate their biological effects (Hamilton, Wu et al. 2013). In particular, a correlation has been reported between MWCNT toxicity, their size (Kim, Song et al. 2010; Hamilton, Wu et al. 2013), contamination with metal catalysts (Aldieri, Fenoglio et al. 2013), and surface functionalization (Hamilton, Wu et al. 2013).
However, it is difficult to find examples in literature where differences between two MWCNT preparations are limited to one parameter and, hence, allow a clear-cut assessment of its contribution to the toxicological properties of the nanomaterial. In this study, a panel of MWCNTs of comparable length, that differ for diameter (range 15-100 nm), has been preliminarily compared. Each preparation was available in pristine form or after COOH-functionalization. Low acute toxicity was observed with both types of materials in macrophages, although an increase in toxicity was detected for thinner MWCNTs. In general, while it is usually accepted that the longer are the MWCNTs tested, the higher is their toxicity (Kim, Song et al. 2010; Hamilton, Wu et al. 2013; Sweeney, Grandolfo et al. 2015), contrasting reports exist on the role of diameter. According to some authors, the larger is MWCNT diameter, the higher is the toxicity reported either *in vitro* or *in vivo* models (Hamilton, Wu et al. 2013), whereas the converse has been also described (Eom, Jeong et al. 2015). For diameters larger than 40 nm, functionalization had little effect on the biological effects of MWCNT. To study the effect of functionalization more in depth, we have used, therefore, the thinnest MWCNT preparation, functionalized with either carboxyl or amino groups, and found that the presence of either functional group mitigated effects on cell viability.

Functionalization has been described to enhance toxicity in airway epithelial BEAS-2B cells (Chatterjee, Yang et al. 2014; Ursini, Maiello et al. 2015), while, on the contrary, it has been demonstrated to suppress bioactivity in other epithelial models (Liu, Dong et al. 2014) as well as in macrophages (Hamilton, Wu et al. 2013). Also in vivo models have yielded contrasting results, with mitigating (Jain, Thakare et al. 2011; Sager, Wolfarth et al. 2014) or enhancing (Urankar, Lust et al. 2012) effects reported in different models. In our preparations, toxicity is absent for MWCNT diameters wider than 40 nm, and this outcome was not changed by functionalization. To study the effect of functionalization, therefore, the thinnest MWCNT preparation, functionalized with either

carboxyl or amino groups, has been used, and found that the presence of either functional groups mitigated the effects on cell viability.

The extension of the study to other toxicity-related endpoints offered interesting insights on the relationship between toxicity and structural determinants of MWCNTs. Activating effects on macrophages, an endpoint related to the pro-inflammatory activity of MWCNTs *in vivo*, also indicated a clear cut mitigating effect of surface functionalization. This result is at variance with a recently published report (Zhang, Tang et al. 2015) in which, however, the COOH-functionalized MWCNT used were much shorter than the pristine ones. Also the perturbation of epithelial barriers, assessed through TEER measurements in airway epithelial cell monolayers, was clearly more evident for pristine MWCNTs than for carboxyl- or amino-functionalized derivatives.

For all these endpoints, mitigation of toxic effects was observed with either carboxyl- or amino-functionalized MWCNT. As far as we know, while COOH-functionalized MWCNT has been extensively investigated, the effects of amino-functionalization on MWCNT toxicity have been never evaluated in depth. However, it is interesting that mitigation occurs independently of the net charge present on the MWCNT surface, suggesting that this parameter does not account for the effect.

Another structural difference among REF, O-REF and A-REF consists in their agglomeration tendency, with REF forming relatively small agglomerates, while large MWCNT agglomerates are evident in cell cultures treated with carboxyl- or amino-functionalized counterparts, both in phase contrast and in confocal microscopy. A comparable pattern has been described for other MWCNT preparations of commercial origin (Jackson, Kling et al. 2015). Different tendency to agglomeration of the three preparations tested is consistent with the different sedimentation rates exhibited in both albumin supplemented saline solution and in complete, serum-supplemented culture medium. These data are similar to the results of Hamilton *et al.* (Hamilton, Wu et al. 2013) who, comparing the effects of three preparations of pristine and COOH-functionalized MWCNT, found that, when suspended in cell culture medium, functionalized MWCNT formed larger agglomerates than pristine counterparts. Interestingly, this effect was particularly evident for the MWCNT endowed with a length comparable to the materials tested here. The presence of larger agglomerates has the obvious consequence of lowering the surface available for the interaction between cells and MWCNTs. Thus, if it were expressed per area, it is possible that the actual dose is smaller for O-CNT and A-CNT than for CNT.

The reason for the higher agglomeration tendency exhibited by functionalized MWCNT has not been specifically investigated here. However, the data reported in Figure 26 clearly indicate that MWCNT sedimentation is profoundly influenced by the presence of proteins in the suspension medium. Interestingly, recent data demonstrate that COOH-functionalization has marked effects on the type of proteins adsorbed by MWCNT (Shannahan, Brown et al. 2013), a finding fully consistent with the results obtained in the present study. Indeed, REF, O-REF and A-REF not only adsorb different amounts of proteins (A-REF > O-REF > REF), but the pattern of proteins adsorbed is also different for the three samples. It is, therefore, possible that the greater agglomeration tendency exhibited by functionalized MWCNT depends on their different protein corona.

The role of agglomeration in MWCNT toxicity is still incompletely defined. *In vitro* experiments have indicated that agglomerated MWCNTs are usually poorly toxic (Wirnitzer, Herbold et al. 2009). Greater toxicity of dispersed compared to agglomerated MWCNTs has been confirmed with *in vivo* models (Wako, Kotani et al. 2010), although it should be stressed out that the experimental condition adopted to improve dispersion in that paper, i.e. grinding, also substantially modifies the size of the materials. However, recent work from mine laboratory has indicated that agglomerates of MWCNTs may exert a focal toxicity in monolayers of airway epithelial cells that can be ameliorated increasing MWCNT dispersion (Rotoli, Gatti et al. 2015). In that work, agglomerates of either needle-like or tangled MWCNTs were used. In the present work, while the damaging effect of needle-like MWCNTs (the benchmark material NM-401) on the epithelial monolayer has been confirmed, the comparison among the three preparations of tangled MWCNTs would indicate a greater perturbing effect of smaller agglomerates (REF) compared to the larger ones on epithelial monolayers. This information is of potential relevance, given the marked pathogenic role of the interaction between MWCNTs and airway epithelial cells (Beamer, Girtsman et al. 2013).

Most of the contributions that investigate toxicity mitigation by MWCNT functionalization do not address the possible influence of surface modification on agglomeration tendency. A notable exception is represented by the recent contribution by Ursini *et al.* (Ursini, Maiello et al. 2015). These authors have investigated the effects of pristine MWCNTs, MWCNTs-OH and MWCNTs-COOH on two epithelial models (BEAS-2B and A549) finding different entry mechanisms and differential toxicity of the three preparations. The size of agglomerates was also determined in medium, finding comparable sizes of pristine and MWCNT-COOH. Therefore, these Authors did not further consider agglomeration as a possible toxicity modulator. However, at variance with the materials used here, pristine MWCNT were much longer than MWCNT-COOH, thus rendering

difficult a straightforward comparison. Conversely, Hamilton et al. (Hamilton, Wu et al. 2013), comparing MWCNT preparations of comparable length, measured the size of agglomerates formed by pristine and functionalized MWCNT in culture medium and found that COOH functionalization actually increases the size of agglomerates. However, the possible relationship between this behavior and the reduced bioactivity of functionalized MWCNT, exhibited both *in vitro* (Hamilton, Wu et al. 2013) and *in vivo* (Sager, Wolfarth et al. 2014), was not been further discussed.

As a toxicity determinant, agglomeration may be important not only *in vitro* but also *in vivo*. Recent results (Pauluhn and Rosenbruch 2015) indicate that the aerodynamic particle size was much larger for highly agglomerated dry than for wet-dispersed MWCNTs and that, while the initially deposited pulmonary dose of MWCNTs was three times higher and cell penetration much easier for wet-dispersed MWCNTs, the elimination half-time of dry-dispersed MWCNTs was much longer. The different toxicokinetics observed *in vivo*, along with the diverse toxicological effects observed in this *in vitro* study, suggest that, depending on different agglomeration status, MWCNTs may exert different biological effects and, thus, require the assessment of different endpoints for their toxicological characterization.

In conclusion, the data presented here, while confirming that diameter is inversely related to the bioactivity of MWCNT preparations, indicate that the mitigating effects of carboxyl- or amino-functionalization may be attributable, at least in part, to the greater tendency of functionalized MWCNT to form large agglomerates in protein-rich biological fluids (a schematic representation of the mechanism is presented in Figure 33).

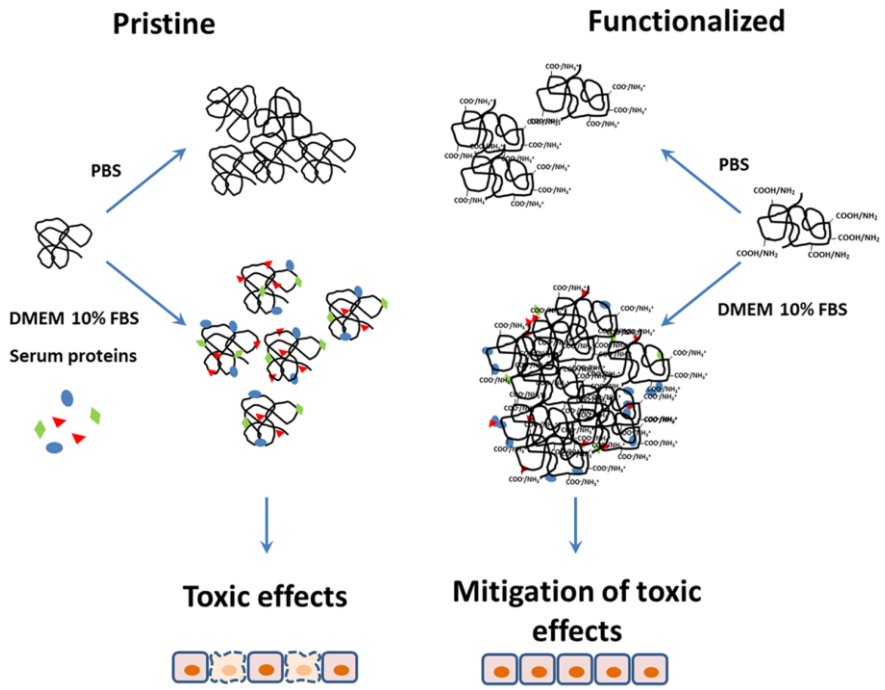

Figure 33. Differential behaviour of pristine and functionalized MWCNT in biological fluids.

CONCLUSIONS

The identification of the biological effects of nanomaterials and the comprehension of the mechanisms underlying their toxic properties has been repeatedly investigated in a lot of studies for a number of years. Many toxicity determinants have been identified for a wide range of nanomaterials. In general, toxicity has been thought to originate from the physico-chemical properties of nanomaterials such as size and surface area, composition, shape and aspect ratio, surface charge, surface roughness, all of which represent extremely important features in determining the interaction of nanomaterials with biological systems.

Two of the most studied toxicity determinants of NM are represented by the shape and aspect ratio. Shape dependent toxicity has been repeatedly reported for several nanoparticles of industrial importance, including carbon nanotubes, silica, nickel, gold and titanium nanomaterials (Ispas, Andreescu et al. 2009) (Hamilton, Wu et al. 2009), and has been codified in the so-called fibre paradigm. In the first part of the thesis this paradigm has been adopted to interpret the effects of length/aspect ratio modification of TiO_2 nanofibres, a novel nanomaterial increasingly used in several industrial fields, on different biological endpoints. Importantly, no modification other than shortening has been introduced, thus allowing a clear cut discrimination of the effects of changes on a single parameter. It has been found that aspect ratio modification can tune the biological behavior of TiO_2 NF. In fact, rather than a generic attenuation of the biological effects, fibre shortening produces a mitigation of endpoints related to cytotoxicity (decrease in cell viability, hemolysis, changes in TEER) but, at the same time, enhances the pro-inflammatory changes in macrophages. Moreover, the interaction with the phagocytic cell has two different outcomes: while long fibres are not efficiently internalized (frustrated phagocytosis), short fibres readily undergo phagocytosis, a process that likely contributes to macrophage activation. TiO_2 nanofibres are a novel material, and no direct experimental evidence on their effects in vivo is available yet. However, extrapolating these findings to an *in vivo* situation, one may speculate that long fibres, through low-grade inflammation and impaired phagocytosis, should be cleared much less rapidly than shorter one. If this hypothesis were validated, long TiO_2 nanofibres would share high bio-persistence with asbestos, a similarity with obvious consequences in terms of possible exposure-associated hazard.

In the second part of the thesis it has been demonstrated that macrophage activation by LPS *in vitro* is markedly enhanced by the simultaneous exposure to TiO_2 NP, suggesting that, when bound to TiO_2 NP, LPS exerts a much more powerful inflammatory effect. Considering these data, it is

possible that some of pro-inflammatory effects elicited by different NM reported in *in vivo* studies could be linked to their capability of binding environmental contaminants such as endotoxins or other PAMPs. Moreover, this aspect is crucial if we consider the exposure to NM that can occur in individuals with inflammatory conditions. In these situations, the composition of biological fluids could be significantly different from normal, with an increased presence of PAMPs or DAMPs, or with higher level of pro-inflammatory molecules such as cytokines. In this scenario, nanomaterials that come into contact with biological fluids may adsorb these biomolecules, delivering them and concentrating them in specific tissues, organs and target cells, likely modulating biological responses *in situ* and, eventually, in the entire organism.

The binding of bioactive immunostimulant molecules onto the surface of nanomaterials and the resulting possibility of positively tuning innate immune system activity is the basic concept of many studies in the field of nanovaccinology. The use of nanotechnology in vaccinology, in particular, has been increasing exponentially in the past decade. In both prophylactic and therapeutic approaches, NP are used as either delivery systems to enhance antigen processing and/or as an immunostimulant adjuvant to activate or enhance immunity.

In general, NP, considered as a high-binding carrier systems, are able to deliver antigens to the immune cells. In this situation, NP co-internalized with the antigen by cells of the immune system, can act as a transient delivery system, or “protect” the antigen until it is released at the target location (Mody, Popat et al. 2013). For these applications, NP have to be endowed with high biocompatibility and have to be easily synthesizable and functionalizable with the desired antigens. Most of the studies in this field adopt polymeric organic NP such as poly(D,L-lactide-co-glycolide) (PLG), poly(D,L-lactic-coglycolic acid) (PLGA) or polystyrene NP as well as inorganic nanoparticles like Gold NP, Silica NP and Carbon NP. Organic and polymeric NP are more biocompatible and, more importantly, biodegradable within the human organism. However, inorganic counterparts are endowed with several advantages such as the rigid structure and controllable synthesis (Kalkanidis, Pietersz et al. 2006).

As far as antigen loading on NP surface are concerned, evidences have been found that complexes of NP and several immunomodulatory compounds can enhance immune cell responses either *in vivo* or *in vitro*. Most of antigens adopted are TLR agonists such as TLR3 agonists (Poly I:C) (Tincer, Yerlikaya et al. 2011; Correia-Pinto, Csaba et al. 2015), TLR1/2 agonists (Heuking, Rothen-Rutishauser et al. 2013) or TLR7/8 agonists such as Imiquimod (Heo and Lim 2014; Stein, Gogoll et

al. 2014). TLR-4 agonists as components of nanocarrier systems have been much less studied then other TLR agonists, while LPS derivatives are commonly used as classical vaccine adjuvants. A very common used LPS derived adjuvant is Monophosphoryl Lipid A (MPL), a detoxified component of LPS derived from *Salmonella minnesota* containing the lipid A moiety that ligates TLR-4 (Ribi, Cantrell et al. 1984). This compound is significantly less toxic than LPS maintaining anyway a strong capability to activate human dendritic cells, which are the most important antigen presenting cells involved in immunomodulatory processes. It also produces a different pro-inflammatory profile compared to LPS, including the production of Type I IFNs, possibly because it may preferentially activate the TRIF *vs.* MyD88 signalling pathways (Okemoto, Kawasaki et al. 2006). Although MPL has been approved for inclusion in different vaccine such as Fendrix ™ (for hepatitis B) and Cervarix ™ (for cervical cancer), its immunomodulatory properties in nanocarrier systems have been much less investigated than those of other TLR agonists. The synergistic effect of LPS and TiO_2 NP shown in this thesis indicate that immunological responses could be tuned also by LPS and, possibly, its derived compounds, included in nanocarrier systems. Supporting this scenario, we have obtained data which demonstrate that the synergistic effect between LPS and TiO_2 NP is not specific for this material but is shared also by other, more biocompatible, NP already used as drug delivery systems, in particular amorphous silica NP (Di Cristo, Movia et al. 2015), gold NP and carboxylated polystyrene NP (unpublished results).

Up to now we have seen that nanostructured materials are endowed with a very high capability to adsorb a wide range of molecules, determining completely different biological effects depending on the adsorbed molecules. We know that in biological fluids, NP or NM tend to adsorb a lot of biomolecules forming the so-called bio-coronae. As already presented in the general introduction of this thesis, one of the most studied bio-coronae is represented by the protein corona. Proteins adsorbed onto the NP/NM surface can modulate their interaction with cells, tissues and organs, depending on the protein corona characteristics. In the third part of the thesis it has been demonstrated that the different biological reactivity of three preparations of MWCNT, pristine or functionalized, was associated with differences in their agglomeration tendency, correlated to their different capability of interacting with culture media proteins. It has been showed that surface chemistry, in particular surface charge, influences the protein adsorption onto the MWCNT surface, allowing to the formation of different protein coronae, which lead to different MWCNT bio-reactivity. While we have clearly demonstrated that functionalization changes the amount and the type of proteins adsorbed to MWCNT, other investigations will be needed to

understand (1) which proteins are selectively adsorbed to pristine and functionalized MWCNT and, even more important, (2) how the structure of adsorbed proteins changes upon the adsorption and how the functionalization modifies the interaction between nanotube surface and the protein. Intuitively, given that pristine MWCNT are extremely hydrophobic, proteins should interact with their surface with hydrophobic domains, usually shielded from protein surface, and this could determine a profound re-arrangement of the protein tertiary structure and even its denaturation. On the contrary, MWCNT functionalized with hydrophilic groups can interact with proteins in their native form. Therefore, functionalization may change not only how many and which proteins are adsorbed, but also the structure (and, hence, the molecular identity) of the proteins adsorbed.

All together, these data demonstrate that the interaction between physico-chemical properties of nanostructured materials and the environment (cells + biological fluids) in which these materials are present is of pivotal importance for the understanding of the biological effects of NM. In particular, bio-persistence and the capability to elicit an effective inflammatory response are attributable to the interaction between NM and macrophages. However, the interaction NM-cells is heavily influenced by the formation at the nano-bio interface of specific bio-coronae that confer a novel biological identity to the nanostructured materials, setting the basis for their specific biological activities.

REFERENCES

Akira, S. and K. Takeda (2004). "Toll-like receptor signalling." Nat Rev Immunol **4**(7): 499-511.
Aldieri, E., I. Fenoglio, et al. (2013). "The role of iron impurities in the toxic effects exerted by short multiwalled carbon nanotubes (MWCNT) in murine alveolar macrophages." J Toxicol Environ Health A **76**(18): 1056-1071.
Anjilvel, S. and B. Asgharian (1995). "A Multiple-Path Model of Particle Deposition in the Rat Lung." Fundamental and Applied Toxicology **28**(1): 41-50.
Aschberger, K., H. J. Johnston, et al. (2010). "Review of carbon nanotubes toxicity and exposure--appraisal of human health risk assessment based on open literature." Crit Rev Toxicol **40**(9): 759-790.
Ashwood, P., R. P. Thompson, et al. (2007). "Fine particles that adsorb lipopolysaccharide via bridging calcium cations may mimic bacterial pathogenicity towards cells." Exp Biol Med (Maywood) **232**(1): 107-117.
Aueviriyavit, S., D. Phummiratch, et al. (2012). "Titanium dioxide nanoparticles-mediated in vitro cytotoxicity does not induce Hsp70 and Grp78 expression in human bronchial epithelial A549 cells." Biological trace element research **149**(1): 123-132.
Bachler, G., N. von Goetz, et al. (2015). "Using physiologically based pharmacokinetic (PBPK) modeling for dietary risk assessment of titanium dioxide (TiO2) nanoparticles." Nanotoxicology **9**(3): 373-380.
Baisch, B. L., N. M. Corson, et al. (2014). "Equivalent titanium dioxide nanoparticle deposition by intratracheal instillation and whole body inhalation: the effect of dose rate on acute respiratory tract inflammation." Part Fibre Toxicol **11**: 5.
Banfield, J. F., D. R. Veblon, et al. (1990). "Transmission electromicroscopy of subsolidus oxidation and weathering olivine." Contributions to Mineralogy and Petrology **106**: 110-123.
Banga, A., F. A. Witzmann, et al. (2012). "Functional effects of nanoparticle exposure on Calu-3 airway epithelial cells." Cell Physiol Biochem **29**(1-2): 197-212.
Beamer, C. A., T. A. Girtsman, et al. (2013). "IL-33 mediates multi-walled carbon nanotube (MWCNT)-induced airway hyper-reactivity via the mobilization of innate helper cells in the lung." Nanotoxicology **7**(6): 1070-1081.
Bhattacharya, K., M. Davoren, et al. (2009). "Titanium dioxide nanoparticles induce oxidative stress and DNA-adduct formation but not DNA-breakage in human lung cells." Part Fibre Toxicol **6**: 17.
Bianchi, M. G., R. Franchi-Gazzola, et al. (2012). "Valproic acid induces the glutamate transporter excitatory amino acid transporter-3 in human oligodendroglioma cells." Neuroscience **227**: 260-270.
Birch, M. E., T. A. Ruda-Eberenz, et al. (2013). "Properties that influence the specific surface areas of carbon nanotubes and nanofibers." Ann Occup Hyg **57**(9): 1148-1166.
Braakhuis, H. M., M. V. Park, et al. (2014). "Physicochemical characteristics of nanomaterials that affect pulmonary inflammation." Part Fibre Toxicol **11**: 18.
Brown, D. M., I. A. Kinloch, et al. (2007). "An in vitro study of the potential of carbon nanotubes and nanofibres to induce inflammatory mediators and frustrated phagocytosis." Carbon **45**(9): 1743-1756.
Bustin, S. A. (2000). "Absolute quantification of mRNA using real-time reverse transcription polymerase chain reaction assays." J Mol Endocrinol **25**(2): 169-193.
Carabineiro, S. A. C., M. F. R. Pereira, et al. (2011). "Effect of the carbon nanotube surface characteristics on the conductivity and dielectric constant of carbon nanotube/poly(vinylidene fluoride) composites." Nanoscale Research Letters **6**.
Casals, E. and V. F. Puntes (2012). "Inorganic nanoparticle biomolecular corona: formation, evolution and biological impact." Nanomedicine (Lond) **7**(12): 1917-1930.
Castranova, V., W. H. Pailes, et al. (1994). "Comparative Cytotoxic Effects of Crocidolite and Its Non-Asbestiform Polymorph on Rat Alveolar Macrophages." Inhaled Particles Vii: 665-673.
Cedervall, T., I. Lynch, et al. (2007). "Understanding the nanoparticle-protein corona using methods to quantify exchange rates and affinities of proteins for nanoparticles." Proc Natl Acad Sci U S A **104**(7): 2050-2055.
Champion, J. A. and S. Mitragotri (2006). "Role of target geometry in phagocytosis." Proc Natl Acad Sci U S A **103**(13): 4930-4934.

Chang, X., Y. Xie, et al. (2015). "Toxicological Characteristics of Titanium Dioxide Nanoparticle in Rats." J Nanosci Nanotechnol **15**(2): 1135-1142.
Charitidis, C. A., P. Georgiou, et al. (2014). "Manufacturing nanomaterials: from research to industry. ." Manufacturing Rev. **1**: 1-19.
Chatterjee, N., J. Yang, et al. (2014). "Potential toxicity of differential functionalized multiwalled carbon nanotubes (MWCNT) in human cell line (BEAS2B) and Caenorhabditis elegans." J Toxicol Environ Health A **77**(22-24): 1399-1408.
Chen, C. C. and J. K. Wang (1999). "p38 but not p44/42 mitogen-activated protein kinase is required for nitric oxide synthase induction mediated by lipopolysaccharide in RAW 264.7 macrophages." Molecular Pharmacology **55**(3): 481-488.
Chen, X., U. C. Tam, et al. (2006). "Interfacing carbon nanotubes with living cells." J Am Chem Soc **128**(19): 6292-6293.
Cheng, C., K. H. Muller, et al. (2009). "Toxicity and imaging of multi-walled carbon nanotubes in human macrophage cells." Biomaterials **30**(25): 4152-4160.
Cho, H. H., H. Huang, et al. (2011). "Effects of Solution Chemistry on the Adsorption of Ibuprofen and Triclosan onto Carbon Nanotubes." Langmuir **27**(21): 12960-12967.
Cho, W.-S., R. Duffin, et al. (2013). "Predictive value of in vitro assays depends on the mechanism of toxicity of metal oxide nanoparticles." Particle and fibre toxicology **10**(1): 55.
Cho, W.-S., R. Duffin, et al. (2012). "Differential pro-inflammatory effects of metal oxide nanoparticles and their soluble ions in vitro and in vivo; zinc and copper nanoparticles, but not their ions, recruit eosinophils to the lungs." Nanotoxicology **6**(1): 22-35.
Cho, W. S., R. Duffin, et al. (2012). "Zeta Potential and Solubility to Toxic Ions as Mechanisms of Lung Inflammation Caused by Metal/Metal Oxide Nanoparticles." Toxicological Sciences **126**(2): 469-477.
Chronopoulos, D. D., C. G. Kokotos, et al. (2015). "Functionalized multi-walled carbon nanotubes in an aldol reaction." Nanoscale **7**(6): 2750-2757.
Correia-Pinto, J. F., N. Csaba, et al. (2015). "Chitosan-Poly (I:C)-PADRE Based Nanoparticles as Delivery Vehicles for Synthetic Peptide Vaccines." Vaccines (Basel) **3**(3): 730-750.
Cui, H. F., S. K. Vashist, et al. (2010). "Interfacing carbon nanotubes with living mammalian cells and cytotoxicity issues." Chem Res Toxicol **23**(7): 1131-1147.
Dankovic, D., E. Kuempel, et al. (2007). "An approach to risk assessment for TiO2." Inhalation toxicology **19 Suppl 1**: 205-212.
Darabi Sahneh, F., C. Scoglio, et al. (2013). "Dynamics of nanoparticle-protein corona complex formation: analytical results from population balance equations." PloS one **8**(5): e64690.
Datsyuk, V., M. Kalyva, et al. (2008). "Chemical oxidation of multiwalled carbon nanotubes." Carbon **46**(6): 833-840.
Davis, J. M., J. Addison, et al. (1986). "The pathogenicity of long versus short fibre samples of amosite asbestos administered to rats by inhalation and intraperitoneal injection." Br J Exp Pathol **67**(3): 415-430.
Davis, J. M., J. Addison, et al. (1991). "Variations in the carcinogenicity of tremolite dust samples of differing morphology." Ann N Y Acad Sci **643**: 473-490.
Davis, J. M. and A. D. Jones (1988). "Comparisons of the pathogenicity of long and short fibres of chrysotile asbestos in rats." Br J Exp Pathol **69**(5): 717-737.
De Volder, M. F., S. H. Tawfick, et al. (2013). "Carbon nanotubes: present and future commercial applications." Science **339**(6119): 535-539.
Delgado-Buenrostro, N. L., E. I. Medina-Reyes, et al. (2015). "Nrf2 protects the lung against inflammation induced by titanium dioxide nanoparticles: A positive regulator role of Nrf2 on cytokine release." Environ Toxicol **30**(7): 782-792.
DeSilva, D. R., E. A. Jones, et al. (1998). "Inhibition of mitogen-activated protein kinase kinase blocks T cell proliferation but does not induce or prevent anergy." J Immunol **160**(9): 4175-4181.
Di Cristo, L., D. Movia, et al. (2015). "Pro-inflammatory effects of pyrogenic and precipitated amorphous silica nanoparticles in innate immunity cells." Toxicol Sci.

Dikalov, S., M. Skatchkov, et al. (1997). "Quantification of peroxynitrite, superoxide, and peroxyl radicals by a new spin trap hydroxylamine 1-hydroxy-2,2,6,6-tetramethyl-4-oxo-piperidine." Biochemical and biophysical research communications **230**(1): 54-57.

Donaldson, K., R. Aitken, et al. (2006). "Carbon nanotubes: a review of their properties in relation to pulmonary toxicology and workplace safety." Toxicol Sci **92**(1): 5-22.

Donaldson, K., F. Murphy, et al. (2011). "Identifying the pulmonary hazard of high aspect ratio nanoparticles to enable their safety-by-design." Nanomedicine (Lond) **6**(1): 143-156.

Donaldson, K. and C. A. Poland (2013). "Nanotoxicity: challenging the myth of nano-specific toxicity." Curr Opin Biotechnol **24**(4): 724-734.

Donaldson, K., A. Schinwald, et al. (2013). "The biologically effective dose in inhalation nanotoxicology." Accounts of chemical research **46**(3): 723-732.

Donaldson, K. and C. L. Tran (2004). "An introduction to the short-term toxicology of respirable industrial fibres." Mutation research **553**(1-2): 5-9.

Eom, H. J., J. S. Jeong, et al. (2015). "Effect of aspect ratio on the uptake and toxicity of hydroxylated MWCNTs in the nematode, Caenorhabditis elegans." Environ Health Toxicol.

Esch, R. K., L. Han, et al. (2010). "Endotoxin contamination of engineered nanomaterials." Nanotoxicology **4**(1): 73-83.

Eswarappa, S. M., V. Pareek, et al. (2008). "Role of actin cytoskeleton in LPS-induced NF-kappaB activation and nitric oxide production in murine macrophages." Innate Immun **14**(5): 309-318.

European-Commission (2011). "COMMISSION RECOMMENDATION of 18 October 2011 on the definition of nanomaterial (2011/696/EU)."

Fenoglio, I., G. Greco, et al. (2009). "Non-UV-induced radical reactions at the surface of TiO2 nanoparticles that may trigger toxic responses." Chemistry **15**(18): 4614-4621.

Flahaut, E., M. C. Durrieu, et al. (2006). "Investigation of the cytotoxicity of CCVD carbon nanotubes towards human umbilical vein endothelial cells." Carbon **44**(6): 1093-1099.

Franken, N. A., H. M. Rodermond, et al. (2006). "Clonogenic assay of cells in vitro." Nat Protoc **1**(5): 2315-2319.

Fubini, B. (1997). "Surface reactivity in the pathogenic response to particulates." Environ Health Perspect **105 Suppl 5**: 1013-1020.

Gangloff, M. (2012). "Different dimerisation mode for TLR4 upon endosomal acidification?" Trends Biochem Sci **37**(3): 92-98.

Gebauer, J. S., M. Malissek, et al. (2012). "Impact of the Nanoparticle-Protein Corona on Colloidal Stability and Protein Structure." Langmuir : the ACS journal of surfaces and colloids **28**(25): 9673-9679.

Gebel, T., H. Foth, et al. (2014). "Manufactured nanomaterials: categorization and approaches to hazard assessment." Archives of toxicology **88**(12): 2191-2211.

Gerloff, K., I. Fenoglio, et al. (2012). "Distinctive toxicity of TiO2 rutile/anatase mixed phase nanoparticles on Caco-2 cells." Chemical research in toxicology **25**(3): 646-655.

German, R. M. and S. J. Park (2008). "Handbook of mathematical relations in particulate materials processing." Wiley

Getts, D. R., L. D. Shea, et al. (2015). "Harnessing nanoparticles for immune modulation." Trends Immunol **36**(7): 419-427.

Gilmour, P. S., D. M. Brown, et al. (1997). "Free radical activity of industrial fibers: role of iron in oxidative stress and activation of transcription factors." Environ Health Perspect **105 Suppl 5**: 1313-1317.

Goodglick, L. A. and A. B. Kane (1990). "Cytotoxicity of long and short crocidolite asbestos fibers in vitro and in vivo." Cancer Res **50**(16): 5153-5163.

Grassian, V. H., T. O'Shaughnessy P, et al. (2007). "Inhalation exposure study of titanium dioxide nanoparticles with a primary particle size of 2 to 5 nm." Environ Health Perspect **115**(3): 397-402.

Gu, Z., Z. Yang, et al. (2015). "Surface Curvature Relation to Protein Adsorption for Carbon-based Nanomaterials." Sci Rep **5**: 10886.

Gustafsson, A., E. Lindstedt, et al. (2011). "Lung exposure of titanium dioxide nanoparticles induces innate immune activation and long-lasting lymphocyte response in the Dark Agouti rat." J Immunotoxicol **8**(2): 111-121.

Guzman, K. A., M. R. Taylor, et al. (2006). "Environmental risks of nanotechnology: National Nanotechnology Initiative funding, 2000-2004." Environ Sci Technol **40**(5): 1401-1407.
Hahon, N., V. Vallyathan, et al. (1986). "In vitro biologic responses to native and surface-modified asbestos." Environmental Research **39**(2): 345-355.
Hamilton, R. F., Jr., Z. Wu, et al. (2013). "Effect of MWCNT size, carboxylation, and purification on in vitro and in vivo toxicity, inflammation and lung pathology." Part Fibre Toxicol **10**(1): 57.
Hamilton, R. F., N. Wu, et al. (2009). "Particle length-dependent titanium dioxide nanomaterials toxicity and bioactivity." Part Fibre Toxicol **6**: 35.
Hamilton, R. F., N. Wu, et al. (2014). "Synthesis, characterization, and bioactivity of carboxylic acid-functionalized titanium dioxide nanobelts." Part Fibre Toxicol **11**: 43.
Hansen, K. and B. T. Mossman (1987). "Generation of superoxide (O2-.) from alveolar macrophages exposed to asbestiform and nonfibrous particles." Cancer Res **47**(6): 1681-1686.
Heo, M. B. and Y. T. Lim (2014). "Programmed nanoparticles for combined immunomodulation, antigen presentation and tracking of immunotherapeutic cells." Biomaterials **35**(1): 590-600.
Heuking, S., B. Rothen-Rutishauser, et al. (2013). "Fate of TLR-1/TLR-2 agonist functionalised pDNA nanoparticles upon deposition at the human bronchial epithelium in vitro." Journal of Nanobiotechnology **11**.
Hirayama, T., Y. Tamaki, et al. (2011). "Toll-like receptors and their adaptors are regulated in macrophages after phagocytosis of lipopolysaccharide-coated titanium particles." J Orthop Res **29**(7): 984-992.
Hurbankova, M., S. Cerna, et al. (2013). "Effect of TiO2 nanofibres on selected bronchoalveolar parameters in acute and subacute phase--experimental study." Cent Eur J Public Health **21**(3): 165-170.
Husain, M., A. T. Saber, et al. (2013). "Pulmonary instillation of low doses of titanium dioxide nanoparticles in mice leads to particle retention and gene expression changes in the absence of inflammation." Toxicol Appl Pharmacol **269**(3): 250-262.
Hussain, S., L. C. Thomassen, et al. (2010). "Carbon black and titanium dioxide nanoparticles elicit distinct apoptotic pathways in bronchial epithelial cells." Part Fibre Toxicol **7**: 10.
Ii, M., N. Matsunaga, et al. (2006). "A novel cyclohexene derivative, ethyl (6R)-6-[N-(2-Chloro-4-fluorophenyl)sulfamoyl]cyclohex-1-ene-1-carboxylate (TAK-242), selectively inhibits toll-like receptor 4-mediated cytokine production through suppression of intracellular signaling." Molecular Pharmacology **69**(4): 1288-1295.
Iijima, S. (1991). "Helical Microtubules of Graphitic Carbon." Nature **354**(6348): 56-58.
Inoue, K.-i. (2011). "Promoting effects of nanoparticles/materials on sensitive lung inflammatory diseases." Environmental health and preventive medicine **16**(3): 139-143.
ISO/TR16197:2014 (2014). Compilation and description of toxicological screening methods for manufactured nanomaterials.
Ispas, C., D. Andreescu, et al. (2009). "Toxicity and Developmental Defects of Different Sizes and Shape Nickel Nanoparticles in Zebrafish." Environmental Science & Technology **43**(16): 6349-6356.
Jackson, P., K. Kling, et al. (2015). "Characterization of genotoxic response to 15 multiwalled carbon nanotubes with variable physicochemical properties including surface functionalizations in the FE1-Muta(TM) mouse lung epithelial cell line." Environ Mol Mutagen **56**(2): 183-203.
Jacobs, M., M. Ellenbecker, et al. (2014). Precarious Promise: A Case Study of Engineered Carbon Nanotubes, University of Massachusetts Lowell.
Jain, S., V. S. Thakare, et al. (2011). "Toxicity of multiwalled carbon nanotubes with end defects critically depends on their functionalization density." Chem Res Toxicol **24**(11): 2028-2039.
Ji, Z., X. Wang, et al. (2012). "Designed synthesis of CeO2 nanorods and nanowires for studying toxicological effects of high aspect ratio nanomaterials." ACS nano **6**(6): 5366-5380.
Jia, G., H. F. Wang, et al. (2005). "Cytotoxicity of carbon nanomaterials: Single-wall nanotube, multi-wall nanotube, and fullerene." Environmental Science & Technology **39**(5): 1378-1383.
Jiang, W. (2011). Amherst, University of Massachusetts. **Ph.D**.
Jones, A. D. (1993). "Respirable industrial fibres: deposition, clearance and dissolution in animal models." Ann Occup Hyg **37**(2): 211-226.

Jones, E., I. M. Adcock, et al. (2007). "Modulation of LPS stimulated NF-kappaB mediated Nitric Oxide production by PKCepsilon and JAK2 in RAW macrophages." J Inflamm (Lond) **4**: 23.

Jugan, M. L., S. Barillet, et al. (2011). "Cytotoxic and Genotoxic Impact of TiO2 Nanoparticles on A549 Cells." Journal of Biomedical Nanotechnology **7**(1): 22-23.

Kagan, V. E., Y. Y. Tyurina, et al. (2006). "Direct and indirect effects of single walled carbon nanotubes on RAW 264.7 macrophages: Role of iron." Toxicology Letters **165**(1): 88-100.

Kalkanidis, M., G. A. Pietersz, et al. (2006). "Methods for nano-particle based vaccine formulation and evaluation of their immunogenicity." Methods (San Diego, Calif) **40**(1): 20-29.

Kamp, D. W. (2009). "Asbestos-induced lung diseases: an update." Transl Res **153**(4): 143-152.

Kang, J. L., C. Moon, et al. (2008). "Comparison of the biological activity between ultrafine and fine titanium dioxide particles in RAW 264.7 cells associated with oxidative stress." Journal of toxicology and environmental health Part A **71**(8): 478-485.

Kim, J. S., K. S. Song, et al. (2010). "Determination of cytotoxicity attributed to multiwall carbon nanotubes (MWCNT) in normal human embryonic lung cell (WI-38) line." J Toxicol Environ Health A **73**(21-22): 1521-1529.

Knuckles, T. L., J. Yi, et al. (2012). "Nanoparticle inhalation alters systemic arteriolar vasoreactivity through sympathetic and cyclooxygenase-mediated pathways." Nanotoxicology **6**(7): 724-735.

Kobayashi, N., M. Naya, et al. (2009). "Comparative pulmonary toxicity study of nano-TiO(2) particles of different sizes and agglomerations in rats: different short- and long-term post-instillation results." Toxicology **264**(1-2): 110-118.

Kohyama, N., Y. Shinohara, et al. (1996). "Mineral phases and some reexamined characteristics of the International Union Against Cancer standard asbestos samples." American journal of industrial medicine **30**(5): 515-528.

Kostarelos, K., L. Lacerda, et al. (2007). "Cellular uptake of functionalized carbon nanotubes is independent of functional group and cell type." Nat Nanotechnol **2**(2): 108-113.

Kumar, S., M. S. Jiang, et al. (1999). "Pyridinylimidazole compound SB 203580 inhibits the activity but not the activation of p38 mitogen-activated protein kinase." Biochemical and biophysical research communications **263**(3): 825-831.

Lam, C. W., J. T. James, et al. (2006). "A review of carbon nanotube toxicity and assessment of potential occupational and environmental health risks." Crit Rev Toxicol **36**(3): 189-217.

Lam, C. W., J. T. James, et al. (2004). "Pulmonary toxicity of single-wall carbon nanotubes in mice 7 and 90 days after intratracheal instillation." Toxicological Sciences **77**(1): 126-134.

Landsiedel, R., U. G. Sauer, et al. (2014). "Pulmonary toxicity of nanomaterials: a critical comparison of published in vitro assays and in vivo inhalation or instillation studies." Nanomedicine (Lond) **9**(16): 2557-2585.

Lanone, S., P. Andujar, et al. (2013). "Determinants of carbon nanotube toxicity." Adv Drug Deliv Rev **65**(15): 2063-2069.

LeBlanc, A. J., J. L. Cumpston, et al. (2009). "Nanoparticle inhalation impairs endothelium-dependent vasodilation in subepicardial arterioles." J Toxicol Environ Health A **72**(24): 1576-1584.

Lee, Y. K., E. J. Choi, et al. (2015). "Effect of the protein corona on nanoparticles for modulating cytotoxicity and immunotoxicity." International journal of nanomedicine **10**: 97-112.

Lesniak, A., F. Fenaroli, et al. (2012). "Effects of the presence or absence of a protein corona on silica nanoparticle uptake and impact on cells." ACS nano **6**(7): 5845-5857.

Li, B., Y. Ze, et al. (2013). "Molecular mechanisms of nanosized titanium dioxide-induced pulmonary injury in mice." PloS one **8**(2): e55563.

Lindenschmidt, R. C., K. E. Driscoll, et al. (1990). "The comparison of a fibrogenic and two nonfibrogenic dusts by bronchoalveolar lavage." Toxicology and applied pharmacology **102**(2): 268-281.

Liu, R., X. Zhang, et al. (2010). "Small-sized titanium dioxide nanoparticles mediate immune toxicity in rat pulmonary alveolar macrophages in vivo." J Nanosci Nanotechnol **10**(8): 5161-5169.

Liu, Z., X. Dong, et al. (2014). "Carboxylation of multiwalled carbon nanotube enhanced its biocompatibility with L02 cells through decreased activation of mitochondrial apoptotic pathway." J Biomed Mater Res A **102**(3): 665-673.

Liu, Z., W. Li, et al. (2012). "Enhancement of lipopolysaccharide-induced nitric oxide and interleukin-6 production by PEGylated gold nanoparticles in RAW264.7 cells." Nanoscale **4**(22): 7135-7142.
Long, C. M., H. H. Suh, et al. (2001). "A pilot investigation of the relative toxicity of indoor and outdoor fine particles: in vitro effects of endotoxin and other particulate properties." Environ Health Perspect **109**(10): 1019-1026.
Lu, X., I. R. Miousse, et al. (2015). "Short-term exposure to engineered nanomaterials affects cellular epigenome." Nanotoxicology: 1-11.
Lundqvist, M., J. Stigler, et al. (2008). "Nanoparticle size and surface properties determine the protein corona with possible implications for biological impacts." Proceedings of the National Academy of Sciences of the United States of America **105**(38): 14265-14270.
Luo, Y. H., L. W. Chang, et al. (2015). "Metal-Based Nanoparticles and the Immune System: Activation, Inflammation, and Potential Applications." Biomed Res Int **2015**: 143720.
Lynch, I., T. Cedervall, et al. (2007). "The nanoparticle-protein complex as a biological entity; a complex fluids and surface science challenge for the 21st century." Advances in colloid and interface science **134-135**: 167-174.
Ma-Hock, L., S. Burkhardt, et al. (2009). "Development of a short-term inhalation test in the rat using nano-titanium dioxide as a model substance." Inhalation toxicology **21**(2): 102-118.
Ma-Hock, L., S. Treumann, et al. (2009). "Inhalation toxicity of multiwall carbon nanotubes in rats exposed for 3 months." Toxicol Sci **112**(2): 468-481.
Manna, S. K., S. Sarkar, et al. (2005). "Single-walled carbon nanotube induces oxidative stress and activates nuclear transcription factor-kappaB in human keratinocytes." Nano Lett **5**(9): 1676-1684.
Marchesan, S. and M. Prato (2015). "Under the lens: carbon nanotube and protein interaction at the nanoscale." Chem Commun (Camb) **51**(21): 4347-4359.
Meena, R., K. Kajal, et al. (2015). "Cytotoxic and genotoxic effects of titanium dioxide nanoparticles in testicular cells of male wistar rat." Appl Biochem Biotechnol **175**(2): 825-840.
Meng, H., T. Xia, et al. (2009). "A predictive toxicological paradigm for the safety assessment of nanomaterials." ACS Nano **3**(7): 1620-1627.
Mercer, R. R., A. F. Hubbs, et al. (2011). "Pulmonary fibrotic response to aspiration of multi-walled carbon nanotubes." Part Fibre Toxicol **8**: 21.
Mercer, R. R., J. F. Scabilloni, et al. (2013). "Distribution and fibrotic response following inhalation exposure to multi-walled carbon nanotubes." Part Fibre Toxicol **10**: 33.
Miclaus, T., V. E. Bochenkov, et al. (2014). "Spatial mapping and quantification of soft and hard protein coronas at silver nanocubes." Nano letters **14**(4): 2086-2093.
Mills, C. D., K. Kincaid, et al. (2000). "M-1/M-2 macrophages and the Th1/Th2 paradigm." J Immunol **164**(12): 6166-6173.
Misko, T. P., R. J. Schilling, et al. (1993). "A fluorometric assay for the measurement of nitrite in biological samples." Anal Biochem **214**(1): 11-16.
Mody, K. T., A. Popat, et al. (2013). "Mesoporous silica nanoparticles as antigen carriers and adjuvants for vaccine delivery." Nanoscale **5**(12): 5167-5179.
Monopoli, M. P., C. Aberg, et al. (2012). "Biomolecular coronas provide the biological identity of nanosized materials." Nature nanotechnology **7**(12): 779-786.
Monopoli, M. P., D. Walczyk, et al. (2011). "Physical-chemical aspects of protein corona: relevance to in vitro and in vivo biological impacts of nanoparticles." Journal of the American Chemical Society **133**(8): 2525-2534.
Moon, C., H. J. Park, et al. (2010). "Pulmonary inflammation after intraperitoneal administration of ultrafine titanium dioxide (TiO2) at rest or in lungs primed with lipopolysaccharide." J Toxicol Environ Health A **73**(5): 396-409.
Moore, R. A., N. C. Bates, et al. (1986). "Interaction of polycationic antibiotics with Pseudomonas aeruginosa lipopolysaccharide and lipid A studied by using dansyl-polymyxin." Antimicrob Agents Chemother **29**(3): 496-500.

Morishige, T., Y. Yoshioka, et al. (2010). "Titanium dioxide induces different levels of IL-1beta production dependent on its particle characteristics through caspase-1 activation mediated by reactive oxygen species and cathepsin B." Biochemical and biophysical research communications **392**(2): 160-165.

Muller, J., F. Huaux, et al. (2008). "Structural defects play a major role in the acute lung toxicity of multiwall carbon nanotubes: toxicological aspects." Chemical research in toxicology **21**(9): 1698-1705.

Muller, J., F. Huaux, et al. (2005). "Respiratory toxicity of multi-wall carbon nanotubes." Toxicology and applied pharmacology **207**(3): 221-231.

Muller, J., F. Huaux, et al. (2005). "Respiratory toxicity of multi-wall carbon nanotubes." Toxicol Appl Pharmacol **207**(3): 221-231.

Murphy, F. A., A. Schinwald, et al. (2012). "The mechanism of pleural inflammation by long carbon nanotubes: interaction of long fibres with macrophages stimulates them to amplify pro-inflammatory responses in mesothelial cells." Part Fibre Toxicol **9**: 8.

Murray, A. R., E. R. Kisin, et al. (2012). "Factoring-in agglomeration of carbon nanotubes and nanofibers for better prediction of their toxicity versus asbestos." Part Fibre Toxicol **9**: 10.

Murray, P. J., J. E. Allen, et al. (2014). "Macrophage Activation and Polarization: Nomenclature and Experimental Guidelines (vol 41, pg 14, 2014)." Immunity **41**(2): 339-340.

Nel, A., T. Xia, et al. (2006). "Toxic potential of materials at the nanolevel." Science **311**(5761): 622-627.

Noel, A., Y. Cloutier, et al. (2013). "Generating nano-aerosols from TiO(2) (5 nm) nanoparticles showing different agglomeration states. Application to toxicological studies." J Occup Environ Hyg **10**(2): 86-96.

O'Brien, J., I. Wilson, et al. (2000). "Investigation of the Alamar Blue (resazurin) fluorescent dye for the assessment of mammalian cell cytotoxicity." European journal of biochemistry / FEBS **267**(17): 5421-5426.

Oberdorster, G., J. N. Finkelstein, et al. (2000). "Acute pulmonary effects of ultrafine particles in rats and mice." Res Rep Health Eff Inst(96): 5-74; disc 75-86.

Oberdorster, G., E. Oberdorster, et al. (2005). "Nanotoxicology: an emerging discipline evolving from studies of ultrafine particles." Environ Health Perspect **113**(7): 823-839.

Okemoto, K., K. Kawasaki, et al. (2006). "A potent adjuvant monophosphoryl lipid A triggers various immune responses, but not secretion of IL-1beta or activation of caspase-1." J Immunol **176**(2): 1203-1208.

Oostingh, G. J., E. Casals, et al. (2011). "Problems and challenges in the development and validation of human cell-based assays to determine nanoparticle-induced immunomodulatory effects." Part Fibre Toxicol **8**(1): 8.

Orazizadeh, M., E. Daneshi, et al. (2015). "Protective effect of beta-carotene against titanium dioxide nanoparticles induced apoptosis in mouse testicular tissue." Andrologia **47**(7): 816-825.

Pacurari, M., V. Castranova, et al. (2010). "Single- and multi-wall carbon nanotubes versus asbestos: are the carbon nanotubes a new health risk to humans?" J Toxicol Environ Health A **73**(5): 378-395.

Park, E. J., N. E. Zahari, et al. (2014). "SWCNTs induced autophagic cell death in human bronchial epithelial cells." Toxicol In Vitro **28**(3): 442-450.

Pauluhn, J. and M. Rosenbruch (2015). "Lung burdens and kinetics of multi-walled carbon nanotubes (Baytubes) are highly dependent on the disaggregation of aerosolized MWCNT." Nanotoxicology **9**: 242-252.

Peigney, A., C. Laurent, et al. (1998). "Carbon nanotubes Fe alumina nanocomposites. Part I: Influence of the Fe content on the synthesis of powders." Journal of the European Ceramic Society **18**(14): 1995-2004.

Pelegrin, P., C. Barroso-Gutierrez, et al. (2008). "P2X7 receptor differentially couples to distinct release pathways for IL-1beta in mouse macrophage." J Immunol **180**(11): 7147-7157.

Philippe, R., B. Caussat, et al. (2009). "An original growth mode of MWCNTs on alumina supported iron catalysts." Journal of Catalysis **263**(2): 345-358.

Poland, C. A., F. Byrne, et al. (2012). "Length-dependent pathogenic effects of nickel nanowires in the lungs and the peritoneal cavity." Nanotoxicology **6**: 899-911.

Poland, C. A., R. Duffin, et al. (2008). "Carbon nanotubes introduced into the abdominal cavity of mice show asbestos-like pathogenicity in a pilot study." Nature nanotechnology **3**(7): 423-428.
Ponti, J., A. Kinsner-Ovaskainen, et al. (2014). Interlaboratory comparison study of the Colony Forming Efficiency assay for assessing cytotoxicity of nanomaterials. Luxembourg, European Commission.
Porter, D. W., A. F. Hubbs, et al. (2013). "Acute pulmonary dose-responses to inhaled multi-walled carbon nanotubes." Nanotoxicology **7**(7): 1179-1194.
Porter, D. W., N. Wu, et al. (2013). "Differential mouse pulmonary dose and time course responses to titanium dioxide nanospheres and nanobelts." Toxicol Sci **131**(1): 179-193.
Preocanin, T., A. Cop, et al. (2006). "Surface potential of hematite in aqueous electrolyte solution: hysteresis and equilibration at the interface." J Colloid Interface Sci **299**(2): 772-776.
Pulskamp, K., S. Diabate, et al. (2007). "Carbon nanotubes show no sign of acute toxicity but induce intracellular reactive oxygen species in dependence on contaminants." Toxicol Lett **168**(1): 58-74.
Raffaini, G. and F. Ganazzoli (2013). "Surface topography effects in protein adsorption on nanostructured carbon allotropes." Langmuir : the ACS journal of surfaces and colloids **29**(15): 4883-4893.
Ramanathan, T., F. T. Fisher, et al. (2005). "Amino-functionalized carbon nanotubes for binding to polymers and biological systems." Chemistry of Materials **17**(6): 1290-1295.
Ramkumar, K. M., C. Manjula, et al. (2012). "Oxidative stress-mediated cytotoxicity and apoptosis induction by TiO2 nanofibers in HeLa cells." Eur J Pharm Biopharm **81**(2): 324-333.
Rao, K. M., T. Meighan, et al. (2002). "Role of mitogen-activated protein kinase activation in the production of inflammatory mediators: differences between primary rat alveolar macrophages and macrophage cell lines." J Toxicol Environ Health A **65**(10): 757-768.
Rasmussen, K., J. Mast, et al. (2014). Multi-walled Carbon Nanotubes, NM-400, NM-401, NM-402, NM-403: Characterisation and Physico-Chemical Properties. Luxembourg, European Commission.
Rasmussen, K., J. Mast, et al. (2014). Titanium Dioxide, NM-100, NM-101, NM-102, NM-103, NM-104, NM-105: Characterisation and Physico-Chemical Properties. Ispra, Varese, Italy, Joint Research Centre – Institute for Health and Consumer Protection.
Ribi, E., J. L. Cantrell, et al. (1984). "Lipid A and immunotherapy." Rev Infect Dis **6**(4): 567-572.
Rittinghausen, S., A. Hackbarth, et al. (2014). "The carcinogenic effect of various multi-walled carbon nanotubes (MWCNTs) after intraperitoneal injection in rats." Particle and Fibre Toxicology **11**.
Rotoli, B. M., O. Bussolati, et al. (2009). "Airway barrier dysfunction induced by exposure to carbon nanotubes in vitro: which role for fiber length?" Hum Exp Toxicol **28**(6-7): 361-368.
Rotoli, B. M., O. Bussolati, et al. (2008). "Non-functionalized multi-walled carbon nanotubes alter the paracellular permeability of human airway epithelial cells." Toxicology letters **178**(2): 95-102.
Rotoli, B. M., O. Bussolati, et al. (2012). "Comparative effects of metal oxide nanoparticles on human airway epithelial cells and macrophages." Journal of Nanoparticle Research **14**(9).
Rotoli, B. M., R. Gatti, et al. (2015). "Identifying contact-mediated, localized toxic effects of MWCNT aggregates on epithelial monolayers: a single-cell monitoring toxicity assay." Nanotoxicology **9**(2): 230-241.
Rushton, E. K., J. Jiang, et al. (2010). "Concept of Assessing Nanoparticle Hazards Considering Nanoparticle Dosemetric and Chemical/Biological Response Metrics." Journal of Toxicology and Environmental Health-Part a-Current Issues **73**(5-6): 445-461.
Ryman-Rasmussen, J. P., M. F. Cesta, et al. (2009). "Inhaled carbon nanotubes reach the subpleural tissue in mice." Nature nanotechnology **4**(11): 747-751.
Sager, T. M., M. W. Wolfarth, et al. (2014). "Effect of multi-walled carbon nanotube surface modification on bioactivity in the C57BL/6 mouse model." Nanotoxicology **8**(3): 317-327.
Salem, L. B., C. Bosquillon, et al. (2009). "Sparing methylation of beta-cyclodextrin mitigates cytotoxicity and permeability induction in respiratory epithelial cell layers in vitro." Journal of controlled release : official journal of the Controlled Release Society **136**(2): 110-116.
Salvati, A., A. S. Pitek, et al. (2013). "Transferrin-functionalized nanoparticles lose their targeting capabilities when a biomolecule corona adsorbs on the surface." Nature nanotechnology **8**(2): 137-143.

Sang, X., B. Li, et al. (2013). "Toxicological mechanisms of nanosized titanium dioxide-induced spleen injury in mice after repeated peroral application." Journal of agricultural and food chemistry **61**(23): 5590-5599.
Sanghera, J. S., S. L. Weinstein, et al. (1996). "Activation of multiple proline-directed kinases by bacterial lipopolysaccharide in murine macrophages." J Immunol **156**(11): 4457-4465.
Saquib, Q., A. A. Al-Khedhairy, et al. (2012). "Titanium dioxide nanoparticles induced cytotoxicity, oxidative stress and DNA damage in human amnion epithelial (WISH) cells." Toxicol In Vitro **26**(2): 351-361.
Scherbart, A. M., J. Langer, et al. (2011). "Contrasting macrophage activation by fine and ultrafine titanium dioxide particles is associated with different uptake mechanisms." Part Fibre Toxicol **8**: 31.
Schinwald, A., T. Chernova, et al. (2012). "Use of silver nanowires to determine thresholds for fibre length-dependent pulmonary inflammation and inhibition of macrophage migration in vitro." Particle and Fibre Toxicology **9**.
Schinwald, A. and K. Donaldson (2012). "Use of back-scatter electron signals to visualise cell/nanowires interactions in vitro and in vivo; frustrated phagocytosis of long fibres in macrophages and compartmentalisation in mesothelial cells in vivo." Part Fibre Toxicol **9**: 34.
Shannahan, J. H., J. M. Brown, et al. (2013). "Comparison of nanotube-protein corona composition in cell culture media." Small **9**(12): 2171-2181.
Sheng, L., X. Wang, et al. (2013). "Cardiac oxidative damage in mice following exposure to nanoparticulate titanium dioxide." Journal of biomedical materials research Part A **101**(11): 3238-3246.
Sheng, L., Y. Ze, et al. (2015). "Mechanisms of TiO2 nanoparticle-induced neuronal apoptosis in rat primary cultured hippocampal neurons." Journal of biomedical materials research Part A **103**(3): 1141-1149.
Shi, H., R. Magaye, et al. (2013). "Titanium dioxide nanoparticles: a review of current toxicological data." Part Fibre Toxicol **10**: 15.
Shi, Y., S. Yadav, et al. (2010). "Endotoxin promotes adverse effects of amorphous silica nanoparticles on lung epithelial cells in vitro." J Toxicol Environ Health A **73**(11): 748-756.
Shukla, R. K., V. Sharma, et al. (2011). "ROS-mediated genotoxicity induced by titanium dioxide nanoparticles in human epidermal cells." Toxicol In Vitro **25**(1): 231-241.
Shvedova, A. A., E. Kisin, et al. (2008). "Inhalation vs. aspiration of single-walled carbon nanotubes in C57BL/6 mice: inflammation, fibrosis, oxidative stress, and mutagenesis." American Journal of Physiology-Lung Cellular and Molecular Physiology **295**(4): L552-L565.
Shvedova, A. A., E. R. Kisin, et al. (2005). "Unusual inflammatory and fibrogenic pulmonary responses to single-walled carbon nanotubes in mice." Am J Physiol Lung Cell Mol Physiol **289**(5): L698-708.
Silva, R. M., C. Teesy, et al. (2013). "Biological response to nano-scale titanium dioxide (TiO2): role of particle dose, shape, and retention." J Toxicol Environ Health A **76**(16): 953-972.
Smulders, S., J.-P. Kaiser, et al. (2012). "Contamination of nanoparticles by endotoxin: evaluation of different test methods." Particle and fibre toxicology **9**: 41.
Song, L., K. Yang, et al. (2012). "Adsorption of bovine serum albumin on nano and bulk oxide particles in deionized water." Colloids Surf B Biointerfaces **94**: 341-346.
Soukup, J. M. and S. Becker (2001). "Human alveolar macrophage responses to air pollution particulates are associated with insoluble components of coarse material, including particulate endotoxin." Toxicol Appl Pharmacol **171**(1): 20-26.
Stanton, M. F., M. Layard, et al. (1981). "Relation of particle dimension to carcinogenicity in amphibole asbestoses and other fibrous minerals." J Natl Cancer Inst **67**(5): 965-975.
Stanton, M. F., M. Laynard, et al. (1977). "Carcinogenicity of fibrous glass: pleural response in the rat in relation to fiber dimension." J Natl Cancer Inst **58**(3): 587-603.
Stein, P., K. Gogoll, et al. (2014). "Efficacy of imiquimod-based transcutaneous immunization using a nano-dispersed emulsion gel formulation." PloS one **9**(7): e102664.
Sweeney, S., D. Grandolfo, et al. (2015). "Functional consequences for primary human alveolar macrophages following treatment with long, but not short, multiwalled carbon nanotubes." International journal of nanomedicine **10**: 3115-3129.
Tagmatarchis, N. and M. Prato (2004). "Functionalization of carbon nanotubes via 1,3-dipolar cycloadditions." Journal of Materials Chemistry **14**(4): 437-439.

Tan, Y. and J. C. Kagan (2014). "A cross-disciplinary perspective on the innate immune responses to bacterial lipopolysaccharide." Mol Cell **54**(2): 212-223.

Taylor, E. L., A. G. Rossi, et al. (2004). "GEA 3162 decomposes to co-generate nitric oxide and superoxide and induces apoptosis in human neutrophils via a peroxynitrite-dependent mechanism." Br J Pharmacol **143**(1): 179-185.

Tenzer, S., D. Docter, et al. (2011). "Nanoparticle size is a critical physicochemical determinant of the human blood plasma corona: a comprehensive quantitative proteomic analysis." ACS nano **5**(9): 7155-7167.

Tincer, G., S. Yerlikaya, et al. (2011). "Immunostimulatory activity of polysaccharide-poly(I:C) nanoparticles." Biomaterials **32**(18): 4275-4282.

Toyokuni, S. (2013). "Genotoxicity and carcinogenicity risk of carbon nanotubes." Adv Drug Deliv Rev **65**(15): 2098-2110.

Treuel, L., S. Brandholt, et al. (2014). "Impact of protein modification on the protein corona on nanoparticles and nanoparticle-cell interactions." ACS nano **8**(1): 503-513.

Triboulet, S., C. Aude-Garcia, et al. (2015). "Comparative proteomic analysis of the molecular responses of mouse macrophages to titanium dioxide and copper oxide nanoparticles unravels some toxic mechanisms for copper oxide nanoparticles in macrophages." PloS one **10**(4): e0124496.

Urankar, R. N., R. M. Lust, et al. (2012). "Expansion of cardiac ischemia/reperfusion injury after instillation of three forms of multi-walled carbon nanotubes." Part Fibre Toxicol **9**: 38.

Ursini, C. L., R. Maiello, et al. (2015). "Evaluation of uptake, cytotoxicity and inflammatory effects in respiratory cells exposed to pristine and -OH and -COOH functionalized multi-wall carbon nanotubes." J Appl Toxicol.

Vallhov, H., J. Qin, et al. (2006). "The importance of an endotoxin-free environment during the production of nanoparticles used in medical applications." Nano letters **6**(8): 1682-1686.

W.H.O. (1997). Determination of airborne fibre number concentrations. A recommended method, by phase-contrast optical microscopy membrane filter method. Geneva, World Health Organization.

Wako, K., Y. Kotani, et al. (2010). "Effects of preparation methods for multi-wall carbon nanotube (MWCNT) suspensions on MWCNT induced rat pulmonary toxicity." Journal of Toxicological Sciences **35**(4): 437-446.

Walczyk, D., F. B. Bombelli, et al. (2010). "What the cell "sees" in bionanoscience." Journal of the American Chemical Society **132**(16): 5761-5768.

Wang, X., T. Xia, et al. (2010). "Quantitative techniques for assessing and controlling the dispersion and biological effects of multiwalled carbon nanotubes in mammalian tissue culture cells." ACS Nano **4**(12): 7241-7252.

Wang, Y., H. Cui, et al. (2015). "Cytotoxicity, DNA damage, and apoptosis induced by titanium dioxide nanoparticles in human non-small cell lung cancer A549 cells." Environ Sci Pollut Res Int **22**(7): 5519-5530.

Warheit, D. B., T. R. Webb, et al. (2006). "Pulmonary instillation studies with nanoscale TiO2 rods and dots in rats: toxicity is not dependent upon particle size and surface area." Toxicol Sci **91**(1): 227-236.

Webb, J. L., M. W. Harvey, et al. (2001). "Macrophage nitric oxide synthase associates with cortical actin but is not recruited to phagosomes." Infect Immun **69**(10): 6391-6400.

Wick, P., P. Manser, et al. (2007). "The degree and kind of agglomeration affect carbon nanotube cytotoxicity." Toxicol Lett **168**(2): 121-131.

Winter, M., H.-D. Beer, et al. (2011). "Activation of the inflammasome by amorphous silica and TiO2 nanoparticles in murine dendritic cells." Nanotoxicology **5**(3): 326-340.

Wirnitzer, U., B. Herbold, et al. (2009). "Studies on the in vitro genotoxicity of baytubes, agglomerates of engineered multi-walled carbon-nanotubes (MWCNT)." Toxicol Lett **186**(3): 160-165.

Wright, G. W. and M. Kuschner (1975). "The influence of varying lengths of glass and asbestos fibres on tissue response in guinea pigs." Inhaled Part **4 Pt 2**: 455-474.

Wu, W. T., H. Y. Liao, et al. (2014). "Effect of nanoparticles exposure on fractional exhaled nitric oxide (FENO) in workers exposed to nanomaterials." Int J Mol Sci **15**(1): 878-894.

Xia, T., R. F. Hamilton, et al. (2013). "Interlaboratory evaluation of in vitro cytotoxicity and inflammatory responses to engineered nanomaterials: the NIEHS Nano GO Consortium." Environ Health Perspect **121**(6): 683-690.

Xiong, S., S. George, et al. (2013). "Size influences the cytotoxicity of poly (lactic-co-glycolic acid) (PLGA) and titanium dioxide (TiO(2)) nanoparticles." Arch Toxicol **87**(6): 1075-1086.

Yang, M., K. Flavin, et al. (2013). "Functionalization of carbon nanoparticles modulates inflammatory cell recruitment and NLRP3 inflammasome activation." Small (Weinheim an der Bergstrasse, Germany) **9**(24): 4194-4206.

Yu, K. N., J. H. Sung, et al. (2015). "Inhalation of titanium dioxide induces endoplasmic reticulum stress-mediated autophagy and inflammation in mice." Food Chem Toxicol.

Zhang, T., M. Tang, et al. (2015). "Surface modification of multiwall carbon nanotubes determines the pro-inflammatory outcome in macrophage." J Hazard Mater **284**: 73-82.

Zhao, Z. Y., Z. H. Yang, et al. (2013). "Multiple functionalization of multi-walled carbon nanotubes with carboxyl and amino groups." Applied Surface Science **276**: 476-481.

Zhu, Y., T. Ran, et al. (2006). "Dependence of the cytotoxicity of multi-walled carbon nanotubes on the culture medium." Nanotechnology **17**(18): 4668-4674.